

The telomeric DNA damage response: Insights into telomere compaction and identification of novel damage signaling factors

THÈSE N° 8945 (2018)

PRÉSENTÉE LE 12 OCTOBRE 2018

À LA FACULTÉ DES SCIENCES DE LA VIE

UNITÉ DU PROF. LINGNER

PROGRAMME DOCTORAL EN APPROCHES MOLÉCULAIRES DU VIVANT

ÉCOLE POLYTECHNIQUE FÉDÉRALE DE LAUSANNE

POUR L'OBTENTION DU GRADE DE DOCTEUR ÈS SCIENCES

PAR

Aleksandra VANCEVSKA

acceptée sur proposition du jury:

Prof. P. Gönczy, président du jury

Prof. J. Lingner, directeur de thèse

Prof. S. Gasser, rapporteuse

Prof. M. Altmeyer, rapporteur

Prof. S. Manley, rapporteuse



ÉCOLE POLYTECHNIQUE
FÉDÉRALE DE LAUSANNE

Suisse
2018

Acknowledgements

"If I have seen further it is by standing on the shoulders of Giants." Isaac Newton, 1675

Primarily, I would like to thank my advisor Prof. Joachim Lingner for his wholehearted support and critical insight during five amazing years of my PhD studies. Working together with such an outstanding scientist and analytical thinker was a great challenge and a beautiful collaboration. I would like to thank Joachim for his extraordinary patience which allows every lab member an opportunity to fail safely and for his help to successfully recover from failures. In my case, I especially thank him for keeping his calm when I have breached all the possible deadlines. I would also like to thank him for being available for discussion at any time and for sparking excitement even when my internal motivation was not at its best. The safe environment that he creates allowed me to pursue challenging projects and develop to extents that I could not envision at the start of my studies. For all of that and many more things, THANK YOU!

I would also like to express gratitude to all the past and present members of the Lingner lab who are the heart and soul of my PhD studies. I would not be who I am today without the discussions about life, science, the universe and everything with all of them. I owe many thanks to Ivo Zemp, an outstanding scientist, who is a mentor and a friend and who is culpable for my decision in joining the Lingner lab family. In addition, I would like to thank Larissa Grolimund for supervision and initiation of both of my projects and Verena Pfeiffer for being a great mentor and collaborator. To Janka, Patricia and Anna Reis, I would like to thank for all their PhD-student comradery and help. I owe special thanks to Marianna Feretzaki, my bench mate and friend for all the daily discussions and help that really shaped me into being a calmer, more understanding and patient person and scientist, as well for all the technical help that she wholeheartedly provided. I also want to thank Galina Glousker for her directness and embodiment of amazing strength that provided me with a model of a scientist that I strive to become. To Reyes Babiano I would like to thank for making me more self-reliant, for encouraging me to trust my intuition, and for not allowing me to repeat experiments in the same way expecting a different result. To Thomas Lunardi I thank for all the laughs and for keeping us all in check. To Gérald Loassaint I thank for introducing me to the wonderful world of DNA replication. Last but not least, I would like to thank Wareed Ahmed for all the great discussions about politics, humanity and experiments and for amazing critical insights. I also want to thank my collaborators Prof. Suliana Manley and Dr. Kyle M. Douglass for outstanding discussions and great collaboration. Their work has been indispensable for the successful realization of my PhD project. Their approach to scientific questions has helped me to be more systematic and precise in the way I perform experiments and organize my day.

I owe deep gratitude to Tatiana Dubi who was always there to guide me and support me through all the requirements of the PhD program.

I thank Prof. Pierre Gönczy for the support and careful mentorship during my PhD studies. I am also grateful to Prof. Susan Gasser, Prof. Matthias Altmeyer, Prof. Suliana Manley and Prof. Gael Cristofari for accepting to take part in my candidacy and PhD thesis committees and to provide constructive feedback on our work.

I thank the EPFL Bioimaging & Optics Platform (BIOP), especially Arne Seitz, Romain Guet, Thierry Laroche and Oliver Burri for constant support and knowledge transfer with all my microscopy requirements.

On a more personal note, I could never thank enough my parents Blagoj and Valentina Vančevski and my sister Jovana Vančevska who have always supported me in all my crazy pursuits and gave me enough space to make my own choices. No words are enough to express the gratitude I have for them and I hope to become at least a tiny bit the moral giants they are. I also want to thank my "adopted" Lausannois family, Stana and Dragan Rakić, who have made my life in Lausanne feel like home. To Vischwachi Tripathi I thank for being an amazing roommate and always understanding of my shortcomings. I thank Dr. Aleksandra Nikolić, my scientific mother who was watching my baby scientific steps and was there to support and correct me while growing up as a scientist. I would like to thank Prof. Bato Korać for allowing me to pass my last exam without whom I won't be able to attend these PhD studies. I thank my best friend Tamara Spasojevic for being there to share with me all the beautiful moments while discovering the secrets of biology and life. I owe big thanks to my crazy curious friends Marjan Biočanin, Đorđe Marković and Petar Šćepanović for all the enriching conversations. And I thank my five friends from the University of Belgrade (Aleksandra Djurić, Lena Arizanović, Sandra Bulatović, Ana Boljević and Ivana Uglješić) for making the unbearable years of the undergraduate studies beautiful. In the end, I want to thank Aleksandar Salim, my fiancée, my trusted confidante, my best friend, my life companion who helped me to battle all the internal and external wars and with whom any moment in life is worth living.

Lausanne, October 12th, 2018

Захвалница

„Ако сам видео даље од других, то је зато што сам стајао на плећима дивова.” Исак Њутн, 1675

Најпре желим да се захвалим свом ментору, Проф. Јоаким Лингнер-у за његову свесрдну подршку и критички приступ током пет предивних година докторских студија. Сарадња са врхунским научником и аналитичким мислиоцем као што је Проф. Лингнер јер била за мене велики изазов али и дивна колаборација. Желим да се захвалим Јоакиму за његово изузетно стрпљење које омогућава сваком члану лабораторије да се безбедно избори са неуспесима и личним недостацима. У мом случају, специјално му се захваљујем на смирености у тренуцима када сам пробила све задате рокове. Такође, желим да му се захвалим што су његова врата била увек отворена, што је увек расположен за дискусију и што је успевао да у мени пробуди узбуђење за науку чак и када је моја интерна мотивација била доведена у питање. Осећај сигурности који је Проф.Лингнер успео да створи у својој лабораторији ми је омогућио да се не бојим рада на изузетно захтевним и ризичним пројектима што ми је помогло да се интелектуално и емотивно развијем до граница које нисам могла да наслутим на почетку докторских студија. За све ово и још много тога- ХВАЛА ВАМ!

Желила бих да се захвалим и свим прошлим и садашњим члановима Лингнер лабораторије који су чинили потку мојих докторских студија. Да није разговора о животу, науци, универзуму и свему осталом са људима који су били део ове лабораторије моја личност се не би формирала на исти начин и била би сиромашнија. Дугујем дубоку захвалност Иви Цемпу, изванредном научнику, који је такође мој ментор и пријатељ и кривац штос сам постала део Лингнер породице. Такође, желим да се захвалим Лариси Гролимунд за менторство и иницијацију пројеката на којима сам радила током доктората и Верени Фајфер, сјајном ментору и сараднику. Јани, Патрисији и Ани желим да се захвалим због братске докторантске подршке. Специјалну захвалност дугујем Мариани Ферецаки, пријатељу и сараднику, за свакодневне дискусије које су ме обликовале у мирнију, разумнију и стрпљивију особу и научника као и за сву техничку помоћ коју ми је безрезервно пружала. Галини Глускер дугујем захвалност за њену искреност и лични пример изузетне снаге и интегритета који ми је постао модел научника коме тежим. Захваљујем се и Рејес Бабијано која ми је помогла да пратим сопствену интуицију и да се осамосталим и која ме је научила да не понављам експерименте на исти начин очекујући другачији резултат. Томасу Лунардију се специјално захваљујем на смесима које свакодневно изазива у лабораторији а Жералду Лосанту на томе што ме је увео у магичан свет ДНК репликације. На крају, захваљујем се Вариду Ахмеду за све сјајне дискусије о политици, човечанству и експериментима и за фантастичне критичке увиде у мој рад. Такође, желим да се захвалим мојим сарадницима Проф. Сулиани Манли и Др Кајлу Дагласу чији је допринос био круцијалан за успешну реализацију ове дисертације.

Захваљујем се Проф.Пјеру Гонзију, мом екстерном ментору, за подршку и критички приступ мом раду. Захвална сам и Проф. Сузан Гасер, Проф. Матијас Алтмајеру, Проф.Сулиани Манли и Проф. Гаелу Кристофарију што су прихватили да буду део комитета за одбрану докторске дисертације и што су били вољни да конструктивним саветима начине наш рад бољим.

Из мало личнијег угла, никада нећу моћи да се довољно захвалим својим родитељима Благоју и Валентини Ванчевској и мојој сестри Јовани Ванчевској који су ме подржавали у свим мојим лудим настојањима и давали ми довољно порстора да доносим самосталне одлуке. Речи нису довољне да опишу све што осећам према њима и заиста се надам да ћу једног дана достићи бар хиљадити део њихове моралне величине. Такође желим да се захвалим члановима моје В.Д. породице из Лозане, Стани и Драгану Ракићу што су учинили да се у овом граду осећам као код куће. Мојој цимерки, Вишвачи Трипати, желим да се захвалим што је била пуна разумевања за све моје недостатке. Др Александри Николић, мојој научној мајци, желим да се захвалим што ме је подржавала и обликовала ме у мом научном путовању. Огромну захвалност дугујем и Проф. Бати Кораћу, без чије дозволе да полажем последњи испит на факултету уопште не бих могла да похађам докторске студије. Мојој пријатељици, Тамари Спасојевић, се захваљујем што је била уз мене да делимо све лепоте одрастања и што смо заједно откривале тајне биологије и живота. Мојим пријатељицама са факултета (Лени Аризановић, Александри Ђурић, Сандри Булатовић, Ивани Угљеша и Ани Бољевић) желим да се захвалим што су ми улепшале тмурне факултетске дане и што су биле непрестана подршка чак и када сам ја губила веру у себе. За крај, желим да се захвалим Александру Салиму, мом веренику, животном сапутнику, пријатељу који је био ту да ми помогне да истрајем у свим унутрашњим и спољашњим ратовима и са ким је сваки дан вредан живљења.

У Лозани, 12. Октобра 2018. године

Abstract

Telomeres are dynamic nucleo-protein structures capping the ends of all eukaryotic chromosomes. Together with telomerase, they counteract replication-dependent telomere attrition. Additionally, they disguise the linear ends of the chromosome from the DNA damage response (DDR) machinery. Otherwise, the chromosome end would be recognized as a double strand break and would elicit a deleterious DDR signal. Both of these functions contribute greatly to the maintenance of genome stability. Telomeres are composed of long repetitive DNA sequences, protein complex dubbed shelterin and telomeric repeat-containing RNAs (TER-RAs). In addition to the core protein complex, other proteins are important for proper telomere structure and function. Our laboratory has a longstanding interest in the discovery of novel factors that have indispensable roles in telomere biology. For that purpose, previous lab members developed a Quantitative Telomeric Chromatin Isolation protocol (QTIP) and detected binding of two new proteins to long telomeres, SMCHD1 and LRIF1. Their function at telomeres is not yet described but they are shown to function in higher-order chromatin organization and genome-wide DDR. Understanding their role in telomere biology is important because the list of players involved in DDR at telomeres is far from complete and we know very little about how chromatin structure affects DDR activation. Thus, this thesis provides insights into the DDR at telomeres by studying the functions of SMCHD1 and LRIF1 and describes the implementation of a novel super-resolution microscopy-based method to study the role of these proteins and shelterins in early steps of the DDR.

Firstly, we describe crucial roles for SMCHD1 and LRIF1 in DDR activation at telomeres lacking shelterin protein TRF2. Removal of TRF2 leads to activation of the ATM kinase and elicits a DDR giving rise to persistent chromosome fusions. We show that LRIF1 and SMCHD1 removal leads to attenuation of ATM activation and subsequent DDR defect as well as impairment in classical non-homologous end joining (NHEJ) at unprotected telomeres. Considering that these phenotypes are rescued by removal of TPP1 and activation of the ATR kinase, we propose that these proteins mainly participate in DDR signaling operating at uncapped telomeres. They are among the rare ones described to act early in the DDR cascade upon TRF2 removal.

Stimulated by the discovery that SMCHD1 and LRIF1 function in X-chromosome compaction, we sought to test if they would function in remodeling telomeric chromatin. To do that, we have implemented super-resolution microscopy method (STORM) to measure sizes and shapes of normal human telomeres and ones lacking SMCHD, LRIF1, and shelterin proteins. We have shown, by examination of thousands of telomeres, that removal of shelterin proteins leads to decompaction of only a very small subset of telomeres. This decompaction does not seem to be required for efficient DDR activation, as the DDR was also efficiently elicited from compacted TRF2-depleted telomeres. Thus, we propose that DDR is triggered by changes at the molecular level in protein recruitment upon telomere deprotection. In addition, transient removal of SMCHD1 and LRIF1 did not affect the compaction state of telomeres as they do in the X-chromosome. Overall, we have described two novel factors that are important for DDR at uncapped telomeres and excluded the need for decompaction as the initial step of DDR activation.

Keywords

Telomere, DNA damage response, SMCHD1, LRIF1, STORM, telomere compaction, ATM kinase

Résumé

Les télomères sont des structures dynamiques, constituées à la fois d'acides nucléiques et de protéines. Ils sont présents aux extrémités des chromosomes chez tous les organismes eucaryotes. Ils jouent un rôle majeur dans le maintien de la stabilité génétique en limitant le raccourcissement des chromosomes lié à leur réplication et en empêchant l'activation de la machinerie de réparation de l'ADN, évitant ainsi les fusions chromosomiques. Les télomères consistent en de longues séquences répétées d'ADN, d'un complexe de protéines protectrices appelées "shelterins" ainsi que d'ARN contenant des répétitions télomériques (ou Telomeric repeats-containing RNA; TERRA). En outre, de nombreuses protéines sont importantes pour assurer l'organisation et la fonction des télomères. Notre laboratoire cherche à identifier et caractériser de nouveaux facteurs indispensables à la biologie des télomères. Grâce au développement d'une technique de biologie moléculaire particulière appelée QTIP (Quantitative Telomeric Chromatin Isolation Protocol), deux nouvelles protéines, SMCHD1 et LRIF1, ont été mise en évidence comme interagissant avec les télomères. Toutefois, leurs fonctions respectives restent inconnues. Mon travail de thèse apporte de nouvelles connaissances sur le rôle de ces protéines aux télomères en particulier lorsque ces derniers ne sont plus coiffés par des protéines protectrices telle que TRF2. De plus, j'ai développé une nouvelle méthode de microscopie à haute résolution qui permet d'étudier le rôle de ces nouvelles protéines et des shelterins dans la compaction des télomères.

Premièrement, je démontre le rôle fondamental de SMCHD1 et de LRIF1 dans l'activation de la machinerie de réparation de l'ADN aux télomères dépourvus de la protéine TRF2. Lorsque TRF2 est absente, la kinase ATM est activée ce qui induit la fusion systématique des extrémités chromosomiques suite à l'activation de la machinerie de réparation de l'ADN. En revanche, l'absence de SMCHD1 et de LRIF1 inhibe la réparation de l'ADN en réduisant l'activité de ATM et affecte la jonction d'extrémités non homologues (NHEJ). Dans ce contexte, la suppression de TPP1 permet de restaurer des mécanismes de réparation de l'ADN. Ainsi, je propose que SMCHD1 et de LRIF1 sont impliquées dans l'activation et/ou le recrutement d'ATM ou de protéines accessoires aux télomères non coiffés. Ces protéines font parties des rares associées aux premières étapes de la réponse aux dommages de l'ADN en l'absence de TRF2.

Motivés par la mise en évidence du rôle de SMCHD1 et de LRIF1 dans la condensation du chromosome X, nous avons testé leur implication dans le remodelage de l'ADN télomérique. Dans ce but, nous avons mise en place une technique de microscopie à haute résolution (STORM) afin de comparer la taille et la conformation de télomères humains en conditions normales et en l'absence de SMCHD1, de LRIF1 et de "shelterins". L'observation minutieuse de nombreux télomères a révélée l'état décondensé d'une petite portion des télomères dépourvus de TRF2. Cette décondensation n'est pas liée à une réponse efficace aux dommages de l'ADN puisque celle-ci est aussi optimale aux extrémités condensées. La machinerie de réparation de l'ADN serait plutôt enclenchée par des modifications de la quantité de protéines recrutées aux télomères non coiffés que par des changements de leur état de condensation. De plus, l'absence de SMCHD1 et de LRIF1 n'a pas d'effet sur l'état de condensation des télomères à la différence du chromosome X.

En résumé, nous avons caractérisé le rôle de deux nouveaux facteurs dans l'activation de la réponse aux dommages de l'ADN aux télomères non coiffés et avons démontré que la décondensation de l'ADN télomérique n'est pas requise pour initier cette dernière.

(Translated by Dr Marie Pierron)

Mots-clés

Télomère, réparation de l'ADN, SMCHD1, LRIF1, STORM, Télomère condensation, ATM

Contents

Acknowledgements	i
Захвалница	ii
Abstract	iii
Keywords	iii
Résumé	iv
Mots-clés	iv
Chapter 1 Introduction	1
1.1 Telomere structure and function.....	1
1.1.1 The end replication problem	1
1.1.2 The end protection problem	5
1.1.3 Transcription at telomeres	14
1.1.4 Telomere replication and replication stress.....	14
1.2 Functions of SMCHD1 and LRIF1	16
1.3 Aim of the thesis.....	19
Chapter 2 The telomeric DNA damage response occurs in the absence of chromatin decompaction	21
2.1 Abstract	21
2.2 Highlights	21
2.3 Author contributions	21
2.4 Apendix to Chapter 2.....	38
Chapter 3 SMCHD1 and LRIF1 promote ATM-dependent DNA Damage signaling and repair of uncapped telomeres	41
3.1 Abstract.....	41
3.2 Highlights	41
3.3 Author contributions	41
Chapter 4 Conclusions and perspectives	61
References	65
Curriculum vitae	78

Chapter 1 Introduction

1.1 Telomere structure and function

Although telomeres are found at chromosome ends it was clear very early that they play a central role in maintaining the stability of linear genomes. The term telomere (Greek. telos-end, meros-part) was coined in 1938 by a prolific researcher Herman Müller. In his studies of X-ray induced DNA-breaks, he noticed that the ends of the chromosomes were similar to a protective cap never susceptible to changes such as inversions or deletions (Müller, Hermann, 1938). Around the same time, Barbara McClintock performed seminal experiments in maize also using X-ray irradiation and the observable variegation in color of maize kernels to ask what the fate of broken chromosomes is. She observed that depending on where the break occurs, broken chromosomes could initiate a repeated breakage-fusion-breakage cycle or be stabilized and propagated. The stabilization of broken ends was especially observable in the germline, although it happened in the endosperm with low frequency (McClintock, 1939, 1941). These early experiments had been the basis for defining what we now call the end protection problem. How the ends perform their protective function remained an enigma until the molecular structure of the chromosome end was cracked. Another puzzle that intrigued researchers interested in DNA metabolism in the 1970's was how the end of the chromosome was replicated. Leonard Hayflick observed that somatic cells when cultured have limited replication potential and stop dividing after approximately 50 divisions (Hayflick, 1965). This phenomenon is now known as Hayflick limit or replicative senescence. To explain this observation Russian theoretical biologist Olovnikov proposed a theory of marginotomy (Olovnikov, 1971). He suggested that due to imperfection in the replication machinery the ends of the DNA template would shorten with each replication cycle. He envisioned two possible mechanisms for this shortening. One is that the DNA polymerase used for replication would have a catalytically inactive zone so that the terminal template segment lying in this dead zone would not be replicated. Another takes into account the requirement of some polymerases to use an RNA primer and that the final replica will be shorter for the length of that primer (Olovnikov, 1973). The latter theory was further developed by James Watson and formulated as what we know today to be the end replication problem (Watson, 1972). Interestingly, Olovnikov proposed that with each division the end genes (he called them "telogenes") will be shortened and that these end genes will have a special feature to enable them to be used as "buffers" and be sacrificed without consequences during successive mitoses. Although these two problems related to telomere biology were postulated very early in the scientific journey through the ends of linear chromosomes, there was no mechanistic explanation how these problems are solved by the cells. As many things related to genome biology answers to these questions came primarily from knowing the DNA sequence of chromosome ends. The following chapters will dive into the experiments that enabled us to explain how telomeres solve the end protection and the end replication problem.

1.1.1 The end replication problem

The nature of the end replication problem became apparent when we learned that replicative DNA polymerases can synthesize DNA in the 5' to 3' direction and that they require a free 3'-OH group stemming from an RNA primer to initiate synthesis. As explained in Figure 1, due to the inherent imperfections of the replication machinery, the synthesis can't be initiated *de novo*, and after the completion of semi-conservative replication the terminal RNA primer is removed. This leads to the formation of a gap at the 5' end and loss of DNA sequence. The emergence of this problem prompted scientists to infer that there might be specialized factors dedicated to solve this difficulty. But to fish out these factors the nature of the "telogene" had to be understood. By using an inhabitant of freshwater ponds *Tetrahymena thermophila*, Elizabeth Blackburn was able to derive the terminal sequence flanking the extrachromosomal palindromic rDNAs. She found that the sequence was 5'-TTGGGG-3', but most surprisingly she observed that this sequence was tandemly repeated between 20 and 70 times and seen as a heterogeneous smear of fragments on agarose gels (Blackburn and Gall, 1978). This turned out to be a general feature of telomeres conserved throughout the tree of life with few

exceptions (such as in *Drosophila melanogaster* (Pardue et al., 1996)) suggesting that this might be an ancestral mechanism for the stabilization of linear genomes. Addition of this sequence to yeast artificial chromosome DNA (YAC) stabilized this DNA after transformation and allowed for isolation of the yeast telomere sequence. But interestingly, over time the *Tetrahymena* sequence was extended by the addition of yeast telomeric sequence, opposite of what the end replication problem model was predicting (Shampay et al., 1984; Szostak and Blackburn, 1982; Walmsley et al., 1984). This led the authors to propose that there might be some enzyme with a terminal-transferase activity that would be capable of *de novo* nucleotide addition to the chromosome ends. The fraction with enzyme activity was isolated by Carol Greider and the enzyme turned out to be a specialized ribonucleoprotein complex called telomerase (Greider and Blackburn, 1985). Ciliated organisms proved to be a great model organism to isolate this enzyme because they contain an unusually large number of chromosomes and are abundant in telomerase (reviewed in Prescott, 1994). Telomerase core that catalyzes the addition of new telomeric sequence consists of an RNA moiety that is used as a template and protein subunit that catalyzes the formation of the phosphodiester bond (Greider and Blackburn, 1987; Pfeiffer and Lingner, 2013).

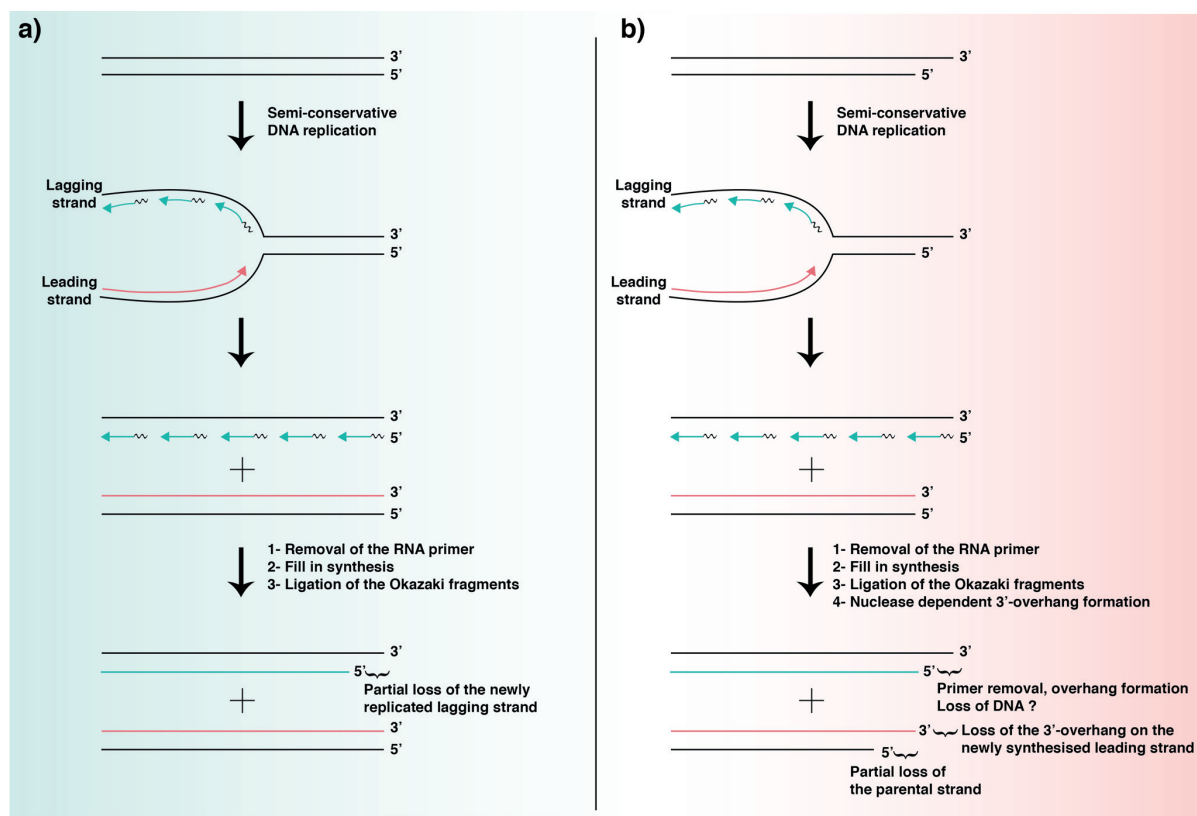


Figure 1. The end replication problem. A) The model for the end replication problem proposed by James Watson. The leading strand (pink line) is continuously synthesized by DNA polymerase in 5' to 3' direction. The lagging strand (cyan lines) is discontinuous and is synthesized by the formation of Okazaki fragments with an RNA primer at the beginning of each (wavy black line). The lagging strand is then processed by removal of the RNA primers, DNA polymerase-alpha primase dependent fill in and ligation. This process leads to removal of the terminal RNA primer and the emergence of a gap at the position of the primer. The final result is a partial loss of DNA sequence in the newly synthesized lagging strand. B) The revised model for the end replication problem that takes into account that telomers end in a 3'-overhang. This model predicts that the end replication problem is not a problem of the lagging strand but the leading strand due to nuclease dependent formation of the 3'-overhang. Telomeric sequence is lost from the 5' of the parental strand after nuclease processing. (Image is adapted from Larissa Grolimund thesis [10.5075/epfl-thesis-6022](https://doi.org/10.5075/epfl-thesis-6022); Lingner et al., 1995)

After the discovery of telomerase and understanding of the basic structure, the main question became what the mechanism of telomerase action is. In the search for the mechanism, other conserved features of the telomeres themselves became apparent. Telomeres were shown to end in a G-rich overhang at their 3' end, in contrast to the belief that the chromosome ends are blunted (Henderson and Blackburn, 1989; Klobutcher et al., 1981). This overhang was shown to be crucial for the extension of telomeres and a preferred substrate for telomerase (Lingner and Cech, 1996). A revised model of the end replication problem that incorporates this new finding was proposed. In this model, the telomere shortening is a problem of the leading strand due to blunting of the end after replication. This blunt end would be processed by nucleases and part of the parental C-rich strand would be lost. For the lagging strand it is uncertain if the processing includes simply RNA primer removal or some additional steps (Lingner et al., 1995). The traditional and the revised model of the end replication problem are shown in Figure 1.

1.1.1.1 *Telomerase structure*

In spite of the fact that telomerase RNA was isolated shortly after telomerase activity was detected in the cell free *T. thermophila* extracts (Greider and Blackburn, 1989), isolation of the catalytic subunit was challenging. The first essential protein coding gene whose dysfunction lead to an ever shorter telomeres (*est*) phenotype was identified in *Saccharomyces cerevisiae* (Lundblad and Szostak, 1989), after which a total of four EST genes were shown to exist (Lendvay et al., 1996). Affinity purification of telomerase from the ciliate *Euplotes aediculatus* lead to the identification of the core catalytic subunit of telomerase. This organism is a very distant ciliate from *T. thermophila* but it contains hundreds of times more DNA molecules and therefore higher amount of telomerase molecules (Lingner and Cech, 1996). Notably, this study prefaced the discovery that the p123 is the core catalytic subunit of telomerase and that it is a reverse transcriptase phylogenetically related to those found in retroviruses (Lingner et al., 1997). In addition, this protein was homologous to the Est2 protein identified in *S. cerevisiae* and the homologs of telomerase in human and *Saccharomyces pombe* were also identified (Nakamura et al., 1997), suggesting that this is another highly conserved component in telomere biology.

Today we know that human telomerase reverse transcriptase (hTERT) protein is characterized by three main domains. The reverse transcriptase domain was already discussed and it contains palm, fingers and thumb subdomains with conserved aspartate required for catalysis (Lingner et al., 1997). TERT RNA binding domain (TRBD) is required for binding of the telomerase RNA component and the telomerase essential N-terminal domain (TEN) is proposed to stabilize the ssDNA:RNA hybrid used as the substrate for catalysis (Akiyama et al., 2015; Lue, 2005). Although this core is sufficient for *in vitro* function of telomerase, proper physiological function is maintained by association with accessory factors such as Dyskerin, NHP2, NOP10 and TCAB1. These proteins are required for recruitment of telomerase to telomeres, maturation of the RNP particle, and stimulation of telomerase activity (Cohen et al., 2007; Cristofari et al., 2007; Freund et al., 2014; Venteicher et al., 2009). Telomerase RNA (hTR) has two important functions: to provide the template for telomere synthesis and to act as a scaffold for binding of the TERT subunit and accessory proteins. The RNA components of telomerase are divergent in sequence across species but key structural elements are conserved (Lin et al., 2004). These include the pseudoknot/template (PK/T) domain folded into a triple helical structure and essential for interaction with TERT, catalysis and positioning the template into the active site (Cash and Feigon, 2017; Qiao and Cech, 2008) and a three-way junction element (CR4/5 domain) also essential for TERT binding catalysis (Mitchell and Collins, 2000). Human TR involves a non-conserved third element, the small Cajal body (*sca*) domain required for binding of dyskerin (the H/ACA subdomain) and the Cajal body box (CAB) subdomain required for mediation of telomerase trafficking to Cajal bodies where maturation of the enzyme occurs (Chen et al., 2018; Cristofari et al., 2007; Jády et al., 2004; Venteicher et al., 2009; Zhu et al., 2004). The major components of telomerase are outlined in Figure 3a. Telomerase possesses a unique ability to realign with the same DNA substrate after addition of the first telomeric repeat and continue the synthesis. The proclivity of telomerase to continuously add several repeats to the growing DNA chain is referred to as Repeat Addition Processivity (Parks and Stone, 2014).

1.1.1.2 *Consequences of telomerase malfunction*

In his premonitory theoretical paper Olovnikov proposed “It seems quite expedient to search for cellular factors controlling the mechanisms of marginotomy and antimarginotomy in template synthesis of polynucleotides, which might repress or derepress, correspondingly, genes determining monosegment DNA-polymerase and tandem-DNA-polymerase or other means of antimarginotomy. Such factors (“marginotomites” and “antimarginotomites”) would, probably, regulate the duration of life of different cell clones and of the organisms which are composed of them.” And “Tandem-DNA-polymerases are present in cells capable of unlimited division, for example, in tumor cells, in permanent cell lines, in stem cells, in germ cells, and in some other cases.” These two excerpts illustrate the importance of telomerase (an “antimarginotomy” factor) in regulating cellular lifespan. Early experiments have shown that improper telomere maintenance leads to senescence (Yu et al., 1990). The latter statement was experimentally confirmed by detecting elevated telomerase activity in highly replicating and cancerous cell lines and tissues (Kim et al., 1994) and when the human telomerase protein sequence was discovered increased expression of TERT was observed in a human cancer cell line (Nakamura et al., 1997). Introduction of telomerase in cultured epithelial cells lead to increased replicative potential rendering them immortal (Bodnar et al., 1998). Thus, limitation of the cellular lifespan is thought to be a major tumor suppressing mechanism. Majority of human cancers require telomerase for survival and telomerase reactivation is a hallmark of cancer (reviewed in Hanahan and Weinberg, 2000). In addition, when telomerase is inactivated, other pathways may arise to circumvent the problem of telomere maintenance, as was first shown in bakers yeast (Lundblad and Blackburn, 1993). A small percentage of cancers (about 12-14%) is telomerase negative and depends on a recombination based Alternative Lengthening of Telomeres (ALT) pathway (Bryan et al., 1997). This discovery suggested that there might be more than one way to go about the end replication problem. The exact mechanisms by which the ALT pathway operates are largely unclear but the initial observation that a tag inserted into the telomere can be copied to multiple other telomeres in telomerase negative cells suggested that the ALT occurs via homologous recombination (Dunham et al., 2000). Furthermore, association of telomeres with HR proteins (including Rad51, Rad52, BRCA1, MRN complex, BLM, SLX4) in ALT cells strengthens this model and suggests that telomeres are copied from sister chromatids by a sequence of typical HR events such as strand invasion, polymerization, and resolution of the HR intermediate structures (reviewed in Pickett and Reddel, 2015). Hallmarks of ALT cancer cells are recombination-based telomere lengthening mechanism, high telomere length heterogeneity, high level of telomere sister chromatid exchanges (t-SCE), association of telomeres with promyelocytic leukemia (PML) bodies, increased levels of extrachromosomal telomeric repeat DNA (ECTRs), disrupted structure of the telomeric chromatin, and frequent loss of chromatin modifiers ATRX and DAXX (reviewed in Dilley and Greenberg, 2015). Understanding these specificities of ALT cancers allowed for investigation of the occurrence frequencies of ALT positive cancers in patient cohorts and opened new avenues for exploring therapeutic targets that would specifically eliminate cancer cells by disrupting a crucial mechanism required for autonomous cell survival.

In the same way that telomerase hyperactivity if not regulated can be detrimental to the normal functioning of an organism, malfunction in telomerase and its accessory subunits as well as telomere binding proteins can give rise to several human diseases. These are called telomeropathies and include dyskeratosis congenita (DC), Coats plus, the Werner syndrome, ICF (immunodeficiency, centromeric instability, facial anomalies) syndrome, Idiopathic pulmonary fibrosis and Bloom’s syndrome (reviewed in Lansdorp, 2009; Townsley et al., 2014).

1.1.1.3 *Telomerase regulation mechanisms*

Because of the fact that both overly active and impaired telomerase can have pathological impact it is clear that its action has to be tightly regulated. The expression of telomerase is restricted to embryonic and highly proliferative tissues (Wright et al., 1996) by transcriptional repression of the hTERT gene (Cong et al., 1999, 2002) while hTR remains ubiquitously expressed. Telomerase should act at telomeres only in the S-phase of the cell cycle and it has been shown that during interphase it is confined to specialized nuclear

structures called Cajal bodies (Jády et al., 2006; Tomlinson et al., 2006). Upon maturation in Cajal bodies telomerase has to be recruited to telomeres through interaction with the TEL-patch domain of TPP1 (Abreu et al., 2010; Nandakumar et al., 2012; Sexton et al., 2014). Although the ssDNA binding telomeric protein Protection of Telomeres 1 (POT1) inhibits telomerase *in vitro* by binding to telomerase substrate (Kelleher et al., 2005; Lei et al., 2005), in association with TPP1 it increases telomerase repeat processivity several fold *in vivo* (Latrick and Cech, 2010; Wang et al., 2007). One of the negative regulators of telomerase action at telomeres is the trimeric protein complex CST (CTC1-STN1-TEN1). This complex binds at the end of S-phase and it is thought to bind at already extended telomeres to ensure that only one extension event per telomere would occur (Chen et al., 2012). Therefore, it acts as a terminator of telomerase activity. Lastly, the telomere itself is a regulator of telomerase activity. Human telomeric proteins TRF1 and TRF2 are the negative regulators of telomerase *in cis* by providing a counting mechanism similar to the one described for the yeast telomeric protein Rap1 (Marcand et al., 1997; Smogorzewska et al., 2000). It has been observed that telomere length in different organisms and telomerase-positive cell lines is maintained in a very limited range. The telomere length homeostasis is a balance point between telomere elongation and telomere shortening events. Until recently, we thought the only shortening event that was happening at the telomere was passive attrition due to the end replication problem. But a new protein called Telomeric Zinc Finger Associated Protein (TZAP) was discovered to bind to over elongated telomeres when the density of the shelterin proteins is lowered (Grolimund et al., 2013). The binding of TZAP unlocks an active trimming pathway to prevent accumulation of aberrantly long telomeres (Li et al., 2017). A summary of how different telomere proteins regulate telomerase is depicted in Figure 5a.

Although discovery and cloning of human telomerase components were fueled simply by interest in basic biological questions, they have accelerated discovery in basic research by providing valuable tools for scientists and have a tremendous impact on understanding human physiology and pathology.

1.1.2 The end protection problem

1.1.2.1 Introduction to mammalian DNA damage response pathways

Deoxyribonucleic acid (DNA) is an extremely stable molecule and it is possibly for that stability, among other things, that it was selected during evolution to be the carrier of genetic information. Despite that, different kinds of chemical and physical stresses are constantly threatening to affect the integrity of DNA and therefore pose a threat to faithful information transfer through generations. To cope with this, cells have evolved a highly coordinated network of molecular interactions collectively called DNA damage response (DDR) and repair signaling pathways. This network involves the ability of cells to sense DNA lesions, to signal and transduce the information to effectors involved in repair, to block cell cycle progression and to eliminate cells with unreparable lesions (Figure 2). The importance of DDR mechanisms is highlighted by the fact that mutations in some of the components of the pathway cause genomic instability which is the basis of several different congenital diseases and hallmark of virtually all types of cancer (reviewed in Jackson and Bartek, 2009).

The major operators of the DDR signaling networks in eukaryotes are three kinases that belong to the Phosphatidylinositol-3 kinase-related kinases (PIKKs). This family of kinases responds to different kinds of cellular stresses including DNA damage (reviewed in Lempiäinen and Halazonetis, 2009; Lovejoy and Cortez, 2009). The family includes ATM (Ataxia-telangiectasia mutated), ATR (ATM- and Rad3-related) and DNA-PKcs (DNA-dependent protein kinase), among others. In response to various types of DNA damage ATM and ATR phosphorylate thousands of substrates important for DNA repair or signaling at conserved serine and threonine residues followed by Gln (SQ/TQ motifs), while DNA-PKcs have a more modest range of interactors and are required for Non Homologous End Joining (NHEJ) (reviewed in Bakkenist and Kastan, 2004). In addition, they start the second cascade of phosphorylation events through activation of Chk1 (ATR-dependent), Chk2 (ATM-dependent) and MK2 protein kinases (Liu et al., 2000; Matsuoka et al., 1998; Reinhardt et al., 2007). This leads to delayed cell cycle progression via destabilizing phosphorylation of Cdc25A phosphatase required to remove inhibitory phosphate groups from Cyclin Dependent Kinases (CDKs) (Mailand et al., 2000; Sanchez

et al., 1997). Although ATM and ATR phosphorylation networks overlap to some extent, these two kinases act in distinct contexts and are activated by different types of DNA lesions (reviewed in Marechal and Zou, 2013).

ATM kinase is activated at sites of double strand breaks (DSB) (reviewed in Marechal and Zou, 2013; Shiloh and Ziv, 2013). Double strand break lesions occur when both strands of the DNA molecule are simultaneously broken at proximal sites in the backbone. These lesions can arise as direct consequence of telomere uncapping, physical damage (such as γ -irradiation) and damage induced by chemicals or indirectly when DNA replication machinery encounters another lesion.

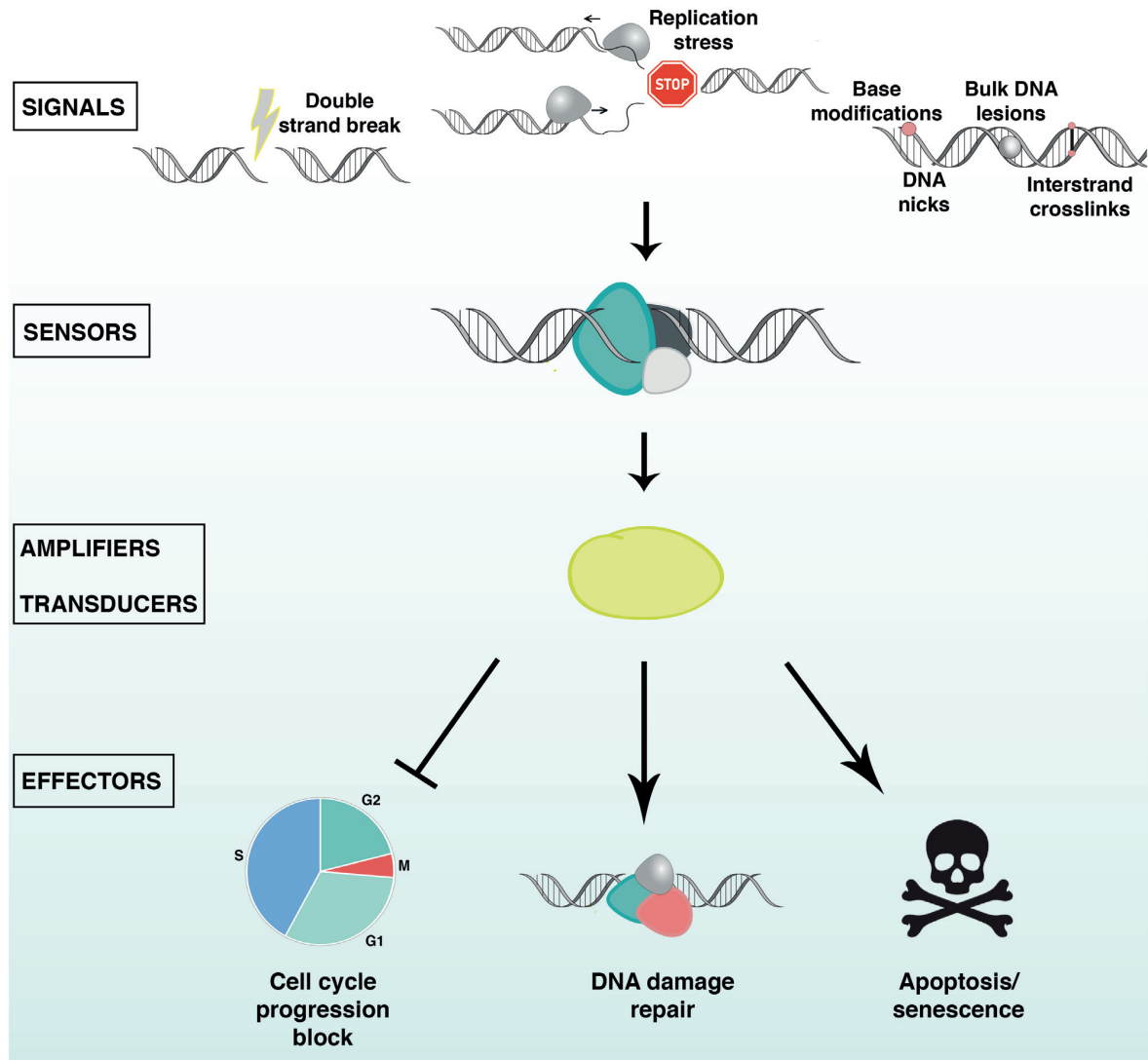


Figure 2. Generalized scheme of the DNA damage response signal-transduction cascade.

Different types of genotoxic lesions that are primary signals for DNA damage response activation are depicted under signals (double strand DNA breaks, replication stress and ssDNA lesions, base modifications, bulky DNA lesions, DNA nicks and interstrand crosslinks). These signals are recognized by dedicated sensory molecules that have specificity for a certain type of lesion. After the lesion is sensed molecules that transfer the information about the occurrence of a problem and locally amplify the signal are recruited and activated. The signal is transferred to effector molecules that will act to repair the lesion, to ones that will block the cell cycle progression until the repair happens, and in case of a prolonged and unresolved problem to molecules that will eventually lead the cell into senescence or apoptosis.

If not repaired correctly they can have deleterious consequences such as chromosome translocations or loss of chromosome parts and start a vicious cycle of breakage-fusion-breakage ultimately leading to tumorigenesis or cell death (McClintock, 1939). Interestingly, there are certain physiological processes that require orchestrated double strand break induction as part of their mechanism of action. These include the meiotic recombination events, where DSBs are required to initiate crossing over and V(D)J and class switch recombination pathways which are important for the generation of B- and T- receptor variability in the cells of the immune system (reviewed in Lukaszewicz et al., 2018). The first responder at DSBs is the MRN (Mre11-NBS1-RAD50) complex and thus it acts as a sensor for this type of lesions. Purified MRN complex binds directly to DSBs with nanomolar affinity (Lee and Paull, 2004, 2005; Lee et al., 2003). The exact mechanism of ATM activation by MRN is not fully understood. ATM under normal conditions exists as an inactive dimer and upon MRN binding to dsDNA ATM is autophosphorylated at S-1981 which leads to monomerization. In the initial *in vitro* experiments activation of ATM by MRN requires free dsDNA ends or ds ends with short ss-overhangs and is stimulated in DNA length-dependent manner (Lee and Paull, 2005; Shiotani and Zou, 2009). Within the complex, MRE11 binds to the DNA end and also interacts with ATM, and NBS1 interacts with ATM through its C-terminal domain. How the signal is transmitted through this molecular network is unclear but DNA-binding dependent conformational changes might provide one explanation (Falck et al., 2005; Schiller et al., 2012). ATM recruitment and activation might also be chromatin context dependent. Although ATM knock out in human cells is not lethal, upon DSB induction only about 20% of the breaks are dependent on ATM for repair. These breaks are occurring in the context of heterochromatin where ATM might be activated by Tip60 dependent acetylation (Sun et al., 2005). Heterochromatin DSBs are repaired much slower than ones occurring in euchromatin due to the increased complexity of the chromatin surrounding the break. Upon ATM activation in heterochromatin, ATM phosphorylates Krüppel-associated box (KRAB)-associated protein (KAP1) which aids in dissociation of Heterochromatin Protein 1 (HP1) and consequent exposure of H3K9me3 histone mark which acts as a substrate for Tip60 binding. This creates a positive feedback loop and enables maximal ATM activation (Ayoub et al., 2008; Bolderson et al., 2012; Goodarzi et al., 2008a; Noon et al., 2010). ATM activation unleashes a cascade of events at the chromatin site of the DSB and within the nucleus to regulate proper DNA repair and checkpoint activation (Figure 3a). At the chromatin side, first substrate of ATM is a histone variant H2AX that is phosphorylated at S-139 and is referred to as γ -H2AX (Rogakou et al., 1998). This form of H2AX is recognized by the BRCT domain of Mediator of DNA damage Checkpoint 1 (MDC1) and this binding promotes further H2AX phosphorylation through direct interaction with ATM and interaction with NBS1. This allows the spreading of DNA damage signal sometimes even hundreds of kilobases away from the original site of the DSB (Meier et al., 2007). MDC1 bound to chromatin and phosphorylated by ATM is recognized by E3 ubiquitin ligase RING Finger 8 (RNF8) which ubiquitylates H2AX/ γ H2AX. This is further recognized by another E3 ubiquitin ligase RING Finger 168 (RNF168) and these chains serve as docking molecules for other repair proteins such as 53BP1 and BRCA1. Synchronous accumulation of MDC1, RNF8, RNF168 and 53BP1 is readily detectable in cytological experiments as appearance of DNA damage induced foci or irradiation induced foci (IRIF) (Doil et al., 2009; Huen et al., 2007; Kolas et al., 2007; Lukas et al., 2011; Mailand et al., 2007; Mattioli et al., 2012; Moudry et al., 2012). The exact role of IRIFs was unclear because deletion of H2AX and inability to form IRIFs did not lead to increased DDR sensitivity, did not affect DDR signaling by ATM and genome stability. Only recently through work on telomeres and on V(D)J recombination it has been understood that these foci, specifically 53BP1 binding, are required for chromatin mobility at the site of DSBs. Increased mobility enhances the chances of finding the appropriate end for DNA repair to occur efficiently (Difilippantonio et al., 2008; Dimitrova and de Lange, 2006a; Dion et al., 2012; Lotterberger et al., 2015). After the DNA damage signal has been transduced and all the necessary signaling factors recruited, the DNA break can be repaired by one of two major DNA repair mechanisms, NHEJ or Homology directed Repair (HR). Classical NHEJ is mediated by the Ku70/Ku80 complex required to physically keep separated DNA ends together and recruit the XRCC4- XLF- Ligase 4 complex, DNA PKcs, and accessory proteins to mend the broken ends. Interestingly, a strict inhibition of the c-NHEJ pathway during mitosis is mediated by inhibitory phosphorylation of the E3 ubiquitin ligase RNF8 by CDK1 kinase, in order to prevent aberrant sister telomere fusions (Orthwein et al., 2014). Several alternative NHEJ mechanisms that do not depend on the Ligase 4 complex have been

described and they are dependent on the existence of short microhomology domains for repair to occur (reviewed in Hustedt and Durocher, 2017). Homologous recombination, on the other hand, requires a template sequence for repair and therefore its action is restricted to S/G2 phases of the cell cycle. For the DNA to be able to find a homologous sequence a resection process dependent on CtIP, Exo1, and Dna2 leads to a formation of a long 3' overhang that is used for homology search and invasion (Sartori et al., 2007; Takeda et al., 2007; Tomimatsu et al., 2012; Wawrousek et al., 2010). Pathway choice between these two types of repair is under regulation by the recently discovered 53BP1-Rif1-Rev7-Shld-CST molecular network (Barazas et al., 2018; Dev et al., 2018; Ghezraoui et al., 2018; Gupta et al., 2018; Mirman et al., 2018; Noordermeer et al., 2018). Initial experiments investigating the early steps of the DDR signaling cascade have established that chromatin modifications at DSBs and subsequent binding of 53BP1 are pivotal for limiting resection by counteracting the action of beforementioned nucleases via unknown mechanisms. Interestingly, it became clear that 53BP1 and BRCA1, an HR protein frequently mutated in breast cancers, act in opposing ways in control of end resection as the embryonic lethality, tumor predisposition and HR defects in BRCA1-null mouse models were efficiently rescued by 53BP1 removal (Bouwman et al., 2010; Bunting et al., 2010; Cao et al., 2009). These findings are even more important in the light of the seminal studies that have revealed that BRCA1/BRCA2 deficient cancer cells are sensitive to treatment with Poly(ADP)-ribose polymerase (PARP) inhibitors (Bryant et al., 2005; Farmer et al., 2005) and that 53BP1 loss can confer resistance to this treatment. Further investigation revealed two additional factors acting downstream of 53BP1 to prevent DNA end resection, Rif1 and Rev7 (MAD2L2) acting in response to DNA damaging agents, at uncapped telomeres and in the physiological process of class switch recombination (Boersma et al., 2015; Chapman et al., 2013; Xu et al., 2015; Zimmermann et al., 2013). By studying the interactomes of 53BP1 and Rev7 (Ghezraoui et al., 2018; Gupta et al., 2018) and by synthetic lethal CRISPR-based genetic screens in BRCA1 deficient cells treated with PARP inhibitors (Barazas et al., 2018; Dev et al., 2018; Noordermeer et al., 2018) additional proteins c20orf196 (Shld1), FAM35A (Shld2), and CTC-534A2.2 (Shld3), collectively called the shieldin complex, were discovered. Loss of the components of the shieldin complex phenocopied the loss of 53BP1 and resulted in defective class switch recombination, conferred PARP inhibitor resistance in BRCA-deficient cells and decreased the frequency of telomere fusions upon uncapping. Biochemical analysis of the shieldin complex revealed that shieldin components are the missing link connecting Rif1 to Rev7, specifically that Shld3 interacts with Rif1 and Shld2, which in turn interacts with Rev7 and Shld1 (Gupta et al., 2018). Additionally, Shld2 has an OB-fold domain through which it can bind ssDNA thus providing a bridge between chromatin and ssDNA at DSB sites. As the complex doesn't possess intrinsic enzymatic activity the mechanism by which it prevents resection was still unclear. Considering that telomeres are a good model to study pathway choice, Mirman Z. and colleagues set out to investigate whether active fill in rather than nuclease inhibition was responsible for preventing extensive resection genome wide, similarly to the telomeric mechanism of 3'-overhang maintenance. At telomeres, the CST complex recruits polymerase α -primase for fill-in synthesis of resected 3'-overhangs and, interestingly, Rev7 and shieldin removal also lead to increased resection at uncapped telomeres. On the other hand, the CST complex was epistatic with shieldin for 3'-overhang maintenance and was recruited to sites of DSBs in Rev7-Shld dependent manner, and yeast-two hybrid screens revealed that the two complexes interact through multiple direct interactions. In addition, polymerase α -primase was also recruited to damaged DNA and its activity was required for radial chromosome formation in BRCA1 deficient cells treated with PARP inhibitors suggesting that indeed the CST- polymerase α -primase complex actively counteracts DNA end resection by continuous fill-in synthesis (Mirman et al., 2018). To completely corroborate this model, additional experiments that aim to detect the polymerase α -primase driven DNA synthesis need to be performed (reviewed in Greenberg, 2018). These groundbreaking studies have deepened our understanding of how cells make the choice which pathway will be employed to resolve an emergent DSB and more importantly identified novel factors that might affect and contribute to resistance of cancers treated with PARP inhibitors enabling thus tools for better stratification of cancer types in the clinic.

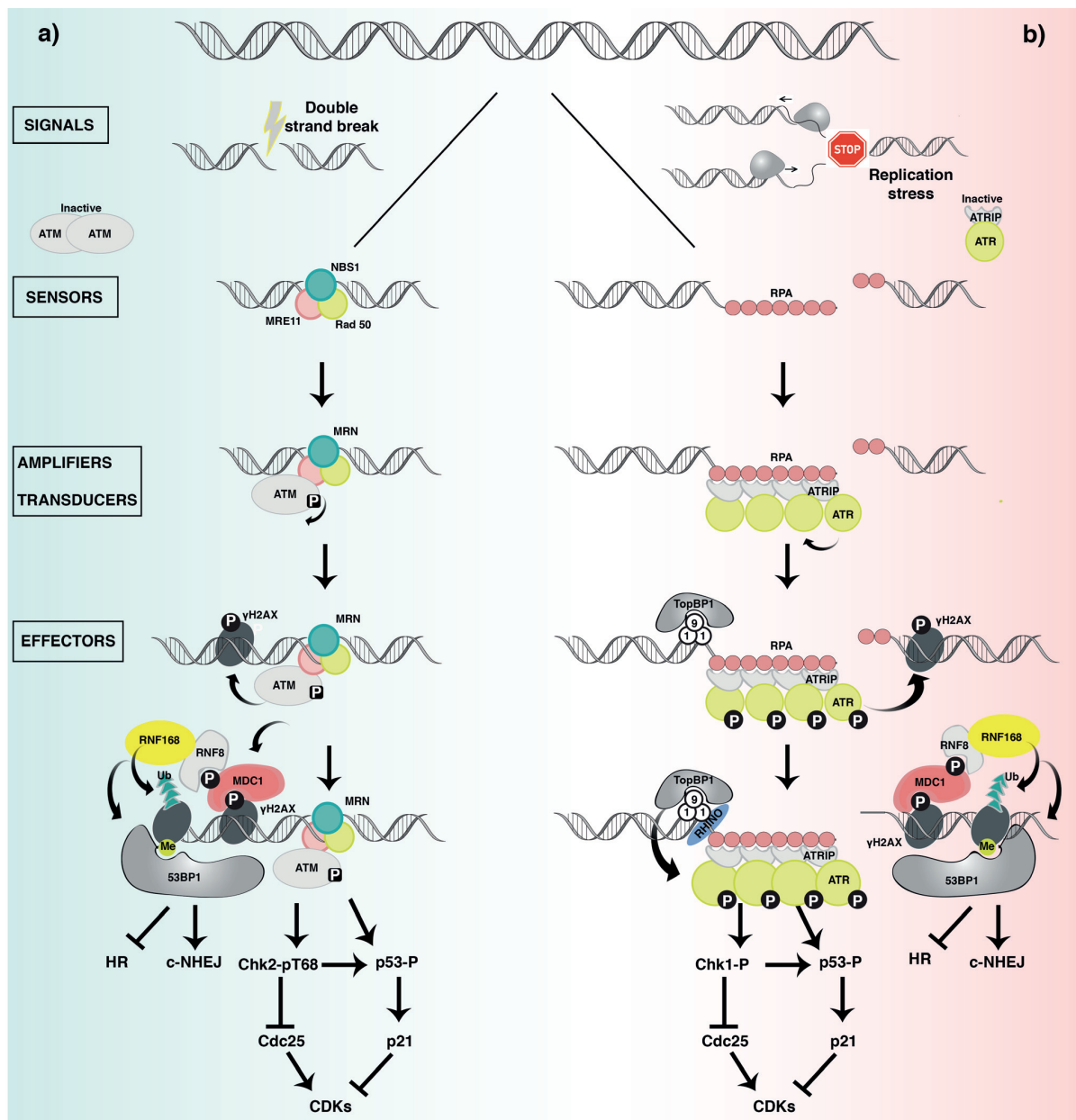


Figure 3. Genome wide DNA damage response to double stranded DNA breaks and ssDNA gaps.

A) Schematic depicting cascade of events upon the occurrence of double stranded DNA break. The break is sensed by a trimeric protein complex MRN (Mre11, Rad50, NBS1). Upon MRN binding, PIKK3 kinase ATM is brought to the double strand break (DSB) and activated by interaction with MRE11. After binding to MRN, ATM is autophosphorylated at S1981 and this leads to dissociation of the inactive homodimer. ATM then transduces the signal locally at the chromatin level leading to the formation of Ionizing Radiation Induced Foci (IRIFs) and to downstream effectors such as CHK2 and p53 through a cascade of phosphorylation and ubiquitination events. The final result is cell cycle progression block. B) Schematic depicting cascade of events when ssDNA region is exposed because of e.g. replication stress. The lesion is sensed by ssDNA binding protein RPA. Binding of several RPA molecules leads to recruitment of the ATR-ATRIP complex. Upon binding ATR phosphorylates itself *in trans* and this leads to recruitment of downstream effectors. In addition, RPA-ssDNA promotes loading of the Rad9-Hus1-Rad1 (9-1-1) complex at the junction between ss and dsDNA. This recruits TopBP1 by interaction with phosphorylated Rad9 and leads to full-blown ATR activity. This multistep process ensures that ATR is activated only when two different features (ssDNA and ssDNA-dsDNA junction) are present and is not aberrantly activated by any ssDNA present in the cell. (Image is adapted from Marechal and Zou, 2013; Palm and de Lange, 2008).

ATR kinase is activated by a variety of different lesions and it took some time to discover what was the common molecular determinant for all of them. Unlike ATM, loss of ATR is embryonically lethal in mouse cells and lethal in cultured human cell lines (Brown and Baltimore, 2000, 2003; Cortez et al., 2001; de Klein et al., 2000). Today we know that this lethality likely stems from the essential role of ATR in DNA replication surveillance mechanisms. Major downstream substrates of ATR in addition to Chk1 and other effector kinases include proteins that are present at DNA replication origins and replication forks in order to regulate the stability of replication forks and to ensure faithful genome duplication (reviewed in Saldivar et al., 2017). The common denominator of DNA lesions at damaged or stalled replication forks, lesions stemming from DNA interstrand crosslink, DNA mismatch repair and base excision repair is generation of a long stretch of ssDNA that can be coated by a heterotrimeric protein complex collectively called Replication Protein A (RPA). This complex is composed of three subunits RPA32-RPA70-RPA14 which bind tightly (app. 10^{-9} - 10^{-10} M affinity) to ssDNA with defined 5'-3' polarity through their oligonucleotide/oligosaccharide-binding (OB) fold domains (reviewed in Maréchal and Zou, 2015). Therefore, RPA is a sensory molecule for DNA lesions that include a long patch ssDNA intermediate. Upon binding of a sufficient number of RPA molecules, an obligate ATR and ATR Interacting Protein (ATRIP) complex is recruited to the site of the lesion through direct interaction of ATRIP with RPA (Zou, 2003). When bound to RPA through ATRIP, ATR is activated by autophosphorylation *in trans* at T-1989. This step is necessary but not sufficient for maximal ATR activation as there are several layers of control for full-blown ATR signaling response (Figure 3b). The lesion is also bound at the ssDNA-dsDNA junction by Rad17-RFC2-5 clamp loader and with assistance from RPA they recruit the Rad9- Hus1-Rad1 (9-1-1) complex through interaction with Rad17 (Ellison and Stillman, 2003; Lee and Dunphy, 2010). ATR then phosphorylates the components of the 9-1-1 complex and phosphorylation of Rad9 and phosphorylation independent recruitment of RHINO engage TOPoisomerase Binding Protein 1 (TopBP1) at the site of the break (Cotta-Ramusino et al., 2011; Delacroix et al., 2007; Lee and Dunphy, 2010). TopBP1 binds the autophosphorylated site of ATR strengthening its association with the site of the lesion and stimulates its activity (Liu et al., 2011; Nam et al., 2011). This multistep fail-safe mechanism of ATR activation ensures that the activation occurs only in the presence of ssDNA and ssDNA-dsDNA junctions and not anytime RPA encounters ssDNA within the cell. ATR and ATM dependent DNA damage responses are not completely mutually restrictive but there is a certain amount of crosstalk between the two kinases both directly through phosphorylation of each other or through phosphorylation of mutual targets such as H2AX (Stiff et al., 2006). They can also influence the localization of each other by phosphorylating chromatin targets and regulating resection at the DSBs (Jazayeri et al., 2006; Myers and Cortez, 2006). This may provide certain redundancy during the DNA damage signaling cascade to ensure proper repair of the lesion and can lead to greater amplification of the signal at unrepairable sites.

1.1.2.2 Latest view on mammalian chromosome ends

Mammalian telomeres are composed of long arrays of 5'-TTAGGG-3' tandem repeats that protrude in a 50-300 bp long 3'-overhang (Henderson and Blackburn, 1989; Moyzis et al., 1988). The overhang sequence at its 5'-end is strictly defined to be ATC-5' while the 3'-end is more inconsistent in sequence (Sfeir et al., 2005). Human telomeres have variable telomere lengths within the range of 5-15 kb, while in *Mus musculus* telomeric tracts can be considerably longer reaching up to 50 kb. Proximal to the telomere there is an array of degenerate telomeric repeats which extend towards the subtelomere. The subtelomeric sequences of human telomeres are poorly characterized due to high sequence similarity between subtelomeres of different chromosomes (Figure 4a). A generally conserved feature of subtelomeres is the presence of so-called 61- 29 - 37 repeat tracts that are methylated (Nergadze et al., 2009).

Knowledge of the sequence of human telomeric DNA has enabled researchers to isolate factors that have a direct binding affinity for telomeric repeat sequence. Two such factors that bind as dimers at the double stranded portion of telomeric repeats are Telomeric-repeat binding factor 1 (TRF1) and Telomeric-repeat binding factor 2 were discovered in pull down experiments using the telomeric sequence as a bait (Bilaud et al., 1997; Broccoli et al., 1997; Chong et al., 1995; Zhong et al., 1992). TRF1-interacting nuclear factor 2 (TIN2) was discovered in a yeast two hybrid screen as an interacting factor of TRF1 but it also binds TRF2 (Broccoli et al., 1997). TIN2 is bound by TPP1 (consensus from TINT1, PTOP, PIP1) and recruits the only single

stranded binding protein of the complex Protection of Telomeres 1 (POT1). Interestingly POT1 is one of the most conserved proteins in the human complex, alongside the TRF2 interacting protein RAP1 (Baumann and Cech, 2001). Collectively this set of 6 proteins clearly demarcates the end of the DNA as a telomere and is called shelterin (Figure 4b) (reviewed in de Lange, 2005).

Alongside a specific sequence and a specifically bound protein complex, the telomeric chromatin is also characterized by specialized structures. It has been observed that telomeres can fold into a lasso like structure by invading the duplex DNA using the free 3'-end to displace one strand of telomeric DNA. This structure resembles a recombination intermediate and is named t-loop (Figure 4c). The formation of this lariat-like structure is dependent on the shelterin protein TRF2 (Doksani et al., 2013; Griffith et al., 1999). In addition, telomeres, as the rest of the DNA, are packed into nucleosomes but these nucleosomes at shorter telomeres have reduced nucleosomal repeat length and increased sensitivity to *Micrococcal nuclease* (MNase) digestion (Pisano et al., 2007; Tommerup et al., 1994). Interestingly these specialized features of telomeric nucleosomes are lost at elongated telomeres and they start to resemble canonical heterochromatin. Telomeric histones are enriched in heterochromatic marks such as H3K9me3 and H3K27me3 and are bound by the Heterochromatin Protein 1 (HP1). Modifiers of chromatin state at telomeres are highly important for regulating telomere length and other aspects of telomere physiology (reviewed in Blasco, 2007).

1.1.2.3 Introduction to the end protection problem

Early experiments performed by Barbara McClintock and Herman Müller established that the telomeres behave differently from broken chromosome ends (McClintock, 1941; Müller, 1938). In addition, Blackburn and Szostak observed that linear DNA introduced into *S.cerevisiae* is unstable and is integrated into the host genome by recombination. When telomeres were added to this piece of DNA it was stabilized and no integration was observed (Szostak and Blackburn, 1982). How exactly telomeres confer stabilization of natural ends of linear DNA and why are they resistant to processing by the DNA repair machinery was the other fundamental question in telomere biology. Furthermore, we know today that the site of a DNA lesion is recognized by fine-tuned molecular sensors and that this signal activates a pathway responsible to block cell cycle progression (reviewed in Marechal and Zou, 2013; Weinert and Hartwell, 1988). Since telomeres are in essence one half of a double strand break it was unclear why they do not activate the DDR pathway and induce persistent cell cycle arrest and apoptosis. This paradox is defined as the end protection problem and after many years of investigation it has become apparent that is solved by the shelterin complex. How different subunits of the shelterin contribute to the end protection problem will be further discussed and is outlined in Figure 5b.

1.1.2.4 ATM kinase dependent DDR pathway at telomeres

In their physiological state telomeres do not elicit an ATM kinase mediated DNA damage response. But when the function of certain shelterin components is undermined by telomere shortening or mutations in certain components of the complex this unleashes a deleterious DNA damage signaling cascade that ends in apoptosis or senescence. Critically short telomeres elicit an ATM dependent signaling response due to loss of binding sites for telomeric proteins (d'Adda di Fagagna et al., 2003, 2004). When telomerase is inactivated in human cells, attrition of telomeric sequence leads to a state called crisis with persistent ATM activation. Some cells manage to escape this crisis (similar to survivors in yeast) and are characterized by Ligase 3 dependent joining of telomeres and inactivation of several major checkpoint signaling proteins (reviewed in Arnoult and Karlseder, 2015; Hayashi et al., 2015). Deletion of individual shelterin components has revealed that the major player in inhibition of ATM-DDR is the shelterin protein TRF2 (Denchi and de Lange, 2007; Karlseder et al., 1999). Removal of TRF2 leads to ATM dependent accumulation of typical DNA damage markers such as γ -H2AX, MDC1, and 53BP1 which can be cytologically detected as Telomere dysfunction induced foci (TIFs). These foci are very similar, if not identical to already described IRIFs that arise upon DNA double strand breaks (Dimitrova and de Lange, 2006a; Takai et al., 2003). Formation of these foci is not cell cycle dependent suggesting that uncapped telomeres pose a threat to the genome at all times (Konishi and de Lange, 2008). Upon uncapping, activated ATM is able to phosphorylate downstream targets such as Chk2 and p53 and induce cell

cycle arrest, apoptosis or senescence. In addition, deprotected telomeres are now aberrantly joined by the action of DNA PKcs and Ku70/80-Lig4 complex leading to the formation of dicentric chromosomes observed microscopically in metaphase spreads as trains of chromosomes with fused telomeres along them (van Steensel et al., 1998). Because of ATM kinase activation and accumulation of aberrantly joined chromosomes, TRF2 loss is lethal (Sfeir and de Lange, 2012; van Steensel et al., 1998). If the checkpoint signaling is inactivated by removal of p53 or blockage of pRb, cells with dicentric chromosomes will continue to divide and enter the next cell cycle with fused chromosomes. This leads to breakage-fusion-breakage cycles and is a very good model to study what happens to cells that surpass telomerase inactivation driven crisis and what happens in early steps during tumorigenesis. Namely, bridges formed during the separation of sister chromatids at the end of mitosis are causative of transient nuclear envelope rupture and are being processed by the cytoplasmic nuclease Three prime repair exonuclease 1 (TREX1). Examination of post-crisis clones revealed signatures of chromothripsis and kataegis similar to chromothripsis induced by micronucleus formation (Maciejowski et al., 2015; Zhang et al., 2013, 2015).

The mechanism by which TRF2 inhibits ATM activation is not fully understood but there are some important advances in tackling that question (reviewed in Lazzerini-Denchi and Sfeir, 2016; Palm and de Lange, 2008). There are probably several layers of ATM inhibition exerted by TRF2 and one of them includes the formation of the t-loop structure. In vitro, TRF2 is able to promote strand invasion and stabilise Holiday Junction like structure via its basic domain (Doksani et al., 2013; Griffith et al., 1999; Schmutz et al., 2017). It is believed that by tucking the telomere end away from DNA damage sensors TRF2 is able to block aberrant activation of the DNA damage signaling cascade. Although a very elegant hypothesis, it is yet unclear to what extent t-loops are physiologically relevant structures and if they contribute to inhibition of DDR. It would be interesting to construct a separation of function mutant of TRF2 that is defective for t-loop formation but have the other functions preserved to address whether t-loops are indeed protective structures. The other model for TRF2 mediated ATM inhibition is through direct protein-protein interactions. It has been shown that TRF2 interacts with ATM and when tethered to non-telomeric sites of DNA damage it dampens the DDR (Karlseder et al., 2004). Additionally, a motif within the TRF2 protein named inhibitor of the DNA Damage Pathway (iDDR) is able to inhibit the activity of RNF168 and prevent accumulation of 53BP1 (Okamoto et al., 2013). This two-layered mode of control of aberrant ATM activation is important because the t-loop has to be unwound during S-phase for proper telomere replication to occur and therefore an additional mechanism is important for protection. In addition, inhibition of a downstream factor in the c-NHEJ pathway functions to protect telomeres from unwanted DDR and signaling. Namely, telomeric proteins TRF1, TRF2, and RAP1 are direct interactors of Ku70/Ku80 heterodimer which plays a role in c-NHEJ. Interestingly, this complex is constitutively present at telomeres and has an important role in telomere maintenance (Ribes-Zamora et al., 2013).

This fact was conflicting with the requirement of the telomere to suppress c-NHEJ. This conundrum was reconciled when it was discovered that TRF2 directly interacts with the alpha-helix 5 domain of Ku70 required for heterotetramerization. This oligomerization of Ku70/80 is required for efficient DDR and by hiding this site, TRF2 prevents telomere fusions in the presence of Ku (Ribes-Zamora et al., 2013). Recently it was discovered that the only mammalian shelterin with yet undescribed roles at telomeres Rap1, is also important for some aspects of telomere end protection. When tethered to telomeres that are depleted of TRF2, it was observed that Rap1 is able to prevent telomere fusions suggesting a role for Rap1 in suppressing c-NHEJ that was previously masked by the presence of TRF2 (Bombarde et al., 2010; Ribes-Zamora et al., 2013). Interestingly, Rap1 also stimulates TRF2-dependent t-loop formation and increases the specificity of TRF2 binding to telomeric DNA (Arat and Griffith, 2012; Janoušková et al., 2015).

Telomeres repress another deleterious repair pathway dubbed Alternative NHEJ (alt-NHEJ). This pathway is only evident when telomeres are depleted of TRF2, TPP1-POT1 and Ku70/80 suggesting that its activation is a major threat to telomere stability. The pathway is initiated by resection conducted by MRE11 and CtIP followed by generation of microhomologies that are then repaired with the action of poly(ADP-ribose) polymerase 1 (PARP1), DNA polymerase θ and DNA ligase III (Kent et al., 2015; Mateos-Gomez et al., 2015, 2017). Although implicated in telomere alt-NHEJ, this pathway operates also in HR-deficient tumors and loss of DNA polymerase θ leads to increased cell death in these tumors, suggesting a potential avenue for tumor specific

treatment (Ceccaldi et al., 2015). In this case, and many others, telomeres become a really important and valuable model and tool to study the components of DDR pathways and to explore putative drug targets.

1.1.2.5 *ATR kinase dependent DDR pathway at telomeres*

ATR kinase can be activated at telomeres by the protruding ssDNA overhang at its 3' end. This activation is counteracted by the shelterin protein that can bind telomeric ssDNA via the OB fold domains (Denchi and de Lange, 2007). Although POT1 and RPA (an OB-fold containing protein also) have similar affinities towards ss telomeric DNA, it is proposed that tethering of POT1 to telomeres by interaction with TPP1 and the rest of the shelterin might increase the local concentration at telomeres and exclude binding of RPA (Takai et al., 2011). An alternative model that includes hnRNPA1/TERRA mediated RPA to POT1 switch was also proposed. In this model, during S phase of the cell cycle, the overhang is bound by hnRNPA1 when TERRA levels are low. Upon completion of S-phase, TERRA levels peak and are thought to sequester hnRNPA1 liberating the 3'-overhang DNA sites for binding of POT1. This study was done with purified proteins and it was shown that TERRA stimulated POT1 binding to ssDNA (Flynn et al., 2011).

1.1.3 Transcription at telomeres

Due to their heterochromatic structure and lack of promoter sequences telomeres have been viewed as transcriptionally silent regions of the genome. Now we know that most telomeres express a long non coding RNA called TERRA for Telomeric Repeat Containing RNA (Azzalin et al., 2007). Transcription of this RNA is initiated in the subtelomere by RNA Polymerase II and protrudes up to 400 nucleotides into the TTAGGG tract (Feuerhahn et al., 2010; Porro et al., 2010a). It has been shown that TERRA promoter sequences are localized in the 61- 29 - 37 repeats which are rich in CpG islands. These islands are methylated by DNMT1 and DNMT3b DNA methyltransferases and their methylation is thought to repress transcription (Nergadze et al., 2009; Porro et al., 2014a). The CpG islands are also associated with CCCTC-binding factor (CTCF) which is shown to have a role in regulating TERRA transcription (Deng et al., 2012). A larger fraction of TERRA molecules are not polyadenylated and are chromatin associated, while the polyA positive fraction is nucleoplasmic (Porro et al., 2010b). TERRA levels are regulated during the cell cycle with lowest TERRA expression during S phase (Porro et al., 2010a). Understanding the exact function of TERRA is one of the great fundamental questions in the field of telomere biology. Current views are that TERRA can act as a protein scaffold in various cellular processes. For example, TERRA expression is upregulated upon telomere uncapping and is involved in binding of Lysine specific demethylase 1 (LSD1) to promote processing of the 3'-overhang by MRE11. In addition, by recruitment of SUV39H1 TERRA increases heterochromatin formation required for efficient NHEJ (Porro et al., 2014b). Although TERRA can have important beneficial functions, there are some aspects where TERRA expression and interaction with telomeres can have possibly deleterious consequences (reviewed in Rippe and Luke, 2015). Chromatin bound TERRA molecules can invade the telomeric duplex to form DNA:RNA hybrids called R-loops. These hybrids if unresolved can potentially impede semi-conservative replication through telomeres and lead to replication stress and telomere damage (Arora et al., 2014). Telomeric R-loops can promote homology-directed repair between telomeres and become essential in cells where telomere maintenance is dependent on recombination events. These include cells with critically short telomeres (Balk et al., 2013; Graf et al., 2017) and cancer cells and yeast survivors that depend on the recombinogenic alternative lengthening of telomeres (ALT) pathway (Arora et al., 2014; Yu et al., 2014).

1.1.4 Telomere replication and replication stress

It is only recently that we have become aware that even the semi-conservative replication through telomeres is challenging and it requires specialized factors. The reason for this is that telomeres share several features with other difficult to replicate regions in the genome dubbed fragile sites. These regions are often places with paucity of origins and poor in dormant origins and therefore unable to rescue collapsed replication forks. In addition, they pose several obstacles to replication fork progression such as that DNA is bound and

It is known that this phenotype arises as a consequence of replication stress and is phenocopied by treatment of the cells with Aphidicolin, a chemical that decouples the replicative polymerase from the DNA unwinding module leading to increased patches of ssDNA and stalled replication forks. The occurrence of this problem elicits an ATR-dependent DDR suggesting that TRF1 indirectly inhibits ATR signaling at telomeres by promoting semi-conservative replication. The mechanism by which TRF1 facilitates replication through telomeres is still not fully understood but it is known that at least partially it is by recruitment of specialized helicases such as Bloom Syndrome Protein (BLM) and Regulator of Telomere Elongation 1 (RTEL1) (Vannier et al., 2012; Zimmermann et al., 2014). RTEL1 is required for unwinding the specialized G4-quadruplex DNA structures at telomeres and in a separated manner to promote t-loop unwinding in S-phase. The latter function of RTEL1 is stimulated by interaction with TRF2, thus implicating also TRF2 in promoting replication at telomeres (Sarek et al., 2015). BLM directly associates with TRF1 and is recruited to promote lagging strand synthesis possibly also by unwinding the G-quadruplex structures at telomeres (Zimmermann et al., 2014). Interestingly, in the occasion of RTEL1 loss telomerase can impede replication by stabilizing reversed forks leading to rampant consequences such as telomere fragility and telomere loss (Margalef et al., 2018). Another helicase, Werner Helicase (WRN) is also required for promoting lagging strand replication and the defects in this helicase can be rescued by expression of telomerase (Arnoult et al., 2009; Crabbe et al., 2004).

1.2 Functions of SMCHD1 and LRIF1

LRIF1 (Ligand dependent nuclear receptor-interacting factor 1)

LRIF1 (also known as HBiX1, RIF1, C1orf103) is a poorly characterized 84.5 kDa large nuclear protein. It was initially discovered in 2007 in a yeast two hybrid screen as an interacting protein of human Retinoic acid receptor α (RAR α). Direct interaction was further confirmed using in vitro translated RAR α and immobilized GST-LRIF1 pull downs (Li et al., 2007). In this study the authors also showed that the interaction with nuclear receptors was hormone independent, that LRIF1 has a bipartite NLS at its C-terminus and that it is localized in the nucleus. LRIF1 was implicated to be the part of the nuclear matrix and to negatively regulate the transcriptional activity of RAR α possibly through recruitment of histone deacetylases (Li et al., 2007). In an independent study, LRIF1 was described as an interacting protein of HP1 α in a proteomic screen using Flag-tagged HP1 α in HEK293T cells (Nozawa et al., 2010). LRIF1 interacts with the chromoshadow domain of HP1 α through its PxVxL motif and a FLAG-tag pulldown of LRIF1 followed by mass-spectrometry revealed interaction with the other two subunits of HP1 (β and γ). Surprisingly, SMCHD1 was also identified in this experiment to interact with the N-terminal coiled-coil domain of LRIF1. An in-depth functional characterization of these interactions was performed and LRIF1 emerged as an epigenetic regulator of X-chromosome inactivation in the RPE-1 female human cell line. The inactive X chromosome (Xi) or Barr body is an example of facultative heterochromatin and is transcriptionally silenced in female cells during gestation. LRIF1 and SMCHD1 were shown to localize at the Xi chromosome and this localization to Xi was dependent on Xist suggesting that these proteins are dispensable for the establishment of X inactivation. Instead, it was suggested that they play an important role in maintaining X chromosome compaction by linking HP1 bound H3K9me3 domains and XIST associated H3K27me3 domains (Figure 6). (Nozawa et al., 2013). Recently, LRIF1 was detected at human alpha satellite repeats by HyCCAPP (hybridization capture of chromatin-associated proteins for proteomics) using biotinylated alpha satellite capture oligonucleotides in K562 cells and its binding was confirmed by ChIP-qPCR suggesting a general function for LRIF1 at heterochromatic loci (Buxton et al., 2017). Remarkably, LRIF1 and SMCHD1 were identified at very long telomeres in HeLa 1.2.11 by an approach similar to HyCCAPP dubbed Proteomics of Isolated Chromatin segments (PiCh) (Déjardin and Kingston, 2009). Our laboratory also identified these proteins at over-elongated telomeres and at telomeres in human fibroblasts by purification of telomeric chromatin using a technique called QTIP for Quantitative Telomeric Chromatin Isolation Protocol (Grolimund et al., 2013; Majerska et al., 2018).

In this study telomere association of LRIF1 was confirmed by chromatin immunoprecipitation (ChIP) of 3xHA-tagged LRIF1. In addition, these proteins were identified at telomeres by proximity labeling techniques such as BioID using overexpressed TRF1 (Garcia-Exposito et al., 2016) or endogenously tagged TRF1 or TRF2

(Anna Reis, Gerald Lossaint, personal communication) leading us to think that there might be yet undescribed important functions for these proteins at telomeres.

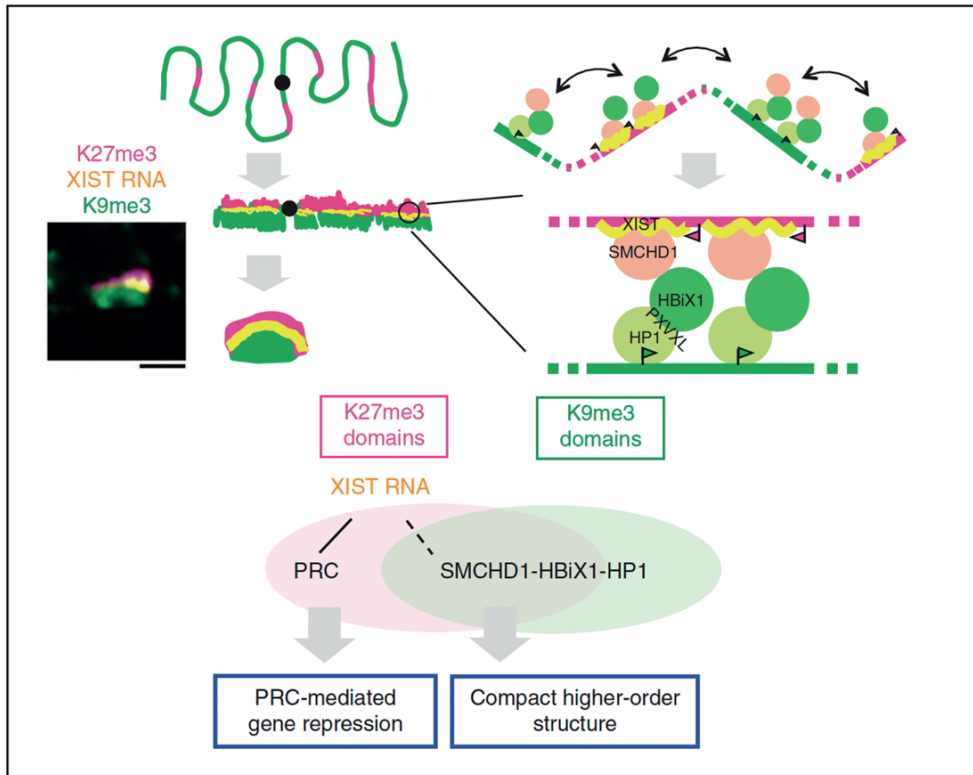


Figure 6. Model depicting SMCHD1 and LRIF1 dependent higher order organization of the inactive X chromosome (Image from Nozawa et al, 2013)

SMCHD1 (*Structural maintenance of chromosomes hinge domain containing protein 1*)

SMCHD1 is a very large 226kDa protein that is functionally well described as an epigenetic regulator. The protein has two conserved domains; the N-terminal GHKL-type ATPase and the C-terminal SMC hinge domain which is flanked by two coiled-coils. Due to the high similarity of the SMC-hinge domain to other Structural maintenance of chromosomes (SMC) proteins, SMCHD1 is considered to be a non-canonical member of this family. This protein family comprises cohesins, condensins and SMC5/SMC6 protein complexes with roles in sister chromatid cohesion, chromatin condensation and DNA damage repair (reviewed in Losada, 2005; Nasmyth and Haering, 2009; Wu, 2012). The ATPase domain, on the other hand, is homologous to the ones of DNA gyrase B, HSP90 and bacterial protein MutL (Brideau et al., 2015). SMCHD1 was originally identified in an N-ethyl-N-nitrosourea (ENU) screen for variegated expression of GFP transgene in mouse erythrocytes (Blewitt et al., 2005). Point mutation produced in the ENU screen was dubbed MommeD1 (Modifier of murine metastable epialleles 1) and was suspected to lead to nonsense mediated mRNA decay of SMCHD1 mRNA phenocopying SMCHD1-null situation. Further characterization of SMCHD1^{MommeD1/MommeD1} mutation carrying mice revealed that female mice die mid-gestation at embryonic day 10.5 while male mice are viable but only half of them survive to weaning. Sex specific embryonic lethality suggested that there might be a critical role for SMCHD1 in X-chromosome inactivation which was then confirmed in further studies in both mouse and human cells (Figure 6) (Ashe et al., 2008; Blewitt et al., 2008; Nozawa et al., 2013). Furthermore, loss of SMCHD1 leads to loss of compartmentalization at the Xi, aberrant Xist spreading and changes in the strength of topologically associated domains (TADs) (Wang et al., 2018). In addition to regulating expression of X-linked genes, SMCHD1 has been shown to regulate expression of several clusters of autosomal genes, especially the ones on the Snrpn and α and β protocadherin loci (Chen et al., 2015; Gendrel et al., 2013; Liu et al., 2016; Massah et al., 2014). Some of the functions of SMCHD1 in the regulation of gene expression might be

contributed to its role in CpG island methylation (Blewitt et al., 2008; Gendrel et al., 2013). Interestingly, a homologous plant protein complex containing GHKL-ATPase and hinge domain on two independent proteins was suggested to have a role in RNA mediated DNA methylation (Lorković et al., 2012). Because of its role in X-linked and autosomal gene regulation SMCHD1 has been suggested to have a tumor promoting function and loss of SMCHD1 was shown to lead to increased tumorigenicity and accelerated tumor growth (Leong et al., 2013). Loss of SMCHD1 and other epigenetic regulators did not affect telomere length in female and male mice *in vivo* (Roberts et al., 2011). Recently, heterozygous mutations in SMCHD1 have been associated with the pathogenesis of two very different diseases Fasioscapulohumoral Muscular Dystrophy (FSHD) and Bosma Arhinia Microphthalmia Syndrome (BAMS) (reviewed in Jansz et al., 2017; Wilkie, 2017). FSHD is a common muscular dystrophy affecting the facial muscles and upper extremities and is characterized by late onset and progressive muscle deterioration. There are two types of FSHD and mutations in SMCHD1 are causative for late-onset progressive FSHD Type 2 and are thought to affect disease severity in FSHD Type 1 (Larsen et al., 2015). Pathogenesis of both diseases is linked to myotoxicity due to aberrant expression of a homeobox factor named DUX4 in the somatic muscle cells. In the germline DUX4 is expressed from a polymorphic repetitive array of D4Z4 macrosatellite repeats on chromosome 4. This array has a variable number of 3.3kb long repeats and each repeat is capable of expressing one DUX4 retrogene. In somatic cells of non-affected individuals this locus is repressed by DNA methylation and enrichment of repressive H3K9me3 histone marks. In FSHD1 affected individuals there is a contraction of the D4Z4 locus to less than 10 repeat units which leads to chromatin relaxation and aberrant DUX4 expression. FSHD2 patients, on the other side, have a normal D4Z4 repeat length but are shown to inherit heterozygous loss-of-function mutations in SMCHD1 and a permissive 4qA haplotype which encodes for a poly-A signal required for stabilization of the DUX4 transcript (van den Boogaard et al., 2016; Lemmers et al., 2012). In this study haploinsufficiency of SMCHD1 was shown to be causative for loss of methylation at the D4Z4 repeat locus and aberrant expression of DUX4 in muscle cells. BAMS is a striking congenital disease phenotypically characterized by nose malformation accompanied by loss of eye function and male infertility. By employing next generation sequencing two groups have identified *de novo* SMCHD1 mutations in affected individuals. Interestingly mutations in SMCHD1 in this disease are concentrated in the ATPase domain of SMCHD1 while in FSHD mutations are spread throughout the protein body (Gordon et al., 2017; Lemmers et al., 2012; Shaw et al., 2017). It is still unclear whether mutations in patients with BAMS are loss or gain of function mutations due to the imperfection of the systems used to test the mutated proteins. Seemingly independent of the function of SMCHD1 as epigenetic regulator of X chromosome inactivation and gene expression two groups have reported that SMCHD1 is recruited to sites of DNA damage and required for efficient c-NHEJ (Coker and Brockdorff, 2014; Tang et al., 2014). Although there is an increasing amount of data tackling the functions of SMCHD1 there is very little known about the biochemistry of the protein itself and there is no mechanistic insight in how SMCHD1 performs its functions. The only known interactors of SMCHD1 so far are LRIF1 and HP1 γ (Brideau et al., 2015; Nozawa et al., 2013). Two studies suggested that SMCHD1 could form homodimers through its N-terminal SMC-hinge domain (HD) and intramolecular coiled-coil interactions (Brideau et al., 2015; Chen et al., 2016a). This is in contrast to canonical SMC proteins whose SMC-hinge domain is located centrally in the protein and is folded to bring together the N- and C-terminal subdomains of the ABC-type ATPase (Figure 7). In addition, canonical SMC proteins form heterodimers through the hinge domains in a non random fashion giving rise to defined SMC complexes with distinct functions with help form non-SMC auxiliary proteins (reviewed in Losada, 2005). Whether the proposed model of SMCHD1 hinge domain mediated dimerization will prevail depends on solving the crystal structure of either the hinge domain or the full length SMCHD1 protein. The hinge domain of SMC proteins has as other function the binding to DNA (Chiu et al., 2004). The DNA binding property of the SMCHD1 HD was addressed and although the HD can putatively bind DNA with micromolar affinity the experiments performed in this study were incomplete (Chen et al., 2015). Therefore, it is still important to understand what mediates SMCHD1 binding to chromatin and whether this binding mode might be context dependent. The beforementioned GHKL-ATPase domain of mouse SMCHD1 was suggested to be functional in ATP hydrolysis and inhibited by a general GHKL-ATPase inhibitor radicicol. The residue important for the catalytic activity in these experiments was shown to be Glutamate 147 (Brideau et al., 2015; Chen et al., 2016b).

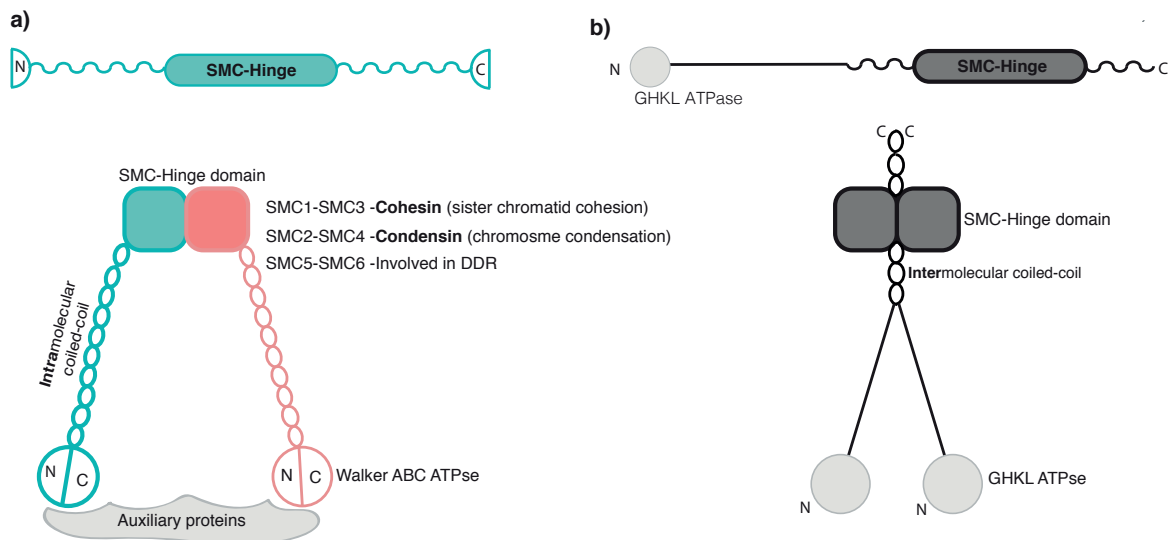


Figure 7. Folding of canonical SMC proteins and SMCHD1. A) (UP) Schematic depicting the domain structure of full-length canonical SMC protein with the SMC-hinge and N- and C- terminal Walker ATPase domains labeled. (DOWN) Canonical structure of the SMC complex with two different SMC proteins labeled with cyan and pink connected by SMC auxiliary proteins. Three distinct SMC protein complexes and their functions are denoted. B) (UP) Schematic depicting domain structure of full-length SMCHD1 protein with the SMC-hinge and GHKL ATPase domain labeled. (DOWN) Putative structure of SMCHD1 based on current evidence. (Image is adapted from Brideau et al., 2015; Chen et al., 2016)

1.3 Aim of the thesis

SMCHD1 and LRIF1 are poorly described interacting proteins with roles in epigenetic silencing and X-chromosome compaction (Blewitt et al., 2008; Nozawa et al., 2013). SMCHD1 is, in addition, recruited to sites of DNA damage via an unknown mechanism and its roles in the process of DDR signaling and repair are not well understood (Coker and Brockdorff, 2014; Tang et al., 2014). Both of them were previously detected at telomeres in several different contexts, by using complementary proteomic approaches to detect telomere associated proteins, but no attempts were made in understanding their roles at telomeres (Déjardin and Kingston, 2009; Garcia-Exposito et al., 2016; Grolimund et al., 2013). Also, how changes in the chromatin structure exerted by these and other heterochromatin proteins, mediated either by physical compaction or molecular changes at the chromatin level, affect the DNA damage response pathway is largely elusive (reviewed in Goodarzi et al., 2010). Therefore, this study aims at understanding the molecular functions of SMCHD1 and LRIF1 at unprotected telomeres. Characterisation of the functions of these proteins in DDR aims to expand the known repertoire of players orchestrating the DDR and to provide further insight into how chromatin changes modulate the activation of DDR signaling. Furthermore, we aim to establish a microscopy-based method to study physical changes in telomere volume mediated by different proteins in order to understand how telomeres are maintained in a compacted state. Previous attempts to study this phenomenon relied on cryo-electron microscopy and atomic force microscopy (AFM) but these have low throughput and do not operate in *in vivo* settings (Benarroch-Popivker et al., 2016; Galati et al., 2015). The method established in this study relies on Stochastic Optical Reconstruction Microscopy (STORM), *in situ* crosslinking of protein-DNA complexes and detection of the telomere by using fluorescently labeled DNA oligonucleotide. By using this method, we aim to understand which components of telomeric chromatin are required for maintenance of the 3D telomere structure and whether changes in this structure affect the DNA damage signaling at uncapped telomeres.

Chapter 2 The telomeric DNA damage response occurs in the absence of chromatin decompaction

Aleksandra Vancevska, Kyle M. Douglass, Verena Pfeiffer, Suliana Manley, Joachim Lingner
(*Genes&Development*, 2017; Vol. 31(6), p.567-577)

2.1 Abstract

“Telomeres are specialized nucleoprotein structures that protect chromosome ends from DNA damage response (DDR) and DNA rearrangements. The telomeric shelterin protein TRF2 suppresses the DDR, and this function has been attributed to its abilities to trigger t-loop formation or prevent massive decompaction and loss of density of telomeric chromatin. Here, we applied stochastic optical reconstruction microscopy (STORM) to measure the sizes and shapes of functional human telomeres of different lengths and dysfunctional telomeres that elicit a DDR. Telomeres have an ovoid appearance with considerable plasticity in shape. Examination of many telomeres demonstrated that depletion of TRF2, TRF1, or both affected the sizes of only a small subset of telomeres. Costaining of telomeres with DDR markers further revealed that the majority of DDR signaling telomeres retained a normal size. Thus, DDR signaling at telomeres does not require decompaction. We propose that telomeres are monitored by the DDR machinery in the absence of telomere expansion and that the DDR is triggered by changes at the molecular level in structure and protein composition.” (Vancevska et al., 2017)

2.2 Highlights

- We apply Stochastic Optical Reconstruction Microscopy (STORM) to measure sizes and shapes of human telomeres
- We are able to detect telomere length dependent changes in telomere volume
- Removal of shelterin proteins doesn't lead to massive telomere decompaction
- Change in telomere structure and possibly decompaction is observed only in a subset of DDR-positive telomeres suggest that telomere decompaction is not a general phenomenon at damaged telomeres
- Our high throughput approach sets the stage to study telomere compaction in various cellular states

2.3 Author contributions

All authors contributed to experimental design. V.P. and A.V. performed preliminary STORM experiments and optimizations, A.V. acquired the STORM data and performed the molecular biological experiments presented in the paper. K.M.D. performed the data analysis with the help of A.V. J.L., with contributions from all authors, wrote the main text. K.M.D. and A.V. wrote the Materials and Methods.

The telomeric DNA damage response occurs in the absence of chromatin decompaction

Aleksandra Vancevska,^{1,4} Kyle M. Douglass,^{2,4} Verena Pfeiffer,^{1,3} Suliana Manley,² and Joachim Lingner¹

¹Swiss Institute for Experimental Cancer Research, School of Life Sciences, Ecole Polytechnique Fédérale de Lausanne (EPFL), 1015 Lausanne, Switzerland; ²Institute of Physics, Laboratory of Experimental Biophysics, EPFL, 1015 Lausanne, Switzerland

Telomeres are specialized nucleoprotein structures that protect chromosome ends from DNA damage response (DDR) and DNA rearrangements. The telomeric shelterin protein TRF2 suppresses the DDR, and this function has been attributed to its abilities to trigger t-loop formation or prevent massive decompaction and loss of density of telomeric chromatin. Here, we applied stochastic optical reconstruction microscopy (STORM) to measure the sizes and shapes of functional human telomeres of different lengths and dysfunctional telomeres that elicit a DDR. Telomeres have an ovoid appearance with considerable plasticity in shape. Examination of many telomeres demonstrated that depletion of TRF2, TRF1, or both affected the sizes of only a small subset of telomeres. Costaining of telomeres with DDR markers further revealed that the majority of DDR signaling telomeres retained a normal size. Thus, DDR signaling at telomeres does not require decompaction. We propose that telomeres are monitored by the DDR machinery in the absence of telomere expansion and that the DDR is triggered by changes at the molecular level in structure and protein composition.

[*Keywords:* telomeres; DNA damage response; chromatin compaction; STORM]

Supplemental material is available for this article.

Received November 21, 2016; revised version accepted February 14, 2017.

Telomeres protect chromosome ends from degradation, DNA rearrangements, and DNA damage signaling, which are seen at DNA double-strand breaks (de Lange 2009; Denchi and Sfeir 2016). The repetitive DNA sequences at human telomeres consist of several kilobases of double-stranded TTAGGG repeats ending in a single-stranded 3' overhang of 100–300 nucleotides. Telomeres are associated with a large number of proteins that mediate their function (Dejardin and Kingston 2009; Grolimund et al. 2013; Bartocci et al. 2014). The shelterin proteins are the main constituents of telomeres, comprising six specialized proteins (de Lange 2005). Among these, both TRF1 and TRF2 bind directly as dimers to the double-stranded portion of telomeric DNA. In contrast, POT1 forms a dimer with TPP1 and binds to the single-stranded G-rich telomeric DNA (Baumann and Cech 2001). TIN2 and Rap1 associate indirectly with telomeres—TIN2 through interactions with TRF1, TRF2, and TPP1, and Rap1 through interactions with TRF2. Shelterin proteins are essential for mediating telomere functions. In particular,

TRF1 is required for efficient replication of the TTAGGG repeats by the DNA replication machinery (Sfeir et al. 2009). TRF1 recruits the BLM helicase, which sustains replication, and TPP1/POT1, which represses ATR kinase signaling (Zimmermann et al. 2014). In the absence of TRF1, replication forks stall, and telomeres obtain a fragile phenotype. Stalled replication forks accumulate ssDNA, which, when bound by replication protein A, recruits ATRIP-ATR to initiate a DNA damage response (DDR) (Zou and Elledge 2003). This can explain how TRF1-depleted telomeres activate the ATR checkpoint kinase in S phase.

The shelterin TRF2 protects chromosomes from end-to-end fusions by nonhomologous end-joining (NHEJ) and suppresses activation of the ATM checkpoint kinase (van Steensel et al. 1998; Denchi and de Lange 2007). When telomeres become critically short, they fail to recruit sufficient TRF2, leading to the activation of a DDR and cellular senescence. Thus, the uncapped telomeres, as DNA double-strand breaks, are sensed and bound by the Mre11–Rad50–Nbs1 (MRN) complex, recruiting and activating the ATM kinase (Uziel et al. 2003; Lee and

³Present address: Institute of Social and Preventive Medicine, University of Bern, 3012 Bern, Switzerland.

⁴These authors contributed equally to this work.

Corresponding authors: joachim.lingner@epfl.ch, suliana.manley@epfl.ch
Article published online ahead of print. Article and publication date are online at <http://www.genesdev.org/cgi/doi/10.1101/gad.294082.116>. Freely available online through the *Genes & Development* Open Access option.

© 2017 Vancevska et al. This article, published in *Genes & Development*, is available under a Creative Commons License (Attribution 4.0 International), as described at <http://creativecommons.org/licenses/by/4.0/>.

Paul 2005). ATM then phosphorylates various substrates, culminating in the DDR cascade.

Telomere-bound TRF2 simultaneously inhibits ATM kinase (Karlseder et al. 2004) and the propagation of DNA damage signaling downstream from ATM (Okamoto et al. 2013). In parallel, MRN recruitment and ATM activation at telomeres may be prevented through t-loops. In t-loop structures, the telomeric 3' overhang is tucked into the double-stranded part of the telomere (Griffith et al. 1999) and may therefore hide the ends of chromosomes from the DNA damage machinery. T-loops were first detected when analyzing psolaren cross-linked telomeric DNA that had been purified from human or mouse cells (Griffith et al. 1999). More recently, when analyzing cross-linked chromatin spreads *in vitro* by stochastic optical reconstruction microscopy (STORM), t loops were found at ~20% of telomeres with varying strand invasion points (Doksani et al. 2013). Intriguingly, depletion of TRF2 caused loss of t loops. Thus, TRF2-dependent suppression of DDR and t-loop formation are correlated. A very different alternative model was proposed recently in which loss of TRF2 would lead to an up to 10-fold decompaction (decrease in density) of telomeric chromatin, rendering telomeres accessible to DDR factors that would otherwise be excluded (Bandaria et al. 2016). Within this model, activation of ATR signaling upon TRF1 depletion was also explained by chromatin decompaction rather than the accumulation of ssDNA at stalled replication forks in S phase as discussed above. The telomere decompaction model was based on data obtained with superresolution microscopy on human cells in which TRF1, TRF2, or other shelterin components were depleted.

Here, we applied STORM superresolution fluorescence microscopy to study telomere structure (Rust et al. 2006). With STORM, we can determine the positions of individual fluorescent probes on a telomere with precision on the order of 10 nm by stochastically switching the fluorophores between fluorescent and dark states. A STORM measurement on a single telomere yields a cluster of fluorophore position estimates (known as localizations) from which structural properties of the telomere, such as its size and shape, were calculated. We depleted TRF1 and TRF2 to assess their roles in telomere compaction and used a large field of view (FOV) flat illumination microscope setup to capture a large number of telomeres (>900 per condition) with high image quality (Douglass et al. 2016). By costaining telomeres with the DNA damage markers 53BP1 and γ H2AX, we were able to unequivocally distinguish telomeres eliciting a DDR from intact telomeres. Our results reveal that the vast majority of DDR-positive telomeres does not differ in size from DDR-negative telomeres, excluding telomere decompaction from being generally associated with the DDR.

Results

STORM imaging of human telomeres

To visualize the TTAGGG repeats of human telomeres, we hybridized fixed HeLa cells with a PNA oligonucleo-

tide (5'-CCCTAA-3')₃ probe that was labeled at its 5' end with the fluorescent dye Alexa fluor 647. Imaging was performed with a custom-built microscope capable of performing STORM on 10–30 cells simultaneously, facilitating the acquisition of large data sets and better ensuring sufficient sampling over the sample heterogeneity. The mean localization precision of fluorophores was 10 nm in the X and Y directions (Supplemental Fig. S1). As expected, wide-field imaging showed telomeres as diffraction-limited spots (Fig. 1A). However, STORM imaging resolved individual fluorophores, forming clusters of localizations corresponding to telomeres. To ensure that every cluster corresponded to a telomere, the localizations were overlaid with wide-field images, and the data were filtered to reject groups of signals that did not correspond to an image of a telomere, had a very low number of localizations (<50), or were not properly clustered. Many telomeres adopted roughly an ovoid structure, but the heterogeneity of shapes suggested a considerable plasticity of telomeres (Fig. 1C; Supplemental Fig. S2).

We assessed telomere sizes by computing each cluster's radius of gyration (R_g), which is the root-mean-square distance between the localizations and the cluster center. Our measured R_g values correlate well with another measure of size, the convex hull area (Supplemental Fig. S1). Unlike the convex hull, however, which uses only localizations at the extreme edges and assumes that cluster outlines have no concavities, R_g uses every localization in the cluster to determine telomere size and makes no assumptions on telomere shape. We compared the telomeres of two isogenic HeLa strains, termed HeLa S (HeLa cells with short telomeres) and HeLa L (HeLa cells with long telomeres), in which the average telomere length was 11 kb and 33 kb as determined by telomere restriction fragment length analysis (Fig. 1D). The long telomeres in HeLa L were obtained upon overexpression of the catalytic subunit of telomerase hTERT together with RNA moiety hTR (Cristofari and Lingner 2006; Grolimund et al. 2013). The average R_g of HeLa S was 68 nm, and the average R_g of HeLa L 88 nm (Fig. 1E,F). Therefore, longer telomeres showed a larger R_g , as expected. The spread in the distributions is consistent with the measured heterogeneity of telomere lengths. Considering that the volume of a sphere increases with the third power of the radius, we estimated that HeLa L telomeres have a slightly higher density (1.4 \times) than HeLa S (see the Materials and Methods).

Telomere sizes of shelterin-depleted telomeres

To study the roles of the shelterin proteins TRF1 and TRF2 in telomere size maintenance, we depleted TRF1 and TRF2 upon expression of shRNAs in HeLa cells from transiently transfected vectors (Fig. 2). Alternatively, we transiently overexpressed a mutant version of TRF2 (TRF2 Δ B Δ M) that is dimerization-competent but DNA-binding-deficient and instrumental in titrating off endogenous TRF2 from telomeres (van Steensel et al. 1998) or used siRNAs targeting TRF1 (Supplemental Fig. S3). The depletion of TRF1 and TRF2 was confirmed on Western blots (Fig. 2A; Supplemental Fig. S3A,D). A loss of

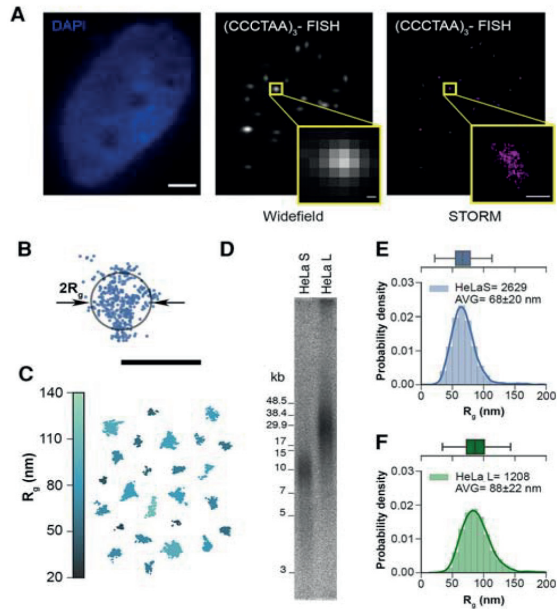


Figure 1. Human telomeres are heterogeneous in length, size, and shape. (A) Wide-field fluorescence images of the HeLa cell nucleus stained with DAPI (left; bar, 3 μm) and telomeres labeled with telomeric (CCCTAA)₃-A647 fluorescence in situ hybridization (FISH) probe (middle) and STORM image of telomeres (right). Enlarged insets show that telomeres are smaller than the diffraction limit. Bar, 0.15 μm . (B) The signal from a single telomere is a cluster of fluorescent molecule position estimates known as localizations. Its size is determined by the radius of gyration (R_g) of the localizations (bar, 0.2 μm), which is the root-mean-square distance of the localizations from the cluster's center of mass. (C) Several clusters of localizations from HeLa L (HeLa cells with long telomeres) illustrating their heterogeneity in shape and R_g (color-coded in the vertical bar). (D) Telomere restriction fragment analysis of telomere length of isogenic HeLa S (HeLa cells with short telomeres) and HeLa L cells used for STORM imaging displays the length heterogeneity of HeLa telomeres. (E) Distribution of R_g for (CCCTAA)₃-FISH-labeled samples of HeLa S telomeres. The solid line on the histogram plot is the kernel density estimate of the distribution, and the solid vertical lines in the box mark the quartiles. Whiskers mark the range of the distribution, excluding outliers. (F) The same as E but for HeLa L telomeres.

function was indicated by the accumulation of the activated and phosphorylated form of the checkpoint kinase ATM (Fig. 2A). The accumulation of the DNA damage marker 53BP1 in foci that colocalized with telomeres indicated that the damage occurred at telomeres (Fig. 2B,C). We then determined the R_g in control cells and TRF1-depleted, TRF2-depleted, and TRF1/2-double-depleted cells. Strikingly, the radii had similar mean values and similar variances (Fig. 2D,E). Therefore, upon strong reduction of shelterin proteins, the telomeric chromatin did not change its compaction in a significant manner. However,

it must be noted that, in depletion experiments, only a fraction of telomeres elicit a DDR, as evidenced by the accumulation of the DDR marker 53BP1 at only a subset of telomeres (Fig. 2C; Supplemental Fig. S3B,E). Therefore, these experiments did not rule out specific changes at DDR-active versus DDR-inactive telomeres.

Telomeric DDR in the absence of decompaction

To identify and compare the sizes of DDR-positive and DDR-negative telomeres, we costained telomeres with antibodies against either 53BP1 or γH2AX , both of which can serve as DDR markers (Fig. 3; Supplemental Fig. S4). The average R_g of DDR-positive telomeres was slightly larger than that of DDR-negative telomeres. However, this shift in the mean value was due to a small subset of DDR-positive telomeres that had a considerably larger R_g (~10% of control telomeres had an R_g of >100 nm, whereas 37% of 53BP1-positive telomeres had an R_g of >100 nm) (Fig. 3D). However, the vast majority of DDR-positive telomeres had an R_g that was indistinguishable from DDR-negative telomeres. This indicates that chromatin decompaction is not required for the telomeric DDR.

Efficient depletion of TRF2 is known to lead to telomere associations and chromosome end-to-end fusions in addition to eliciting a telomeric DDR. We therefore suspected that the small subset of DDR-positive telomeres with larger R_g s contained more telomeric DNA and possibly corresponded to telomere associations. Consistent with this, we observed a positive correlation between the number of localizations and R_g (Fig. 4A), including a population of DDR-positive telomeres with a higher number of localizations and larger R_g s compared with the control (Fig. 4B). For the longer telomeres in HeLa L, we also observed a larger number of localizations (mean $n = 412$) than in HeLa S (mean $n = 299$), although their ratio was not in proportion with their average lengths, which differed by a factor of three. Finally, fluorescence intensity in fluorescence in situ hybridization (FISH) experiments has been correlated with telomere length in numerous studies (Poon and Lansdorp 2001). Altogether, these analyses suggest that the small subset of DDR-positive telomeres in TRF2-depleted cells that had a larger R_g contained more telomeric DNA. Since depletion of TRF2 during a short time period does not induce telomere length changes (Supplemental Fig. S5), this suggests that the larger telomeres were due to telomere–telomere associations. This was supported by inspection of their shapes, which further indicated larger deviations from the ovoid shapes that were seen in DDR-positive telomeres with a near-average R_g as well as control telomeres (cf. Fig. 4C,D and Supplemental Fig. S2). However, these experiments could not fully exclude that a higher number of localizations could be due to increased probe accessibility.

Telomere size measurements by FISH and anti-TRF1 immunofluorescence (IF) are consistent

To further corroborate our analysis, we compared telomeres that were stained with FISH probes with telomeres

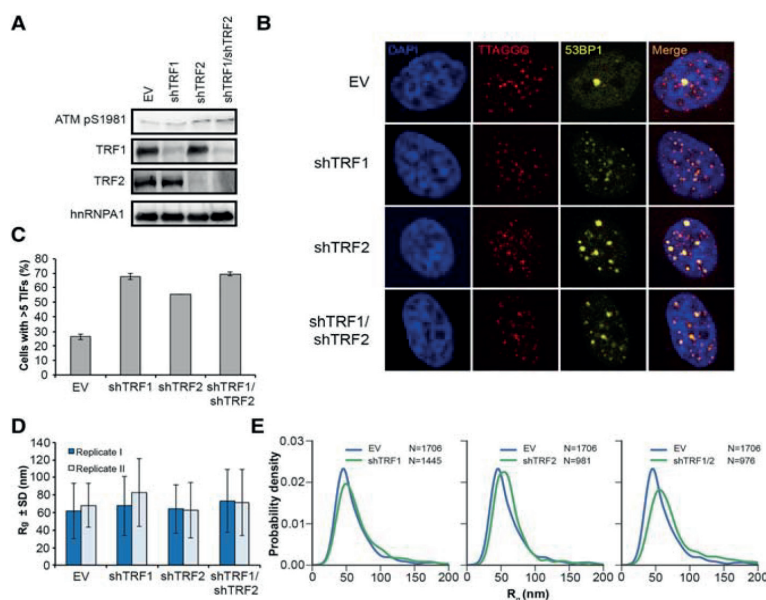


Figure 2. Depletion of shelterin proteins TRF1 and TRF2 does not affect telomere size in HeLa S cells. (A) Western blot analysis of TRF1, TRF2, hnRNPA1, and ATM pS1981 in HeLa cells transfected with the indicated shRNAs (shTRF1, shTRF2, and shTRF1/shTRF2) or empty vector (EV). (B) Representative images for detection of 53BP1 at telomeres in HeLa cells transfected with the indicated shRNAs or empty vector. Immunofluorescence (IF) for 53BP1 (yellow) was combined with telomeric (CCCTAA)₃-FISH (red), and the DNA was stained with DAPI. (C) Quantification of the number of cells containing more than five telomere dysfunction-induced foci (TIFs), detected as in B. Data represent the mean of two independent experiments \pm SD (>130 cells per condition per experiment). (D) Average R_g of telomeric (CCCTAA)₃-FISH-labeled samples obtained by analysis of STORM data. Data represent the mean R_g (in nanometers) of two independent experiments \pm SD (>900 telomeres per condition per experiment). (E) Representative distributions of R_g of telomeric (CCCTAA)₃-FISH-labeled samples obtained by analysis of STORM data.

that were stained by indirect IF with affinity-purified polyclonal antibodies raised against TRF1 (Fig. 5). The experiments were carried out with HeLa L cells with telomeres of an average length of 33 kb, as they gave a good signal over noise (Fig. 5B). The average R_g of HeLa L was 88 nm when telomeres were labeled by FISH (Figs. 1F, 5A) and 103 nm when labeled by IF against TRF1 (Fig. 5C). The slightly larger R_g obtained with IF can be explained by the sizes of primary and secondary antibodies that will place the fluorescent label at an offset distance from TRF1-bound telomeres and therefore lead to an apparent size increase (Lambert and Waters 2017).

We also compared the R_g distributions of telomeres in HeLa L that had been depleted for TRF2. For FISH and IF, the DDR-negative telomeres had a distribution similar to that of empty vector cells. For DDR-positive HeLa L telomeres, we observed with both methods a major peak in the size distribution that was indistinguishable from that of nondepleted cells and a smaller subset of DDR-positive telomeres with larger R_g s as compared with the control. Therefore, the analyses by FISH and IF are consistent. Furthermore, the telomeres of HeLa L and HeLa S responded similarly to the depletion of TRF2. In both cases, the great majority of telomeres eliciting a DDR did not increase in size.

Discussion

In this study, we applied STORM to study the shape and size of human telomeres. Using a large FOV illumination system known as FIFI (Douglass et al. 2016), we were able to simultaneously sample multiple cells that differed in

their telomeric states. The determined telomere sizes demonstrate that telomeric DNA is compacted when assembled as chromatin in cells. A B-DNA double helix of 11,000 base pairs (bp) has a calculated length of 3650 nm. The measured R_g of 68 nm for 11,000 bp of telomeric chromatin suggests a compaction in length of <27-fold. Our measurements are in agreement with previous studies on mouse and human telomeres (Doksani et al. 2013; Bandaria et al. 2016). Our analysis reveals that the volume elements occupied by human telomeres can be approximated by ovoid structures. However, the heterogeneity of shapes indicates substantial plasticity of telomeres.

We addressed the question of whether telomere compaction changes upon depletion of TRF1 or TRF2. We observed no major changes in telomere density. This therefore suggests that, upon shelterin removal, telomeric DNA remains compacted. TRF2 is able to package telomeric DNA in vitro (Benarroch-Popivker et al. 2016), but the lack of this activity upon TRF2 depletion can obviously be compensated for by other factors such as nucleosomes or other proteins that remain unidentified. We also specifically analyzed the sizes of TRF2-depleted telomeres that elicited a DDR. This was possible by co-staining of telomeres with the DDR markers 53BP1 and γ H2AX. This analysis revealed that the majority of telomeres eliciting a DDR did not differ in size in comparison with their DDR-negative counterparts. This therefore strongly indicates that telomere decompaction is not linked to the DDR. In addition, the data suggest that t-loop unfolding does not lead to massive telomere expansions and shape changes. A small subset of DDR-positive telomeres showed a higher R_g . However, these

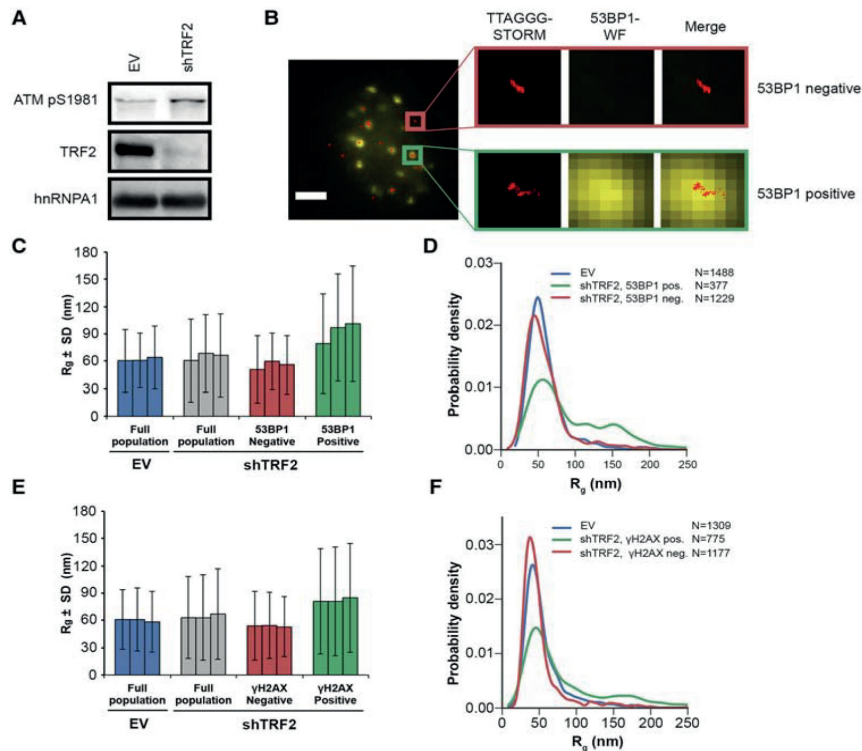


Figure 3. Selection of DDR-positive telomeres of shTRF2-depleted HeLa S cells with two markers (53BP1 and γ H2AX) reveals an increase in telomere size in only a small subset of telomeres. (A) Western blot analysis of TRF2, hnRNPA1, and ATM pS1981 in HeLa cells transfected shTRF2 plasmids. (B) Representative images for detection of 53BP1 at telomeres in HeLa cells transfected with shTRF2 plasmids. IF for 53BP1 (yellow; *middle* panel, wide-field [WF] image) was combined with telomeric (CCCTAA)₃-FISH (red; *left* panel, STORM image) in order to use the wide-field image of 53BP1 as a selection marker for DDR-positive telomeres. One 53BP1-positive and one 53BP1-negative telomere are enlarged. The same procedure was also performed for selection of γ H2AX-positive telomeres. Bar, 4 μ m. (C) Average R_g of telomeric (CCCTAA)₃-FISH-labeled and 53BP1-IF-labeled samples obtained by analysis of STORM data. Data represent the mean R_g (in nanometers) of three independent experiments \pm SD (>900 telomeres per condition per experiment). (D) Representative distributions of R_g of telomeric (CCCTAA)₃-FISH-labeled and 53BP1-IF-labeled samples obtained by analysis of STORM data. (E) Average R_g of telomeric (CCCTAA)₃-FISH-labeled and γ H2AX-labeled samples obtained by analysis of STORM data. Data represent the mean R_g (in nanometers) of three independent experiments \pm SD (>900 telomeres per condition per experiment). (F) Representative R_g distributions of telomeric (CCCTAA)₃-FISH-labeled and γ H2AX-labeled samples obtained by analysis of STORM data.

telomeres had proportionally higher numbers of localizations. Consistent with this, telomeres stained with TRF1 antibody gave similar size distributions, and, again, larger telomere foci had a higher number of localizations. As TRF2 depletion does not lead to rapid telomere elongation, the most straightforward interpretation of these results is that the large telomeres with a high number of localizations correspond to telomere clusters. However, we cannot fully exclude that the small subset of DDR-positive telomeres with a large R_g corresponds to decompacted telomeres that at the same time became more susceptible to labeling with the FISH probe and the TRF1 antibodies.

Our data indicate that decompaction of telomeres is not required for the telomeric DDR. On the other hand, we ob-

served a high plasticity of telomere shapes. This suggests a dynamic nature of telomeres, which may facilitate protein composition changes at telomeres in response to cell cycle, cell differentiation, or stress. We therefore favor the idea that telomeres are constantly accessible to proteins, including the checkpoint machinery, that monitor their intactness. Consistent with this model are several previous observations. A rapid exchange of GFP-tagged TRF1 and TRF2 in the second to minute scale at chromosome ends was demonstrated, supporting a dynamic model for telomeres with a constant flux of its constituents (Mattern et al. 2004). Telomerase was also shown to be able to access telomeres in S phase with high frequency (Schmidt et al. 2016). Finally, Mre11, ATM, and ATR were detected at telomeres in chromatin

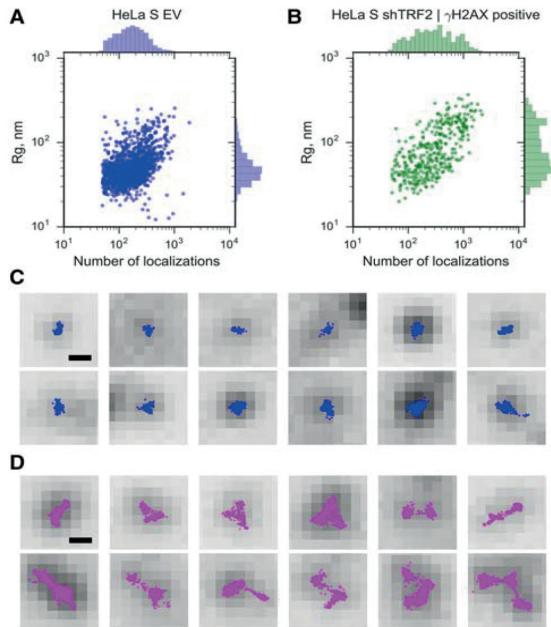


Figure 4. An increase in the size of DDR-positive telomeres of shTRF2-depleted HeLa S cells is accompanied by an increase in the number of localizations. (A) R_g (in nanometers; distribution shown at the *right*; log scale) as a function of the number of localizations (distribution is shown at the *top*; log scale) in HeLa S cells transfected with empty vector controls (EV). Each dot represents a single telomere. (B) R_g as a function of the number of localizations in HeLa S cells transfected with shTRF2 plasmids. The telomeres shown were selected as DNA damage-positive using γ H2AX as a DDR marker. Each dot represents a single telomere. (C) Randomly selected STORM images overlaid with wide-field images of γ H2AX-positive telomeres that have R_g values <80 nm. (D) Randomly selected STORM images overlaid with wide-field images of γ H2AX-positive telomeres that have R_g values >80 nm. Bar, 250 nm.

immunoprecipitation experiments from late S phase to the G2/M transition (Verdun and Karlseder 2006), where they may promote telomerase recruitment (Lee et al. 2015; Tong et al. 2015). Thus, our study and others support the notion that telomeres are physically accessible to non-telomere-bound proteins and that telomeres do not shield chromosome ends from protein access. In this regard, telomeres may not be substantially different from other regions of the genome that are characterized by dynamic nucleosomes, allowing the scanning of genome information (Hihara et al. 2012; Ricci et al. 2015).

Our data are consistent with the accompanying study by the Zhuang and de Lange laboratories (Timashev et al. 2017) in which the size of mouse telomeres was analyzed in the presence and absence of TRF1 and TRF2. These investigators also did not find evidence that DDR requires substantial chromatin decompaction when shel-

terin is compromised. However, our data and conclusions are in striking contrast to the ones put forward by the Yildiz group (Bandaria et al. 2016), who proposed that intact telomeres are excluding the checkpoint proteins because of steric hindrance from the very dense packaging. In their study, TRF1-depleted or TRF2-depleted telomeres were reported to expand up to 10-fold in volume, and, in their model, only expanded telomeres became accessible to the DDR machinery. To better facilitate comparison with other works, we reanalyzed our data using the convex hull as a readout for size (Supplemental Fig. S6). We estimated the convex hull volume by computing the convex hull areas for all of our two-dimensional (2D) clusters and raised these values to the power $3/2$. Considering that the volume increases with the third power of the radius, the

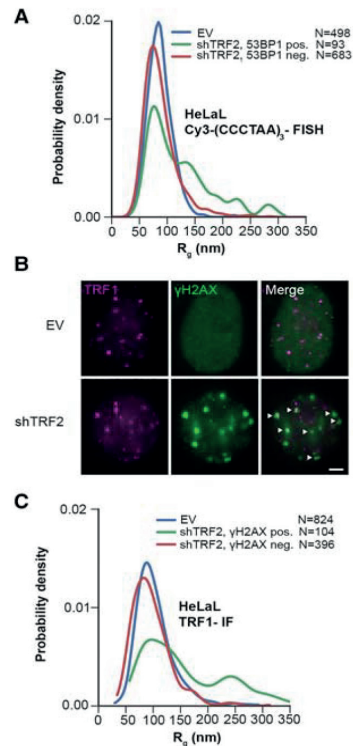


Figure 5. Measurements of HeLa L telomere sizes, labeled by FISH or anti-TRF1 IF, are consistent. (A) Representative distribution of R_g of telomeric (CCCTAA)₃-FISH-labeled and 53BP1-IF-labeled HeLa L samples obtained by analysis of STORM data. (B) Representative images for detection of γ H2AX and TRF1 at telomeres in HeLa L cells transfected with shTRF2 or empty vector (EV) plasmids. Bar, 3 μ m. Both TRF1 (purple) and γ H2AX (green) were detected by IF. Arrows indicate colocalization of telomeres, with γ H2AX used for discrimination of DDR-positive and DDR-negative telomeres. (C) Representative distribution of R_g of telomeric TRF1-IF-labeled and γ H2AX-IF-labeled HeLa L samples obtained by analysis of STORM data.

convex hull comparisons inflated relative differences between HeLa S and HeLa L telomeres and DDR-negative and DDR-positive telomeres as expected (Supplemental Fig. S6A,B). However, in analogy to the R_g comparison, the difference in mean volume of DDR-negative and DDR-positive telomeres was driven by a small subset of very large telomere foci (Supplemental Fig. S6C). Thus, while we are not able to fully explain the discrepancies between the measurements, our study includes the following major advances. First, we developed an imaging platform that allowed the analysis of an unprecedentedly large number of telomeres, providing a very high confidence on our measurements. Second, we visualized telomeric DNA by FISH or endogenous TRF1 by IF without manipulating native telomere protein composition, whereas, in the previous study (Bandaria et al. 2016), key data were acquired by photoactivated localization microscopy (PALM) imaging of cells that overexpressed mEos2-tagged versions of TRF1 and TRF2. Third, we distinguished DDR-positive and DDR-negative telomeres and analyzed them separately, allowing us to identify and characterize the more heterogeneous populations of DDR-positive telomeres. Our technical developments set the stage to study telomere compaction in various cellular states and dissect the roles of telomeric chromatin components for telomere morphology.

Materials and methods

Cell culture

HeLa cell lines harboring 11-kb-long (HeLa S) and 33-kb-long (HeLa L) telomeres were described previously (Grolimund et al. 2013). Both cell lines were maintained at 37°C with 5% CO₂ in Dulbecco's modified Eagle's medium supplemented with 10% fetal calf serum and penicillin/streptomycin.

Telomere restriction fragment length analysis

Genomic DNA was isolated using the Wizard Genomic DNA purification kit (Promega). Genomic DNA (8 µg) was subjected to restriction digestion with *Hinf*I and *Rsa*I and separated by pulse-field gel electrophoresis on 1% agarose in 0.5× TBE at 5 V cm⁻¹ for 16 h at 14°C with switch times ramped from 0.5 to 6 sec. The gel was dried for 2 h at 50°C, denatured with 0.8 M NaOH and 150 mM NaCl, neutralized with 0.5 M Tris-HCl (pH 7.0) and 1.5 M NaCl, prehybridized at 50°C in Church buffer (1% BSA, 1 mM EDTA, 0.5 M Na-phosphate buffer at pH 7.2, 7% SDS), and hybridized overnight at 50°C to a [³²P]-labeled telomeric probe as described (Grolimund et al. 2013). After hybridization, the gel was rinsed in 4× SSC followed by successive 1-h washes at 50°C in 4× SSC, 4× SSC, 0.5% SDS, 2× SSC, and 0.5% SDS. The image was acquired using a FujiFilm Fluorescent Image Analyzer (FLA-3000).

The subtelomere sequence assemblies from the Riethman laboratory at the Wistar Institute (<http://www.wistar.org/lab/haroldc-riethman-phd/page/subtelomere-assemblies>) were used to calculate the average DNA length (419 bp) contributed by subtelomeric DNA to the telomere restriction fragments following *Hinf*I and *Rsa*I cleavage.

Antibodies

The following antibodies were used: TRF1 (Abcam, ab371; a generous gift from Dr. Titia de Lange) for Western blots, TRF1 (affinity-purified rabbit antibody against recombinant TRF1 from serum no. 605 448) (Grolimund et al. 2013) for IF, TRF2 (Millipore, 05-521) for Western blots, γH2AX (Millipore, 05-636) for both Western blots and IF, hnRNPA1 (4B10; Santa Cruz Biotechnology, sc-32301) for Western blots, 53BP1 (Novus Biologicals, NB100-304) for IF, 53BP1 (Novus Biologicals, NB100-305) for Western blots, and phospho-ATM-Ser 1981 (Abcam, ab81292) for Western blots.

Plasmids

Plasmids containing shRNAs used in this study were prepared by restriction cloning of annealed oligonucleotides into pSUPER-puro or pSUPERblast plasmid backbones (Oligoengine). The target sequences of the shRNAs were TRF1 (5'-GAATATTTGG TGATCCAAA-3') cloned into pSuperPURO and TRF2 (5'-GCG CATGACAATAAGCAGA-3') pSuperBLAST (Porro et al. 2014). The pLPC_TRF2_ΔBAM plasmid (a generous gift from Dr. Titia de Lange; Addgene, plasmid 18008) was used for overexpression of TRF2ΔBAM. The pLPC-N-MYC empty plasmid (Addgene, plasmid 12540) was used as a control.

Transfection protocols

For depletion experiments, HeLa S cells were transfected in six-well plates at 60%–80% confluency using Lipofectamine 2000 according to the manufacturer's protocol (ThermoFisher, catalog no. 11668019). Puromycin (1 µg/mL; Invivogen, ant-pr-1) and 5 µg/mL blasticidin (Invivogen, ant-bl-1) were added to the medium 20–24 h after transfection, and the cells were expanded in 10-cm dishes. Selection with the two antibiotics was maintained for 4 d. Empty pSuperPURO and pSuperBLAST plasmids were used as controls in all of the experiments.

For overexpression of the TRF2ΔBAM dominant-negative mutant, HeLa S cells were transfected in six-well plates at 60%–80% confluency using Lipofectamine 2000 according to the manufacturer's protocol (ThermoFisher, catalog no. 11668019) and harvested 48 h after transfection for Western blot and microscopy experiments.

For siRNA-mediated depletion of TRF1 (Supplemental Fig. S2), HeLa S cells were transfected using a standard Ca-phosphate protocol with 0.5 pmol of siRNA at 20%–30% confluency. TRF1-specific siRNAs corresponded to a mix of several siRNAs (Santa Cruz Biotechnology, sc-36722). As a control, a nontargeting siRNA against GFP was used (sequence: 5'-GCAGCAGCACUUCUUAAGUUDtT-3'). Transfected HeLa S cells were harvested 48 h after transfection.

Telomeric PNA-FISH

FISH staining of human telomeric DNA (Celli and de Lange 2005) was performed as follows. For the analyses performed in Figure 1, E and F, HeLa S and HeLa L cells were grown on coverslips (thickness 0.17 mm ± 0.005 mm; Carl Roth, YX04.1) to 80% confluency. For the shRNA-mediated depletion experiments (Figs. 2E, 3E,D), cells were grown on coverslips and harvested for Western blot and microscopy experiments after 4 d of selection. For the overexpression experiments and siRNA-mediated depletion experiments (Supplemental Fig. S2), cells were grown on coverslips and harvested after 48 h. After harvesting, the coverslips were washed in 1× PBS, fixed with 4% formaldehyde in 1× PBS at

room temperature, permeabilized in 1× detergent solution (0.1% Triton X-100, 0.02% SDS in 1× PBS), and dehydrated with increasing amounts of ethanol (70%, 95%, and 100%). Dehydrated coverslips were then placed on slides containing 90 µL of hybridization mix [10 mM Tris-HCl at pH 7.4, 2% blocking reagent (Roche, reference no. 11096176001), 70% formamide, 0.1 µM A647-labeled (CCCTAA)₃ PNA probe (PNA Bio, F1013)] and denatured for 3 min at 80°C in a hybridization oven. Subsequently, the hybridization was allowed to proceed for 3 h in a light-protected humidified chamber at 25°C. Coverslips were removed from the slide and washed twice for 15 min in buffer containing 70% formamide and 10 mM Tris-HCl (pH 7.4) and three times for 15 min with 0.1 M Tris-HCl (pH 7.2), 0.15 M NaCl, and 0.08% Tween-20. For DNA staining, DAPI was added to 1 µg/mL in the second wash. After the washes, coverslips were stored at 4°C in 1× PBS in the dark until imaging.

Indirect IF and telomeric FISH (IF-FISH)

Indirect IF detection of human 53BP1 and γH2AX followed by telomeric FISH staining was performed as described with minor modifications (Celli and de Lange 2005). Cells were grown on coverslips (thickness 0.17 mm ± 0.005 mm [Carl Roth, YX04.1] for STORM imaging or 12 mm [Menzel-Glaser, CS12100] for confocal imaging) as described in the previous section. After harvesting, the coverslips were washed in 1× PBS, fixed with 4% formaldehyde in 1× PBS, and permeabilized in 1× detergent solution (0.1% Triton X-100, 0.02% SDS in 1× PBS). The slides were then preblocked in 2% BSA in 1× PBS, blocked for 30 min in 10% normal goat serum in 2% BSA and 1× PBS, incubated for 1 h at room temperature with either anti-53BP1 (1:2000 dilution) or anti-γH2AX (1:1000) antibody, and washed three times for 5 min in 2% BSA and 1× PBS. Alexa fluor 488-labeled goat anti-rabbit antibody (Thermo Fisher, A-11034) was used for detection of 53BP1 for STORM imaging experiments, and Alexa fluor 633-labeled goat anti-rabbit antibody (Thermo Fisher, A-21070) was used for confocal imaging experiments. Alexa fluor 488-labeled goat anti-mouse antibody (Thermo Fisher, A-11001) was used for detection of γH2AX for both STORM and confocal imaging experiments. After detection with the secondary antibody, the cells were washed three times with 1× PBS, post-fixed with 4% formaldehyde for 5 min, and dehydrated with increasing amounts of ethanol (70%, 95%, and 100%). Dehydrated coverslips were then processed in the same manner as described for the telomeric PNA-FISH procedure using a A647-(CCCTAA)₃ PNA probe (PNA Bio, F1013) for STORM imaging and a Cy3-(CCCTAA)₃ PNA probe (PNA Bio, F1002) for confocal imaging. For simultaneous detection of TRF1 and γH2AX, cells were stained as above except that dehydration and FISH steps were left out.

For the analysis of telomere dysfunction-induced foci after the IF-FISH procedure, the slides were mounted in VectaShield mounting medium (Vector Laboratories). Images were acquired using a Zeiss LSM 700 upright microscope equipped with an Axiocam MRm(B/W) camera and controlled by Zen2009 software. The images were analyzed using the Cell Counter plug-in for FIJI.

Estimation of the ratio of telomere densities of HeLa L to HeLa S

A rough estimate of the ratio of volume densities of chromatin per telomere for HeLa L and HeLa S cells may be made from the data in Figure 1. The mean $R_{g,S}$ for HeLa L and HeLa S were 0.088 µm ± 0.023 µm and 0.068 µm ± 0.021 µm (mean ± standard deviation), respectively. The average lengths for HeLa L and HeLa S were 33 kb and 11 kb, respectively. The ratio of the volume density of HeLa L telomeric chromatin, ρ_L , to HeLa S telomeric chroma-

tin, ρ_S , is therefore

$$\frac{\rho_L}{\rho_S} = \left(\frac{N_L}{R_{g,L}^3} \right) \left(\frac{R_{g,S}^3}{N_S} \right) = \left[\frac{33 \text{ kb}}{(0.088 \text{ } \mu\text{m})^3} \right] \left[\frac{(0.068 \text{ } \mu\text{m})^3}{11 \text{ kb}} \right] \approx 1.4.$$

Due to the large sample sizes, the value for the standard error of the mean R_g is <1 nm. However, sampling bias in the microscopy measurements typically leads to a variation in the observed mean of approximately ±5 nm from experiment to experiment. Taking this as the value for the error in the R_g , the upper value for the range on the estimate is

$$\frac{\rho_L^+}{\rho_S} = \left[\frac{33 \text{ kb}}{(0.088 - 0.005 \text{ } \mu\text{m})^3} \right] \left[\frac{(0.068 + 0.005 \text{ } \mu\text{m})^3}{11 \text{ kb}} \right] \approx 2.0,$$

and the lower value is

$$\frac{\rho_L^-}{\rho_S} = \left[\frac{33 \text{ kb}}{(0.088 + 0.005 \text{ } \mu\text{m})^3} \right] \left[\frac{(0.068 - 0.005 \text{ } \mu\text{m})^3}{11 \text{ kb}} \right] \approx 0.93.$$

The final estimated value for the ratio of densities of telomeric chromatin is therefore $\rho_L/\rho_S = 1.4 + 0.6/-0.5$.

STORM image acquisition

STORM imaging was performed on a custom-built STORM microscope with a 100×100-µm² FOV as described previously (Douglass et al. 2016). The large FOV of this microscope allowed for the simultaneous imaging of between ~10 and 30 nuclei; a flat illumination pattern ensured uniform fluorophore photoswitching across the FOV. For each condition and replicate, three to five FOVs were acquired, depending on the density of the cells. For the present work, an additional laser (Coherent Sapphire, 488-nm peak emission wavelength, 50 mW) was introduced into the setup to image Alexa 488 IF. A dichroic filter (Chroma, Z488bcm) was used for beam combining, and fluorescence emission in the Alexa 488 channel was filtered with a GFP emission filter (Chroma, ET525/50m).

Individual coverslips containing fixed and labeled HeLa cells were placed in a custom-built sample holder containing 1000 µL of imaging buffer (see below) supplemented with an oxygen-scavenging system. Before each STORM acquisition, a wide-field image of the FOV was acquired: one for the Alexa 647 channel (50-msec exposure time at 1.4 mW in the objective back focal plane [BFP]) and one for the Alexa 488 channel (500-msec exposure at ~0.1 mW in the objective BFP). For STORM acquisitions, 20,000 frames per FOV at 10-msec exposure time and zero inter-frame delay were acquired with ~590 mW of 647-nm laser power in the objective BFP; only the Alexa 647 channel was acquired in STORM. A 405-nm laser light was applied at frame number 10,000 and steadily ramped upward between 0 and 4.0 mW in the objective BFP through the end of the acquisition. The 405-nm laser light was applied to return Alexa 647 fluorophores to the emitting state and achieve more complete spatial sampling.

The STORM imaging buffer with oxygen-scavenging system was described previously (Olivier et al. 2013) and uses millimolar concentrations of polyunsaturated hydrocarbon cyclooctatetraene to boost photon yields during STORM imaging. All reagents were purchased from Sigma-Aldrich. The images shown in Figure 1A were taken on an inverted Nikon N-STORM microscope with a 100×/1.49 N.A. apo TIRF objective (Nikon) and an EMCCD camera (Andor, iXon3 897). A 500-mW 640-nm laser (Coherent Sapphire) and a 100-mW 402-nm laser (Coherent Sapphire) were used to induce fluorophore photoswitching and control the switching rate, respectively. Molecule localization and drift correction (using cross-correlation) for data in Figure 1A only were performed in the Nikon NIS-Elements software version

4.30.01. Before the STORM acquisition, wide-field images of the DAPI and Cy5 channels were acquired. The probe used in this experiment was the Cy5-(CCCTAA)₃ PNA probe (Eurogentec, PN-TC055-005), and the DNA was labeled with DAPI. The oxygen-scavenging system used for STORM imaging was glucose oxidase/catalase-based and prepared as described previously (Olivier et al. 2013).

Filtering and cluster analysis of STORM data

The filtering and analysis pipeline used in this work consists of seven discrete steps that were applied to each FOV individually (Supplemental Fig. S1). Unless otherwise stated, analyses were performed in a custom-written Python analysis library (B-Store, versions 0.1.1 and 0.2.0; <https://github.com/kmdouglass/bstore>) for Python 3.5.

Computing localizations from raw image stacks

Input data for the analysis pipeline originated from STORM acquisitions and consisted of stacks of images of single fluorescent molecules labeling the telomeric DNA. All STORM image stacks in this study contained 20,000 frames recorded at 10-msec exposure times with zero delay between each frame. Image stacks were saved to a disk during acquisition as multipage tagged image format (TIF) files; each frame was represented as a 2D array of pixels whose intensities (in analog to digital units) were stored as 16-bit integers. Square subregions that potentially contained single molecules were segmented from each frame using a peak-finding algorithm that incorporated a sCMOS camera-specific noise model and used a difference of smoothing filters followed by a local maximum filter (Huang et al. 2011). Localizations (i.e., estimates of single fluorophore positions in each camera frame) were determined with subpixel accuracy in the candidate regions using a previously described sCMOS camera-specific maximum likelihood estimator fitting algorithm (Huang et al. 2013). Both of these steps were implemented in MATLAB 2014a and CUDA 4.0. We used the values shown in Table 1 for the input parameters for the segmentation and fitting algorithms in all data sets.

Optimal values for the filter sizes and the peak threshold were determined by simultaneously varying their values and visually inspecting a small number of frames from an image stack until the majority of fluorescent spots was successfully identified. The pixel size was determined by focusing on 100-nm-diameter TetraSpeck fluorescent beads emitting light in the Alexa 647 channel (Life Technologies), depositing the beads on a coverslip, and immersing them in deionized water using the pixel size calibration routine in Micro-Manager (version 1.4.22, nightly build 2015-07-27) (Edelstein et al. 2014). Frames earlier than frame 500 were not processed because too many molecules were still emitting to allow for their accurate localization at these times. All other parameters retained their default values.

Drift correction

Axial drift was corrected during acquisition to ~10-nm standard deviation using a TIR laser-based active autofocus method as described previously (Douglass et al. 2016) and the pgFocus open hardware autofocus module (<http://big.umassmed.edu/wiki/index.php/PgFocus>). Localizations were corrected for lateral drift using 100-nm-diameter gold fiducial beads (corpuscular, 5.6 × 10⁹ particles per milliliter) that were first diluted 1:1 in 100 µg/mL poly-L-lysine (Sigma-Aldrich) to promote adhesion to the cell membrane. Prior to imaging, 200 µL of the bead suspension was pipetted onto the coverslips, allowed to sit for 5 min, and then

gently washed once with phosphate-buffered saline before coverslips were immersed in STORM imaging buffer.

Localizations originating from fiducial beads were identified in the localization data sets by rendering 2D histograms with 1 × 1 µm² bin sizes and manually selecting bins containing a number of localizations that was approximately equivalent to the number of frames in the image stacks. For each region, tracks of the *x* and *y* positions of the localizations versus camera frames were fit with a weighted cubic smoothing spline using a Gaussian smoothing filter for weighting whose standard deviation was typically equivalent to 200 frames and whose window size was 800 frames. These numbers were varied slightly on a case-by-case basis if spline fits were poor. The resulting splines for each fiducial track were averaged together to form a final drift trajectory and correct the localizations in that particular FOV. FOVs that contained no good fiducials were discarded from the analysis.

Filtering and merging localizations

Localizations with precision estimated by the fitting algorithm to be >30 nm and log likelihood ratios >250 were discarded from the analysis. (The log likelihood ratio is a measure of how closely a single-molecule image resembles a 2D Gaussian point spread function [PSF] model.) The value for the localization precision filter was chosen to be approximately three times the measured localization precision (Supplemental Fig. S1); with this value, ~99% of all localizations corresponding to a single fluorescent molecule should be retained when their emissions are well separated in time. The maximum log likelihood was selected by varying its value and observing scatter plots of localizations overlaid on the wide-field images. An optimal value struck a balance between rejecting localizations that did not overlap with any features in the wide-field images and accepting all localizations originating from the telomeres.

Because we performed 2D STORM imaging to obtain as high a localization precision as possible, we removed localizations whose fitted PSF images had widths >175 nm (standard deviation of the 2D Gaussian). This ensured that only localizations coming from a focal volume of small axial extent were retained for analysis. The average width of all localizations prior to filtering was typically ~150 nm. After filtering, localizations were merged along the time dimension to reduce stochasticity in the spatial sampling of the telomeres due to rapid blinking of the Alexa 647 molecules, whose off-time distribution displayed two behaviors: a short pronounced peak at the origin and a long tail comprised of relatively few events (Supplemental Fig. S1). The merge radius was set to 30 nm (or three times the measured

Table 1. Input parameters for segmentation and fitting algorithms

Parameter	Values
Smoothing filter size 1	9 × 9 pixels ²
Smoothing filter size 2	3 × 3 pixels ²
Local maximum filter size	5 × 5 pixels ²
Localization region of interest size	7 × 7 pixels ²
Peak rejection threshold	50
Number of iterations for Newton-Raphson fitting routine	50
Pixel size	108 nm
Minimum frame number	500
Fitting routine	Single emitter (low density)

mean localization precision), and the gap time was set to one frame to balance the rapid blinking behavior against the chance to erroneously merge localizations from distinct molecules. This meant that a track of localizations could disappear and reappear for at most one frame and still be merged into a single localization. Merging was performed using a Python implementation of the Crocker-Grier tracking algorithm (Trackpy version 0.3.0; <http://doi.org/10.5281/zenodo.34028>).

Spatial clustering

Localizations were spatially clustered using the DBSCAN clustering algorithm (Martin et al. 1996) from scikit-learn (version 0.17.1). The minimum number of localizations per cluster was set to eight, and the neighborhood radius was set to 90 nm. These values were determined by varying them and simultaneously observing the results of the clustering of localizations overlaid on a corresponding wide-field image. Ideal values did not erroneously group distinct clusters of localizations that originated from separate telomere signals into single clusters; ideal values also did not break up distinct clusters into multiple subclusters.

After clustering, we removed clusters with <50 localizations because these clusters very often did not overlap a feature in the wide-field images as described below.

Alignment to wide-field images

Each set of clustered localizations was binned into a separate 2D histogram with bin side lengths of ~22 nm. The corresponding wide-field fluorescence images in the Alexa 647 channel were upsampled five times to the same pixel size (22 nm) and cross-correlated with the localization histograms using a fast Fourier transform-based implementation (fftconvolve method from Scipy version 0.17.1) to determine and correct any offset between the localizations and the wide-field images. We typically observed an offset that was between 40 and 60 nm in each direction that was attributed to both the stage drift and the drift correction procedure described above. The calculated offsets were applied to the localizations to ensure that they were correctly overlaid on top of their corresponding features in the wide-field images in the next steps of the analysis pipeline.

Wide-field images in the Alexa 488 and Alexa 647 channels were acquired in quick succession so that stage drift between the two acquisitions was effectively zero. We therefore used the same offsets as determined above to overlay the localizations on the wide-field images from the Alexa 488 channel. A small axial displacement of the piezo stage of 0.6 μm was made between channels to correct axial chromatic aberration. Due to the large sizes of the 53BP1 and γH2AX loci, we did not observe the need to correct transverse chromatic aberrations to determine the overlap of a telomeric STORM signal with a DDR locus (Fig. 3B).

Manual cluster rejection

To ensure that each cluster of localizations was telomeric in origin, we performed a semiautomated filtering step for every FOV. Clusters of localizations were overlaid on top of the wide-field images [after applying the offsets described above] and presented one-by-one to the analyst. The analyst chose to keep or reject each cluster based on the following criteria: (1) Clusters were located on top of a fluorescent locus. (2) Clusters were located inside a cell nucleus. (3) The shape of the cluster roughly matched the shape of the corresponding wide-field locus. After each decision, the analysis software recorded the results and automatically progressed to the next cluster. This step was per-

formed with the custom-written Python analysis library described above.

Manual cluster classification

For experiments in which we determined whether a 53BP1 or γH2AX signal was present at any given telomere, the manually filtered clusters of localizations were overlaid on top of the wide-field image from the Alexa 488 channel (applying the lateral offset as described above). Each telomere was then manually classified into one of three groups: (1) no overlap of the cluster with an Alexa 488 locus, (2) partial spatial overlap of the cluster with an Alexa 488 locus, and (3) complete spatial overlap of the cluster with an Alexa 488 locus. Once again, the custom software for this semiautomated analysis is at the URL above.

Data availability

All original data are available from the Dryad Digital Repository (<http://dx.doi.org/10.5061/dryad.h1157>).

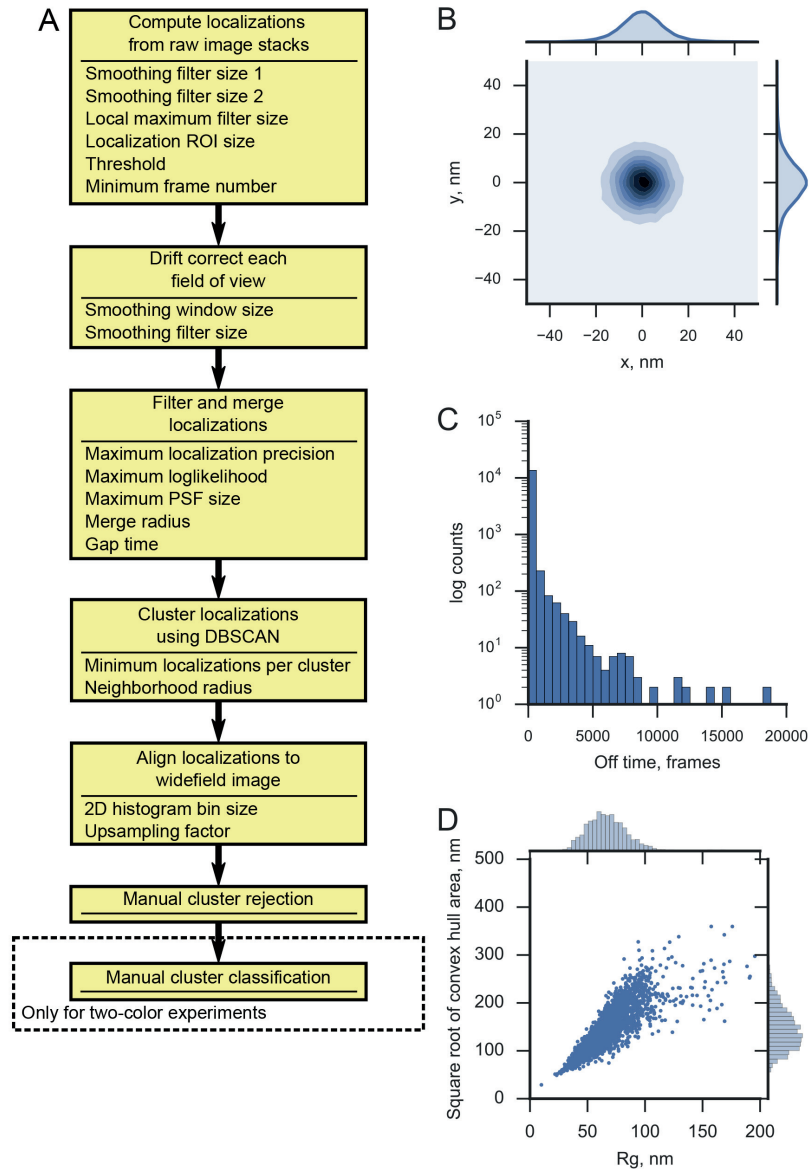
Acknowledgments

We thank Titia de Lange for generously providing material and sharing unpublished results prior to publication. We thank Larissa Grolimund for exploratory STORM experiments, and the École Polytechnique Fédérale de Lausanne (EPFL) Bioimaging and Optics Facility for technical support. Research in J.L.'s laboratory was supported by the Swiss National Science Foundation (SNSF), the SNSF-funded National Center of Competence in Research RNA and Disease Network, an Initial Training Network (ITN) grant (CodeAge) from the European Commission's Seventh Framework Programme (grant agreement no. 316354), the Swiss Cancer League, and EPFL. Research in S.M.'s laboratory was supported by a European Research Council starting grant (grant agreement no. 243016), the Swiss National Science Foundation, and EPFL. K.M.D. is supported by a SystemsX.ch Transition Post-Doc Fellowship. All authors contributed to experimental design. A.V. and V.P. acquired the STORM data and performed the molecular biological experiments. K.M.D. performed the data analysis. J.L., with contributions from all authors, wrote the main text. K.M.D. and A.V. wrote the Materials and Methods.

References

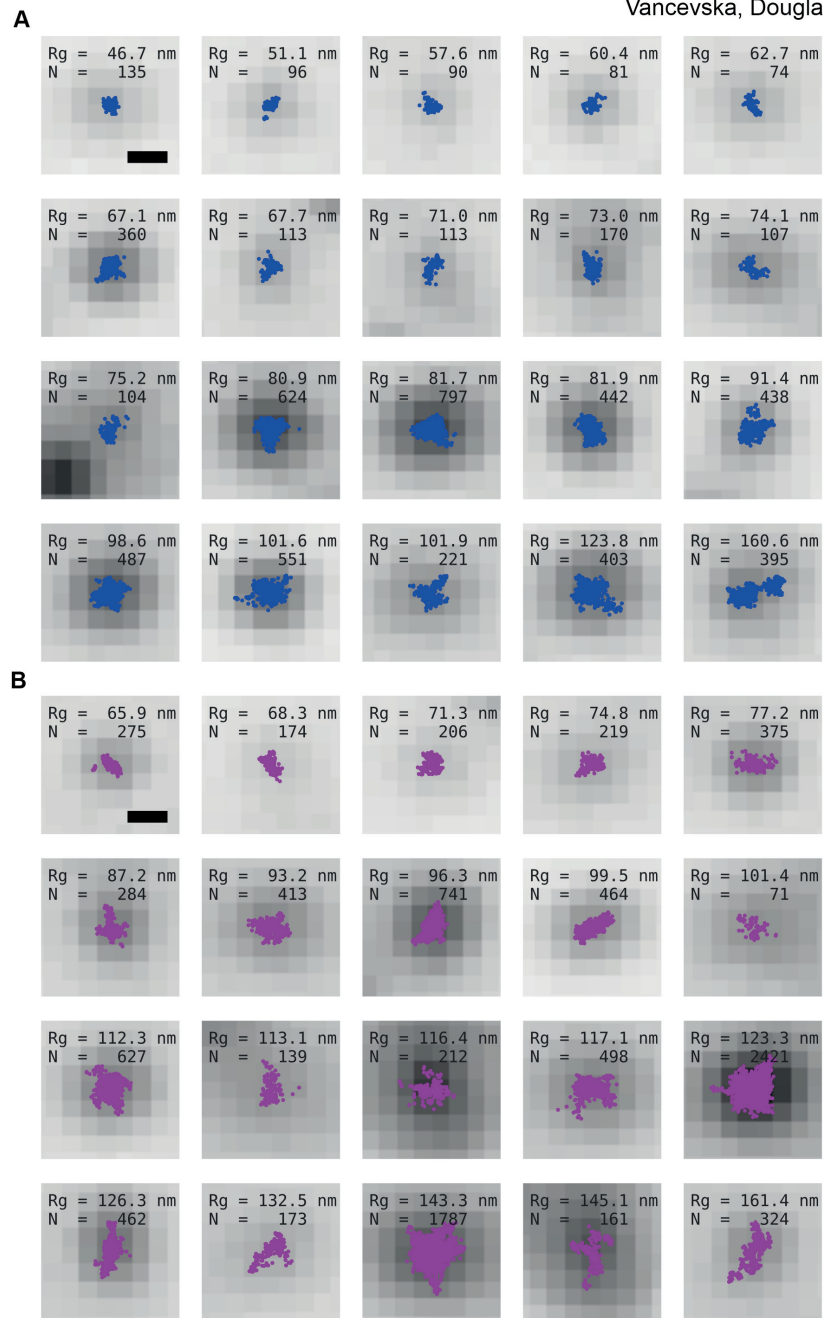
- Bandaria JN, Qin P, Berk V, Chu S, Yildiz A. 2016. Shelterin protects chromosome ends by compacting telomeric chromatin. *Cell* **164**: 735–746.
- Bartocci C, Diedrich JK, Ouzounov I, Li J, Pionti A, Pasini D, Yates JR III, Lazzarini Denchi E. 2014. Isolation of chromatin from dysfunctional telomeres reveals an important role for Ring1b in NHEJ-mediated chromosome fusions. *Cell Rep* **7**: 1320–1332.
- Baumann P, Cech T. 2001. Pot1, the putative telomere end-binding protein in fission yeast and humans. *Science* **292**: 1171–1175.
- Benarroch-Popivker D, Pisano S, Mendez-Bermudez A, Lototska L, Kaur P, Bauwens S, Djerbi N, Latrick CM, Fraissier V, Pei B, et al. 2016. TRF2-mediated control of telomere DNA topology as a mechanism for chromosome-end protection. *Mol Cell* **61**: 274–286.

- Celli GB, de Lange T. 2005. DNA processing is not required for ATM-mediated telomere damage response after TRF2 deletion. *Nat Cell Biol* **7**: 712–718.
- Cristofari G, Lingner J. 2006. Telomere length homeostasis requires that telomerase levels are limiting. *EMBO J* **25**: 565–574.
- Dejardin J, Kingston RE. 2009. Purification of proteins associated with specific genomic loci. *Cell* **136**: 175–186.
- de Lange T. 2005. Shelterin: the protein complex that shapes and safeguards human telomeres. *Genes Dev* **19**: 2100–2110.
- de Lange T. 2009. How telomeres solve the end-protection problem. *Science* **326**: 948–952.
- Denchi EL, de Lange T. 2007. Protection of telomeres through independent control of ATM and ATR by TRF2 and POT1. *Nature* **448**: 1068–1071.
- Denchi EL, Sfeir A. 2016. Stop pulling my strings—what telomeres taught us about the DNA damage response. *Nat Rev Mol Cell Biol* **17**: 364–378.
- Doksani Y, Wu JY, de Lange T, Zhuang X. 2013. Super-resolution fluorescence imaging of telomeres reveals TRF2-dependent T-loop formation. *Cell* **155**: 345–356.
- Douglass KM, Sieben C, Archetti A, Lambert A, Manley S. 2016. Super-resolution imaging of multiple cells by optimised flat-field epi-illumination. *Nat Photonics* **10**: 705–708.
- Edelstein AD, Tsuchida MA, Amodaj N, Pinkard H, Vale RD, Stuurman N. 2014. Advanced methods of microscope control using muManager software. *J Biol Methods* **1**: e10.
- Griffith JD, Comeau L, Rosenfield S, Stansel RM, Bianchi A, Moss H, de Lange T. 1999. Mammalian telomeres end in a large duplex loop. *Cell* **97**: 503–514.
- Grolimund L, Aeby E, Hamelin R, Armand F, Chiappe D, Montatte M, Lingner J. 2013. A quantitative telomeric chromatin isolation protocol identifies different telomeric states. *Nat Commun* **4**: 2848.
- Hihara S, Pack CG, Kaizu K, Tani T, Hanafusa T, Nozaki T, Takemoto S, Yoshimi T, Yokota H, Imamoto N, et al. 2012. Local nucleosome dynamics facilitate chromatin accessibility in living mammalian cells. *Cell Rep* **2**: 1645–1656.
- Huang F, Schwartz SL, Byars JM, Lidke KA. 2011. Simultaneous multiple-emitter fitting for single molecule super-resolution imaging. *Biomed Opt Expr* **2**: 1377–1393.
- Huang F, Hartwich TM, Rivera-Molina FE, Lin Y, Duim WC, Long JJ, Uchil PD, Myers JR, Baird MA, Mothes W, et al. 2013. Video-rate nanoscopy using sCMOS camera-specific single-molecule localization algorithms. *Nat Methods* **10**: 653–658.
- Karlseder J, Hoke K, Mirzoeva OK, Bakkenist C, Kastan MB, Petrini JH, de Lange T. 2004. The telomeric protein TRF2 binds the ATM kinase and can inhibit the ATM-dependent DNA damage response. *PLoS Biol* **2**: E240.
- Lambert TJ, Waters JC. 2017. Navigating challenges in the application of superresolution microscopy. *J Cell Biol* **216**: 53–63.
- Lee JH, Paull TT. 2005. ATM activation by DNA double-strand breaks through the Mre11–Rad50–Nbs1 complex. *Science* **308**: 551–554.
- Lee SS, Bohrsen C, Pike AM, Wheelan SJ, Greider CW. 2015. ATM kinase is required for telomere elongation in mouse and human cells. *Cell Rep* **13**: 1623–1632.
- Martin ES, Kriegel H-P, Sander J, Xu X. 1996. A density-based algorithm for discovering clusters in large spatial databases with noise. *Kdd* **96**: 226–231.
- Mattern KA, Swiggers SJ, Nigg AL, Lowenberg B, Houtsmuller AB, Zijlmans JM. 2004. Dynamics of protein binding to telomeres in living cells: implications for telomere structure and function. *Mol Cell Biol* **24**: 5587–5594.
- Okamoto K, Bartocci C, Ouzounov I, Diedrich JK, Yates JR III, Denchi EL. 2013. A two-step mechanism for TRF2-mediated chromosome-end protection. *Nature* **494**: 502–505.
- Olivier N, Keller D, Gonczy P, Manley S. 2013. Resolution doubling in 3D-STORM imaging through improved buffers. *PLoS One* **8**: e69004.
- Poon SS, Lansdorp PM. 2001. Quantitative fluorescence in situ hybridization (Q-FISH). *Curr Protoc Cell Biol* **12**: 18.4.1–18.4.21.
- Porro A, Feuerhahn S, Delafontaine J, Riethman H, Rougemont J, Lingner J. 2014. Functional characterization of the TERRA transcriptome at damaged telomeres. *Nat Commun* **5**: 5379.
- Ricci MA, Manzo C, Garcia-Parajo MF, Lakadamyali M, Cosma MP. 2015. Chromatin fibers are formed by heterogeneous groups of nucleosomes in vivo. *Cell* **160**: 1145–1158.
- Rust MJ, Bates M, Zhuang X. 2006. Sub-diffraction-limit imaging by stochastic optical reconstruction microscopy (STORM). *Nat Methods* **3**: 793–795.
- Schmidt JC, Zaug AJ, Cech TR. 2016. Live cell imaging reveals the dynamics of telomerase recruitment to telomeres. *Cell* **166**: 1188–1197 e1189.
- Sfeir A, Kosiyatrakul ST, Hockemeyer D, MacRae SL, Karlseder J, Schildkraut CL, de Lange T. 2009. Mammalian telomeres resemble fragile sites and require TRF1 for efficient replication. *Cell* **138**: 90–103.
- Timashev LA, Babcock H, Zhuang X, de Lange T. 2017. The DDR at telomeres lacking intact shelterin does not require substantial chromatin decompaction. *Genes Dev* (this issue). doi: 10.1101/gad.294108.116.
- Tong AS, Stern JL, Sfeir A, Kartawinata M, de Lange T, Zhu XD, Bryan TM. 2015. ATM and ATR signaling regulate the recruitment of human telomerase to telomeres. *Cell Rep* **13**: 1633–1646.
- Uziel T, Lerenthal Y, Moyal L, Andegeko Y, Mittelman L, Shiloh Y. 2003. Requirement of the MRN complex for ATM activation by DNA damage. *EMBO J* **22**: 5612–5621.
- van Steensel B, Smogorzewska A, de Lange T. 1998. TRF2 protects human telomeres from end-to-end fusions. *Cell* **92**: 401–413.
- Verdun RE, Karlseder J. 2006. The DNA damage machinery and homologous recombination pathway act consecutively to protect human telomeres. *Cell* **127**: 709–720.
- Zimmermann M, Kibe T, Kabir S, de Lange T. 2014. TRF1 negotiates TTAGGG repeat-associated replication problems by recruiting the BLM helicase and the TPP1/POT1 repressor of ATR signaling. *Genes Dev* **28**: 2477–2491.
- Zou L, Elledge SJ. 2003. Sensing DNA damage through ATRIP recognition of RPA–ssDNA complexes. *Science* **300**: 1542–1548.



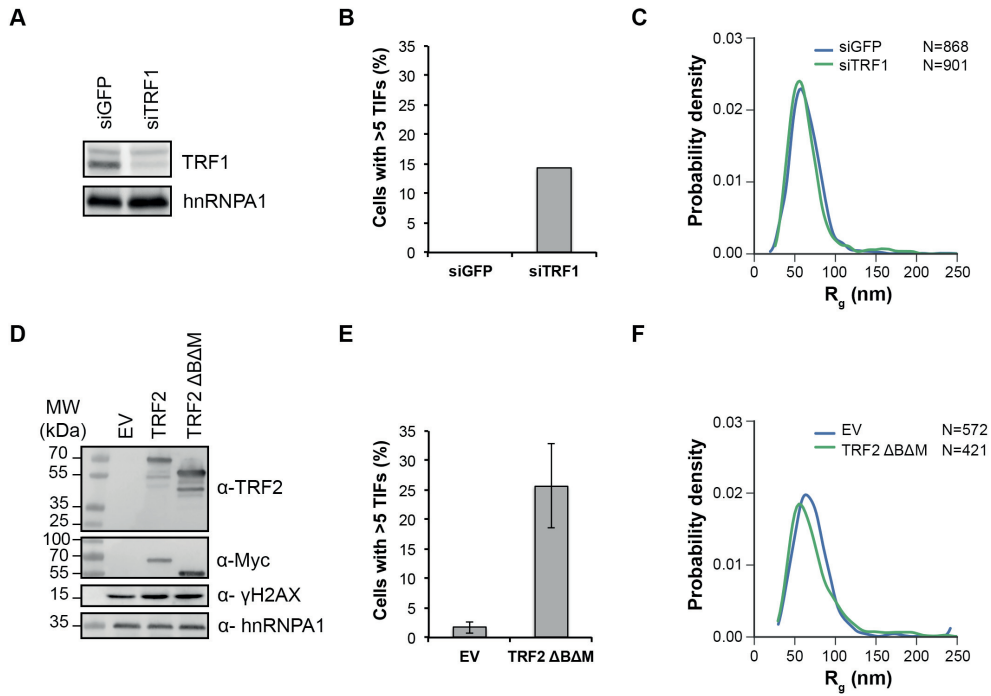
Supplemental Figure S1: Processing pipeline and supplemental data for STORM cluster analyses.

(A) The processing pipeline consists of six (possibly seven) steps that require setting values for the parameters described in the text. (B) 2D kernel density estimate of overlapped clusters of localizations from individual AlexaFluor 647 dye molecules conjugated to PNA oligonucleotides (5'-CCCTAA-3')₃, sparsely distributed on a coverslip in imaging buffer, and imaged using the STORM acquisition parameters described in the text. The 10 nm localization precision is the standard deviation of the distribution in each direction. (C) Off-time distribution of the AlexaFluor 647 molecules shows a strong propensity of the dye to blink rapidly. (D) The convex hull area and the radius of gyration (Rg) both measure the size of a cluster of localizations. Data are taken from HeLa S telomeres (Figure 1).



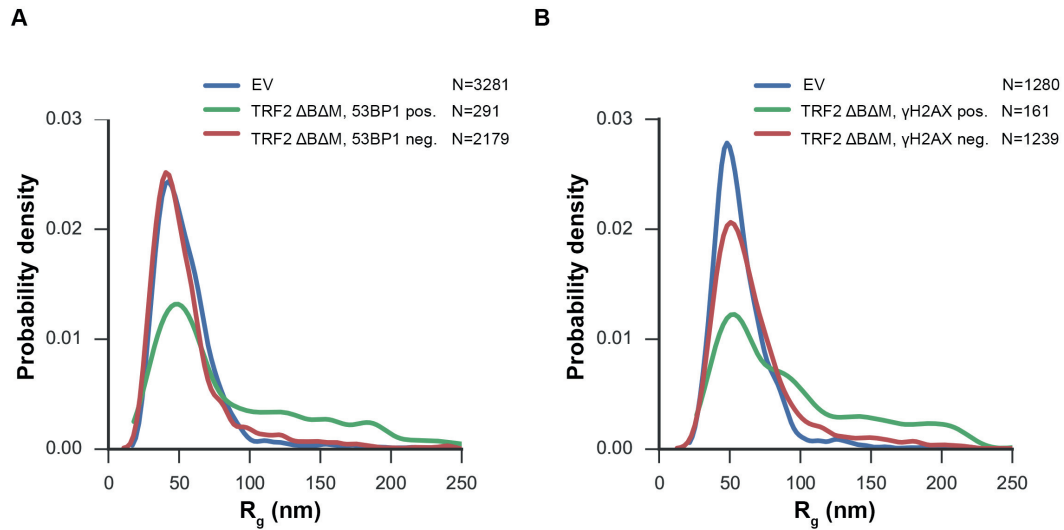
Supplemental Figure S2: Visual comparison of telomeres from populations with different mean lengths.

(A) Scatter plots of localizations overlaid on the corresponding widefield images of twenty telomeres drawn randomly from the HeLa S population of Figure 1. (B) Twenty clusters randomly drawn from the HeLa L population of Figure 1. Rg: radius of gyration. N: number of localizations. Scale bars: 250 nm.



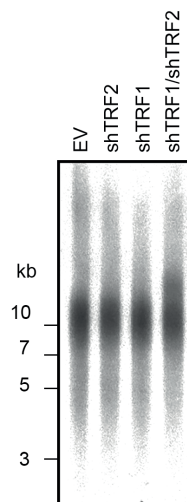
Supplemental Figure S3: Depletion of shelterin proteins TRF1 and TRF2 does not affect telomere size in HeLaS cells.

(A) Western Blot analysis of TRF1 and hnRNPA1 in HeLaS cells transfected with the indicated siRNAs (siGFP and siTRF1). (B) Quantification of the number of cells containing >5 telomere dysfunction induced foci (TIFs) detected as in Figure 2B. Data represent mean of 1 independent experiment (>200 cells/condition/experiment). (C) Distributions of R_g of telomeric (CCCTAA)₃-FISH labeled samples obtained by analysis of STORM data. (D) Western Blot analysis of TRF2, Myc, γ H2AX and hnRNPA1 in HeLaS cells transfected with TRF2 Δ B Δ M and empty vector (EV) control. (E) Quantification of the number of cells containing >5 telomere dysfunction induced foci (TIFs) detected as in Figure 2B. Data represent mean of 2 independent experiments (>190 cells/condition/experiment). (F) The same as in (C) but for TRF2 Δ B Δ M transfected cells.

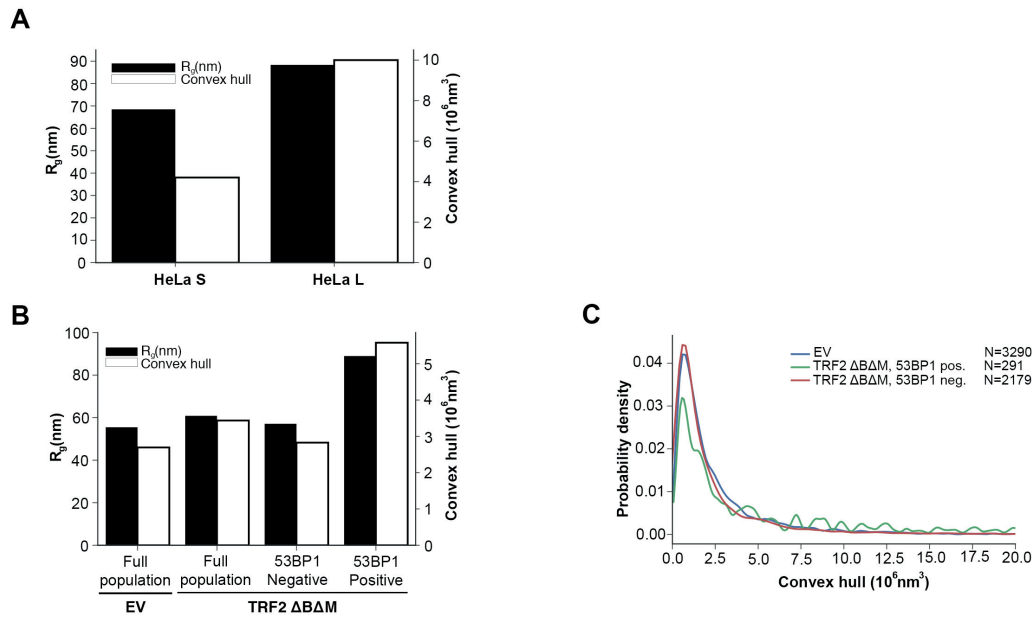


Supplemental Figure S4: Selection of DDR positive telomeres of TRF2 Δ B Δ M transfected HeLa S cells with two markers (53BP1 and γ H2AX) reveals increase in telomeres size in only a small subset of telomeres.

(A) Representative R_g distributions of telomeric (CCCTAA)₃-FISH and 53BP1 labeled samples obtained by analysis of STORM data in HeLaS cells transfected with TRF2 Δ B Δ M and empty vector control (EV). (B) Representative R_g distributions of telomeric (CCCTAA)₃-FISH and γ H2AX labeled samples obtained by analysis of STORM data in HeLaS transfected with TRF2 Δ B Δ M and empty vector control (EV).



Supplemental Figure S5: Telomere restriction fragment (TRF) length analysis of HeLaS cells depleted for TRF1 and TRF2.



Supplemental Figure S6: Comparison of radius of gyration and convex hull measurements of telomere size.

(A) Average radius of gyration (R_g) and average convex hull volume of telomeric (CCCTAA)₃-FISH labeled HeLaS and HeLaL cell lines obtained by analysis of STORM data shown in Figure 1. (B) Average radius of gyration (R_g) and average convex hull volume of telomeric (CCCTAA)₃-FISH and 53BP1 labeled samples obtained by analysis of STORM data in HeLaS transfected with TRF2 $\Delta B\Delta M$ and empty vector control (EV). Data shown is from experiment in Supplementary Figure S4. (C) Representative convex hull distributions of telomeric (CCCTAA)₃-FISH and 53BP1 labeled samples obtained by analysis of STORM data in HeLaS cells transfected with TRF2 $\Delta B\Delta M$ and empty vector control (EV).

2.4 Appendix to Chapter 2

As already mentioned previously in the text SMCHD1 and LRIF1 are two proteins that are among other things involved in X-chromosome compaction (Nozawa et al., 2013). They mediate the compacted state by bridging H3K9me3 and H3K27me3 regions and bringing them closer together thus establishing a higher order chromatin structure. Stimulated by this fact and by the fact that these proteins were found to be enriched at extremely long telomeres (Grolimund et al., 2013) that are enriched for H3K9me3 and H3K27me2 heterochromatin marks (see below) we set out to investigate if SMCHD1 is required for maintaining the compacted state of telomeres. We used the STORM-based method to calculate the Radius of Gyration (R_G) of telomeres that are depleted for SMCHD1 and SMCHD1 and TRF2. We have not observed major changes in compaction upon SMCHD1 removal alone or together with TRF2 in HeLa S cells (Figure 1) and HeLaL cells (not presented). In addition, removal of LRIF1 by siRNA as well did not affect the compaction state of telomeres (Verena Pfeiffer, unpublished).

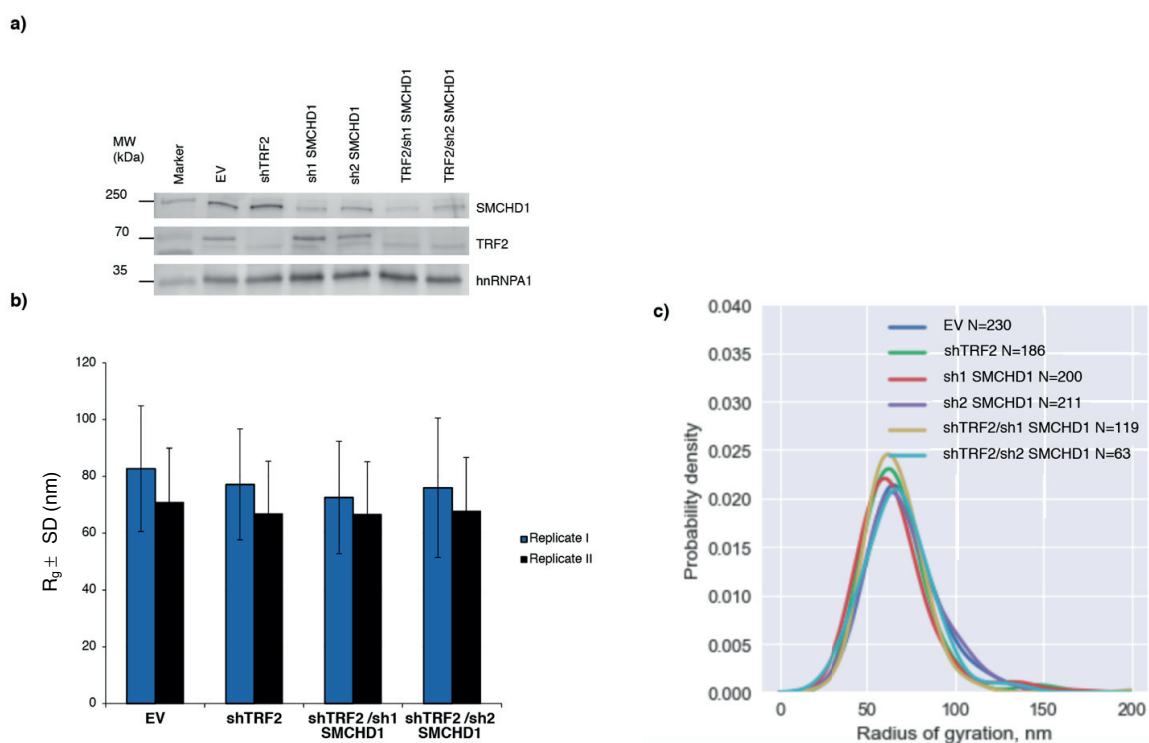
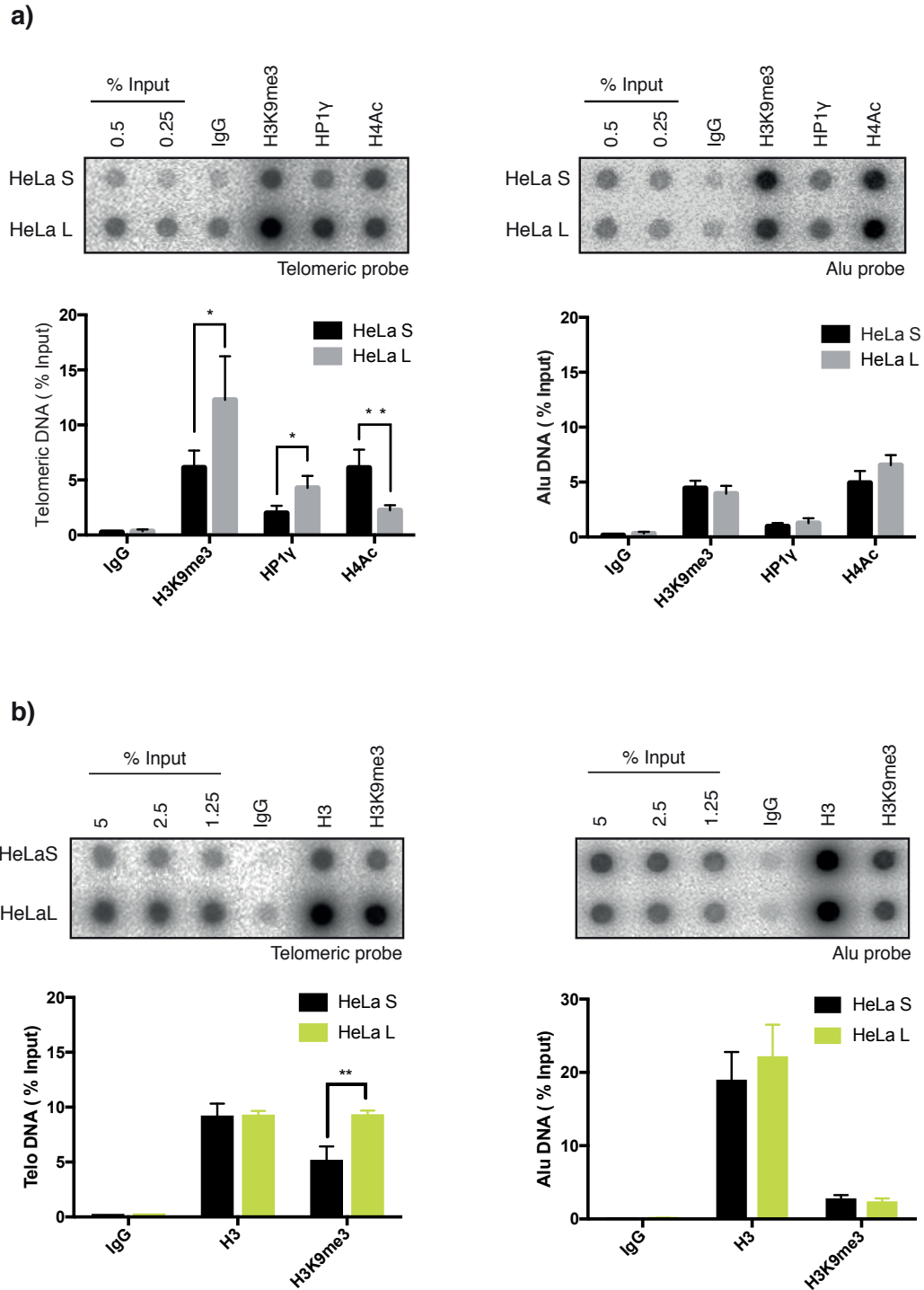


Figure 1. Depletion of SMCHD1 does not affect telomere size in HeLaS cells. A) Western blot analysis of SMCHD1, TRF2 and hnRNPA1 in HeLa cells transfected with the indicated shRNAs (shTRF2, sh1 SMCHD1, sh2 SMCHD1, shTRF2/sh1 SMCHD1, shTRF2/sh2 SMCHD1) or empty vector (EV) control. B) Average R_g of telomeric (CCCTAA)₃-FISH labeled samples obtained by analysis of STORM data. Data represent the mean of Radius of Gyration (R_G) in nanometers of two independent experiments. Error bars represent the standard deviation. C) Representative distributions of R_g of telomeric (CCCTAA)₃-FISH labeled samples obtained by analysis of STORM data.

Interested to characterize the compaction state of short (10kb) and long telomeres (30kb) we have performed ChIP experiments to detect heterochromatin marks in order to complement the STORM experiments published previously. We have observed that telomeres in HeLa L cells are enriched for heterochromatic mark H3K9me3 and binding of HP1 γ while being less abundant in H4Acethyl which is a mark of transcriptionally active chromatin. Our data suggest that long telomeres might be more heterochomatized than short ones and possibly more compacted (Figure 2).



Chapter 3 SMCHD1 and LRIF1 promote ATM-dependent DNA Damage signaling and repair of uncapped telomeres

Aleksandra Vancevska, Verena Pfeiffer, Joachim Lingner (manuscript in preparation)

3.1 Abstract

“SMCHD1 (structural maintenance of chromosomes flexible hinge domain containing protein 1) has been implicated in X-chromosome inactivation, imprinting and DNA damage repair. Mutations in *SMCHD1* can also cause facioscapulohumoral muscular dystrophy. More recently, SMCHD1 and its interacting partner and heterochromatin protein 1 (HP1) binding protein LRIF1/HBiX1 (ligand-dependent nuclear receptor interacting-factor 1) have also been detected as component of telomeric chromatin. Here, we identify requirements of SMCHD1 and LRIF1 for DNA damage signaling and non-homologous end joining (NHEJ) at unprotected telomeres. Co-depletion of SMCHD1 or LRIF1 with TRF2 reduced the rate of 3' overhang removal in time course experiments and the number of telomere end fusions. In SMCHD1 deficient cells, the formation of ATM pS1981, γ H2AX and 53BP1 containing telomere dysfunction induced foci (TIFs) were diminished indicating defects in checkpoint signaling. Strikingly, removal of TPP1 and subsequent activation of ATR signaling rescued telomere fusion events in TRF2-depleted *SMCHD1* knockout cells. Together, these data indicate that SMCHD1 depletion reduces telomere fusions in TRF2-depleted cells due defects in ATM-dependent DNA checkpoint signaling. SMCHD1 mediates DNA damage signaling activation upstream of ATM at uncapped telomeres.”

3.2 Highlights

- SMCHD1 is recruited to dysfunctional telomeres
- SMCHD1 KD/KO and LRIF1 KD lead to impaired c-NHEJ and reduction in the number of telomere fusions upon TRF2 removal
- SMCHD1 KO reduces the rate of 3'-overhang processing after telomere uncapping
- SMCHD1 is required formation of ATM pS1981, γ H2AX and 53BP1 containing telomere dysfunction induced foci (TIFs)
- Removal of TPP1 and activation of ATR dependent DNA damage signaling reinstates telomere fusions in SMCHD1 KO cells

3.3 Author contributions

J.L., A.V. and V.P. designed research, A.V. and V.P. carried out the experiments with transient depletion of SMCHD1, A.V. constructed the SMCHD1 KO cell lines and carried out the experiments in those, and J.L. and A.V. wrote the paper.

Introduction

Arguably the most fundamental function of telomeres is to suppress at chromosome ends DNA damage signaling and DNA end repair (Muller 1938, McClintock 1941). This is achieved through the recruitment of specialized proteins that bind directly or indirectly to telomeric repeat DNA, which consists of hundreds to thousands of 5'-TTAGGG-3'/5'-CCCTAA-3' repeats in vertebrates. Most abundant at telomeres are the shelterin proteins comprising TRF1, TRF2, RAP1, TIN2, TPP1 and POT1 (de Lange 2009; Denchi and Sfeir 2016). TRF1 and TRF2 bind as homodimers to the double stranded telomeric DNA repeats. Depletion of TRF2 from chromosome ends occurs naturally upon telomere shortening in senescent cells (Karlseder et al. 2002; Cesare et al. 2013). TRF2 depletion leads to ATM kinase activation and a long-lasting DNA damage response (DDR) promoting cellular senescence (Denchi and de Lange 2007). Inactivation of the DDR in senescent cells occurs during tumorigenesis (Shay and Wright 2011; Maciejowski and de Lange 2017). The ensuing cell proliferation leads to further telomere shortening and further TRF2 depletion culminating in telomere crisis in which chromosome ends are fused to one another by alternative nonhomologous DNA end joining (alt-NHEJ), which relies on DNA ligase 3 and poly(ADP-ribose) polymerase 1 (PARP1) (Jones et al. 2014). Experimental depletion of TRF2 in cells with normal telomere length also leads to ATM-dependent DDR activation and telomere end joining, which in this case is mediated by the classical NHEJ pathway involving DNA ligase 4 and the KU70/80 heterodimer (Celli and de Lange 2005). Significantly, classical NHEJ at TRF2-depleted telomeres requires DDR activation (Denchi and de Lange 2007).

The DDR promotes genome stability regulating DNA repair, chromatin remodeling, transcription, cell cycle arrest, senescence and apoptosis (Ciccia and Elledge 2010; Panier and Durocher 2013). DDR activation at DNA double strand breaks and uncapped telomeres involves ATM recruitment to chromatin by the MRE11/RAD50/NBS1 (MRN) complex, which also promotes conformational changes stimulating ATM kinase activity (Paull 2015). In addition to the interaction with NBS1 in the MRN complex, ATM activation also depends on Tip60/KAT5-dependent acetylation of K3016 in ATM (Sun et al. 2009; Kaidi and Jackson 2013). Active ATM leads to autophosphorylation at S1981 and phosphorylation and activation of hundreds of downstream DDR substrates (Matsuoka et al. 2007), such as the CHK2 kinase, p53, NBS1, 53BP1, and H2AX.

SMCHD1 is a non-canonical member of the structural maintenance of chromosomes (SMC) protein family (Blewitt et al. 2008), which includes among others the SMC1/3 cohesion and SMC2/4 condensin complex components, the SMC5/6 complex which is involved in homologous recombination and RAD50. As other SMC proteins, SMCHD1 contains a hinge domain flanked by coiled-coil domains. However, unlike SMC1-6, SMCHD1 forms homodimers (Brideau et al. 2015). Furthermore, it contains a GHKL (gyrase, Hsp90, histidine kinase, MutL)-type ATPase rather than the bipartite ABC-type ATPase domain typically seen in SMC proteins (Brideau et al. 2015). SMCHD1 physically associates with LRIF1/HBiX1 (below referred to as LRIF1), which in turn associates with H3K9me3 bound HP1 on chromatin (Nozawa et al. 2013). LRIF1 and SMCHD1 mediate the compaction of the inactive X chromosome in females linking the H3K9me3 and the XIST-H3K27me3 domains (Nozawa et al. 2013). Through mediating chromatin interactions on the inactive X chromosome, SMCHD1 may promote chromatin mixing and drive attenuation of chromosomal compartments and topologically associated domains (TADs) (Wang et al. 2018). Apart from binding the inactive X chromosome, SMCHD1 is also recruited to sites of DNA damage induced by laser micro-irradiation (Coker and Brockdorff 2014) or zeocin drug treatment and it has been implicated in promoting DNA repair by NHEJ over homologous recombination (Tang et al. 2014). Finally, SMCHD1 and LRIF1 have been detected in proteomic analyses of telomeric chromatin (Dejardin and Kingston 2009; Grolimund et al. 2013; Bartocci et al. 2014). Specifically, SMCHD1 and LRIF1 were enriched at telomeres that were overly long and showed a lower density of TRF2 (Grolimund et al. 2013). However, the roles of SMCHD1 and LRIF1 at telomeres remained enigmatic.

Here, we discover critical functions of SMCHD1 and LRIF1 at telomeres that were deprived of TRF2. Significantly, depletion of SMCHD1 and LRIF1 impairs ATM-dependent DNA damage signaling at TRF2-depleted telomeres. At the same time telomere end fusions were diminished indicating crucial roles of SMCHD1 and LRIF1 in DNA damage signaling or repair. Experimental activation of the ATR checkpoint at TRF2-depleted telomeres re-instigated chromosome end fusions in the absence of SMCHD1 unraveling a requirement

of SMCHD1 for checkpoint activation but not directly the DNA repair reaction. Our data indicate that SMCHD1 and LRIF1 are required in the onset of DDR activation upstream of ATM.

Results

SMCHD1 and LRIF1 are required for efficient telomere-end-to-end fusions at TRF2-depleted telomeres

In previous work we observed in HeLa cells enrichment of SMCHD1 and LRIF1 at long telomeres with an average length of 30 kb over telomeres with an average length of 10 kb (Grolimund et al. 2013). In addition, over-elongated telomeres showed a lower density of TRF2. We therefore tested if shRNA-mediated TRF2 depletion in HeLa cells is sufficient to enhance association of SMCHD1 with telomeres of normal length. SMCHD1 association with telomeric DNA was assessed by chromatin immunoprecipitation upon which co-precipitated telomeric DNA was detected by Southern hybridization. Indeed, immunoprecipitated SMCHD1 was associated with more telomeric DNA in TRF2-depleted cells (Supplemental Fig. S1). A probe for Alu-repeat DNA served as a negative control.

TRF2-depleted telomeres trigger an ATM-dependent DNA damage response and they undergo NHEJ-mediated telomere end-to-end fusions (Denchi and de Lange 2007). In order to assess potential roles of SMCHD1 and LRIF1 for these processes, we used CRISPR/Cas9 technology to disrupt the *SMCHD1* gene and we developed shRNA vectors for the depletion of SMCHD1 and LRIF1 (Fig. 1). Three different guide RNAs were used for generating *SMCHD1* knockout clones in HeLa cells and in a HeLa cell clone in which TRF2 could be depleted using an inducible shRNA (Grolimund et al. 2013). Individual clones were screened for loss of SMCHD1 protein expression on Western blots using antibodies recognizing SMCHD1 peptides near the N- and C-termini (Fig. 1A and Supplemental Fig. S2A). This analysis suggested complete loss of SMCHD1 protein expression in all three clones (Supplemental Fig. S2A). Analysis of the knockout clones by PCR amplification of the targeted loci and DNA sequencing revealed introduction of frameshift mutations near the N-terminus of SMCHD1 leading to premature stop codons, which can explain the loss of SMCHD1 protein expression. In addition, two shRNAs mediated efficient depletion of SMCHD1 protein (Fig. 1B and further below) and one shRNA efficient depletion of LRIF1 mRNA (Fig. 1C). ShRNA-mediated TRF2 depletion during 5 days (Fig. 1A) triggered end-to-end fusions at 20% of the chromosome ends as assessed by the analysis of metaphase chromosome spreads (Fig. 1D,E). Strikingly, the telomere fusions were reduced to roughly 3-4% when TRF2 was depleted in the two different *SMCHD1* knockout clones. Similar results were obtained upon shRNA-mediated co-depletion of SMCHD1 or LRIF1 with TRF2 (Fig. 1F,G) confirming critical roles of SMCHD1 and LRIF1 for efficient telomere end-to-end fusions upon TRF2 loss.

SMCHD1 promotes DNA end processing for NHEJ at TRF2-depleted telomeres

Upon TRF2-depletion, telomeric DNA is first processed to remove the 3' overhang. The blunt end telomeres are then fused by NHEJ (Celli and de Lange 2005). To better understand the roles of SMCHD1 in these processes, we followed telomeric DNA processing and fusions in time-course experiments in which TRF2 was depleted using an inducible shRNA in *SMCHD1* wild type and knockout cells (Fig. 2). Quantification of telomere end-to-end fusions showed strong reduction but not abolishment of fusion events in *SMCHD1* knockout cells as seen in Figure 1 (Fig. 2B). Removal of the telomeric 3' overhang was assessed by native in gel hybridization in which the radiolabeled probe detects only the telomeric 3' overhang but not the double stranded telomeric DNA, which remains base-paired (Fig. 2C, left panel). As expected the overhang signal was lost upon *in vitro* treatment of the DNA prior to gel loading with Exonuclease 1 from *E. coli* which removes the 3' overhang (left panel, lanes designated with +Exo). Upon denaturation of the same gel, however, single and double stranded telomeric DNA is detected with the probe (right panel). Inspection of the native gels (Fig. 2C, left panel, see short run) and quantification revealed that the *SMCHD1* knockout cells lost the telomeric 3' overhang considerably slower than the *SMCHD1* wild-type cells (Fig. 2C,D). Furthermore, the signal for fused telomeres which is fully double stranded and therefore can only be detected in the denatured gel (Fig. 2C, right panel, see long

run), was strongly reduced in the *SMCHD1* knockout cells (compare signal of fused to non-fused telomeres in each lane). These results are consistent with the metaphase chromosome analysis of Figure 2B.

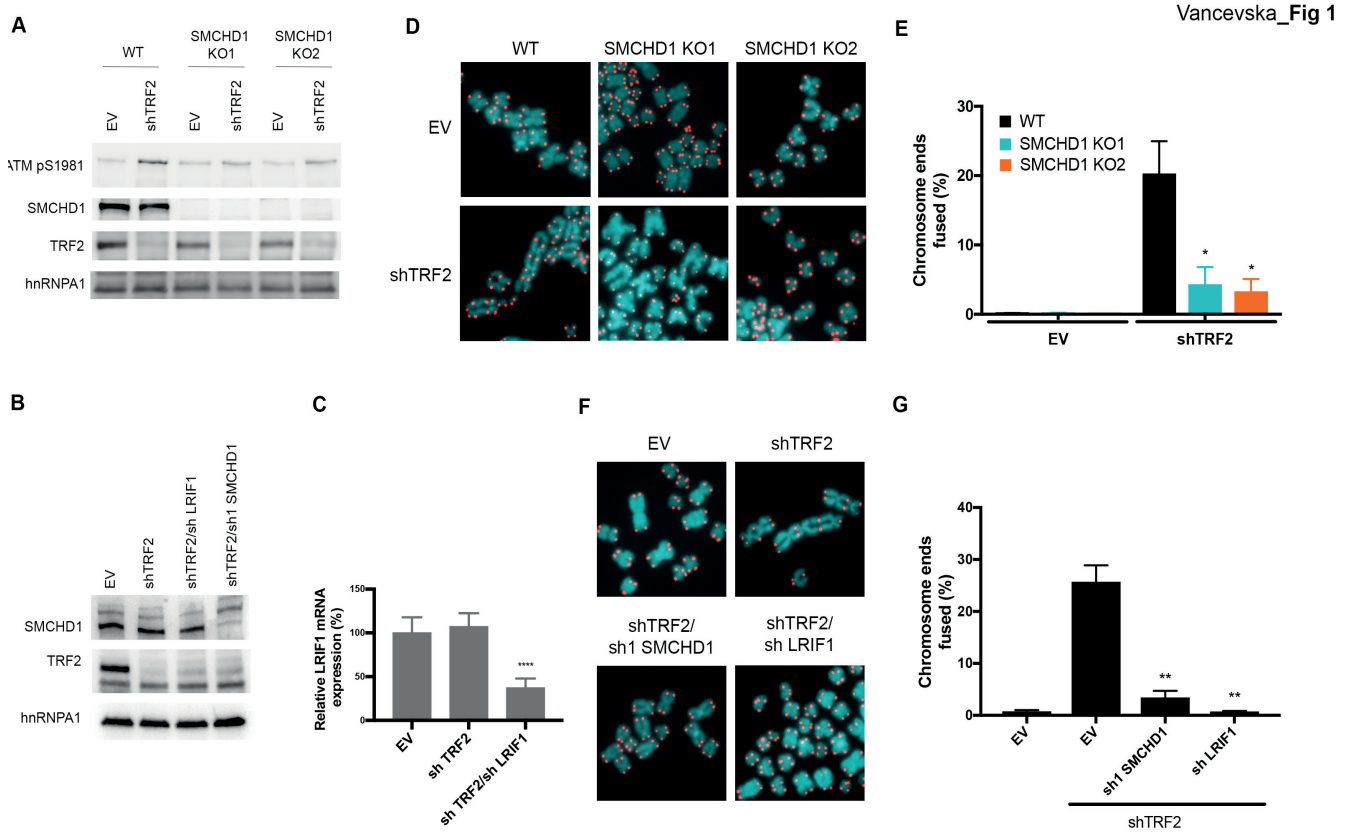


Figure 1. SMCHD1 and LRIF1 promote c-NHEJ at dysfunctional telomeres.

(A) Western Blot detection of ATM pS1981, SMCHD1, TRF2 and hnRNPA1 loading control in wild-type and two SMCHD1 knockout (KO1 and KO2) HeLa cells transfected with shTRF2 plasmid or EV control. (B) Immunoblot analysis of SMCHD1, TRF2 and hnRNPA1 in HeLa cells transfected with indicated shRNAs (shTRF2, shTRF2/sh LRIF1, shTRF2/sh1 SMCHD1) or EV control. (C) RT-qPCR quantification of LRIF1 mRNA levels normalized to GAPDH reference and compared to EV in the samples from the experiment performed in (B). (****) $P < 0.0001$; unpaired two-tailed Student's t-test. The bars represent average value from three biological and two technical replicates for each sample. Error bars represent the SD. (D) Representative metaphase spreads from wild-type and SMCHD1 knockout HeLa cells transfected with shTRF2 plasmid or EV control. Telomeric signals were detected with Cy3-OO-(CCCTAA)₃ and are false colored in red, DNA is stained with DAPI and is false colored in cyan. (E) Quantification of telomere fusions from experiment shown in (D). Bars represent average number of fused chromosome ends. SDs were obtained from 3 independent experiments (>3,000 telomeres counted/condition/experiment). (*) $P < 0.05$; unpaired two-tailed Student's t-test. (F) Representative metaphase spreads from HeLa cells transfected with indicated shRNAs or EV control. Experiment was performed as in (D). (G) Quantification of telomere fusions from experiment shown in (F). Bars represent average number of fused chromosome ends. SDs were obtained from 3 independent experiments (>3,000 telomeres counted/condition/experiment). (****) $P < 0.001$, (**) $P < 0.01$; unpaired two-tailed Student's t-test.

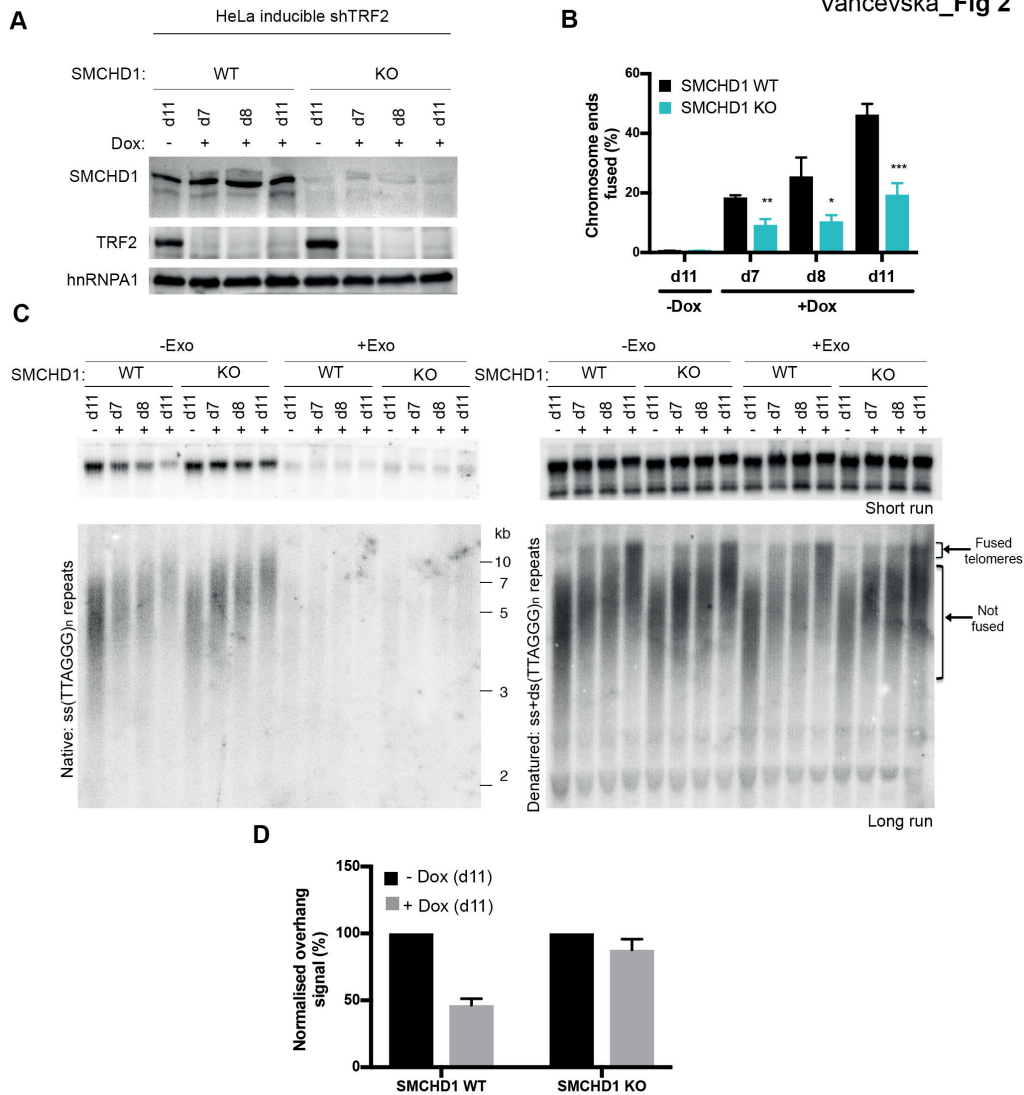


Figure 2. SMCHD1 loss slows down overhang processing at TRF2 depleted telomeres.

(A) Western Blot detection of SMCHD1, TRF2 and hnRNPA1 in SMCHD1 wild-type or SMCHD1 knockout HeLa inducible shTRF2 cells treated with or without doxycycline for the indicated number of days (d7, d8, d11). (B) Quantification of telomere fusions in SMCHD1 wild-type or SMCHD1 knockout HeLa inducible shTRF2 cells treated with or without doxycycline for the indicated number of days (d7, d8, d11). Bars represent average number of fused chromosome ends. SDs were obtained from 3 independent experiments (>1,900 telomeres counted/condition/experiment). (***) $P < 0.001$, (**) $P < 0.01$; (*) $P < 0.01$; unpaired two-tailed Student's t-test. (C) Terminal Restriction Fragment (TRF) analysis of telomeric DNA to detect 3' overhang processing of genomic DNA isolated from SMCHD1 wild-type or SMCHD1 knockout HeLa inducible shTRF2 cells treated as in the experiment in (B). (Left) Radiolabeled (CCCTAA)_n probe was hybridized with a short run (upper panel) and long run (lower panel) native DNA gel to detect the signal of the telomeric 3' overhang. Samples used for the short and the long run were from the same digestion split into two. Exo I treatment (+ Exo) was used as a control that single stranded telomeric signal was terminal. (Right) The total TTAGGG signal in the same lane was detected upon denaturation and hybridization with the same probe. (D) Quantification of the telomeric overhang signal at d11 after doxycyclin addition to SMCHD1 wild-type and SMCHD1 knockout HeLa shTRF2 inducible cells. The bar graph represents the average overhang signal intensity from two biological replicates as percentage of the signal in the cells untreated with doxycycline.

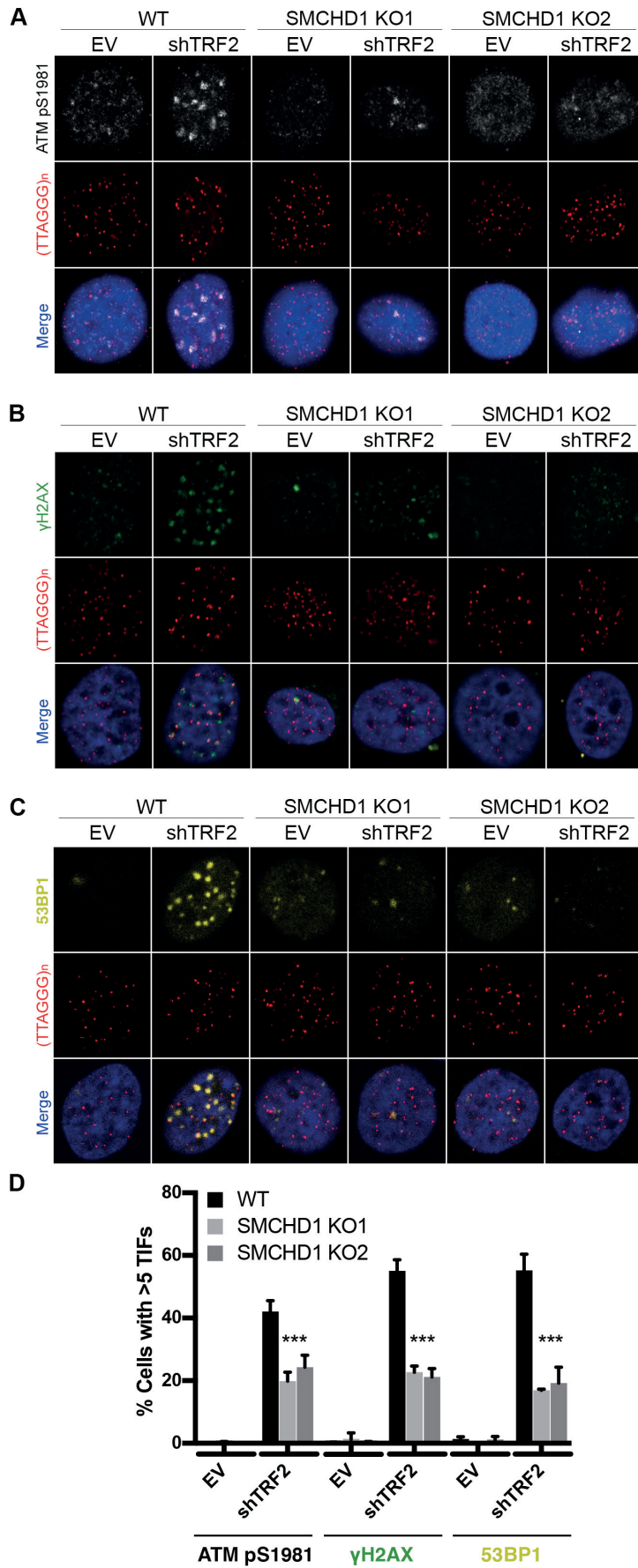


Figure 3. SMCHD1 promotes TIF formation and stimulates ATM signaling from TRF2 depleted telomeres.

(A-C) Representative images for detection of ATM pS9181, γ H2AX, and 53BP1 at telomeres in wild-type (WT) and SMCHD1 knockout HeLa cells transfected with shTRF2 plasmid and empty vector (EV) control. Immunofluorescence (IF) for ATM pS1981 (gray), γ H2AX (green) and 53BP1 (yellow) was combined with telomeric (CCCTAA)₃-FISH (red) and DAPI staining total DNA. (D) Quantification of the number of cells containing >5 Telomere dysfunction Induced Foci (TIFs) detected as in (A)-(C). Data represent the mean of 4 independent experiments \pm SD (>200 cells/condition/experiment) for ATM pS1981 and 3 independent experiments \pm SD (>200 cells/condition/experiment) for γ H2AX and 53BP1.

During the time course, we also observed a shift of the telomeric signals over time towards longer telomeres which was expected as TRF2 negatively regulates telomere elongation by telomerase (Smogorzewska et al. 2000). Altogether, this analysis indicated that the first step of the telomeric DNA end-fusion reaction, the DNA end processing step was strongly delayed in the absence of SMCHD1.

SMCHD1 promotes ATM activation and DDR at TRF2-depleted telomeres

NHEJ of TRF2-depleted telomeres is strictly dependent on activation of the DDR at uncapped telomeres (Denchi and de Lange 2007). Therefore, we tested if SMCHD1 is required for checkpoint signaling. As expected, TRF2-depletion led to induction of telomere dysfunction induced foci (TIFs) (Takai et al. 2003) in which at S1981 phosphorylated ATM (ATM pS1981), phosphorylated H2AX (γ H2AX) and 53BP1 accumulate as foci at telomeres (Fig. 3). Strikingly, depletion of TRF2 in the two *SMCHD1* knockout clones showed a strong reduction but not abolishment of all TIF markers indicating reduced DDR at TRF2-depleted telomeres in the absence of SMCHD1. Similarly, we observed reduced TIFs in TRF2-depleted cells that had been treated with SMCHD1 shRNAs (Supplemental Fig. S3). Finally, we observed in Western blots, that ATM pS1981 was reduced in TRF2-depleted *SMCHD1* knockout cells (Fig. 1A) or upon shRNA-mediated depletion of SMCHD1 (Supplemental Fig. S3A). Altogether, these results indicate that SMCHD1 is required for efficient ATM activation and the subsequent DDR at TRF2-depleted telomeres. Notably, however, SMCHD1 is not absolutely essential for the DDR. Thus SMCHD1 loss has less severe consequences than MRE11 depletion, which completely abolished DDR and NHEJ at TRF2-depleted telomeres (Supplemental Fig. S3A, S3C and S4), reminiscent of results obtained in mouse embryonic fibroblasts (MEFs) in which *Mre11* was deleted (Deng et al. 2009).

SMCHD1 is required for NHEJ at TRF2-depleted telomeres because of ATM activation

The above results unraveled requirements of SMCHD1 for ATM activation and NHEJ of TRF2-depleted telomeres but they could not distinguish if the effects on NHEJ were solely due to its involvement in checkpoint activation or if it also played direct roles in the DNA processing or end ligation reactions. For addressing this question we were inspired by a previous landmark paper (Denchi and de Lange 2007), which discovered the requirement of ATM for NHEJ of TRF2-depleted telomeres and which demonstrated that ATM function could be substituted by activated ATR. To activate ATR at telomeres, we depleted TPP1 with shRNAs (Fig. 4A), which leads to removal of POT1 from the telomeric 3' overhang (Frescas and de Lange 2014). This in turn leads to RPA binding to the single stranded 3' overhang, subsequent ATR/ATRIP recruitment and checkpoint signaling at chromosome ends (Zou and Elledge 2003). Significantly, the shRNA-mediated depletion of TPP1 reinstated efficient chromosome end-to-end fusions in *SMCHD1* knockout cells that had been depleted for TRF2 (Fig. 4B). Concomitant inhibition of the ATR kinase with an inhibitor (VE-821) (Reaper et al. 2011) again prevented efficient end fusions (Fig. 4C) indicating that ATR signaling upon TPP1-depletion was responsible for triggering chromosome end-to-end fusions in the absence of SMCHD1.

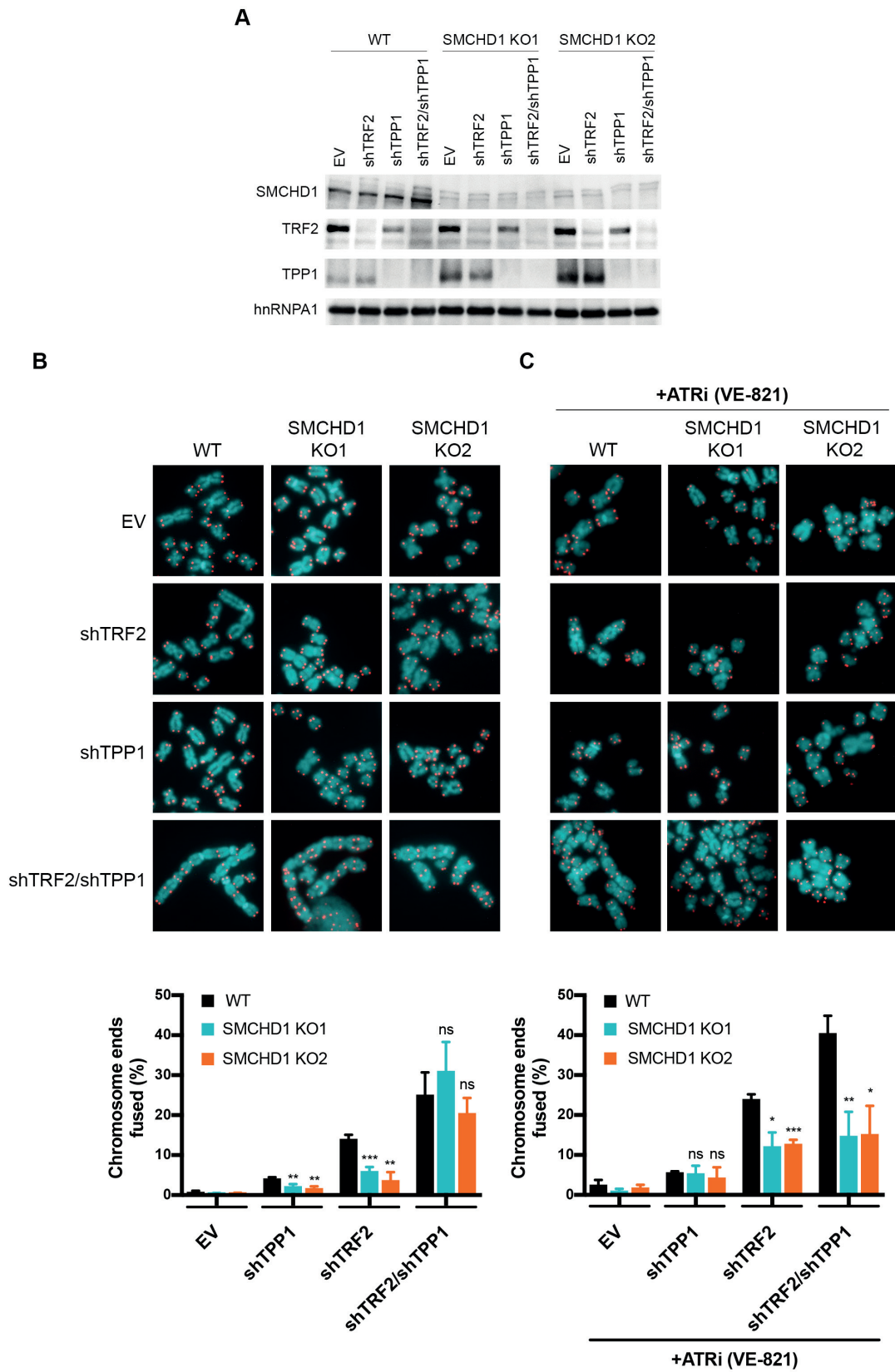


Figure 4. ATR signalling induction by TPP1 removal rescues the telomere fusion defect in SMCHD1 knockout cells.

(A) Western Blot detection of SMCHD1, TRF2, TPP1 and hnrNPA1 in wild-type or SMCHD1 knockout HeLa cells transfected with the indicated shRNAs (shTRF2, shTPP1, shTRF2/shTPP1) or EV control. (B) Representative metaphase spreads from HeLa cells transfected with indicated shRNAs or EV control and quantification of telomere fusions. Bars represent average number of fused chromosome ends. SDs were obtained from 3 independent experiments (>2,800 telomeres counted/condition/experiment). (***) $P < 0.001$, (**) $P < 0.01$, (*) $P < 0.01$, (ns) non significant as compared to WT; unpaired two-tailed Student's t-test. (C) Representative metaphase spreads from HeLa cells transfected with indicated shRNAs or EV control treated for 4 days with ATRi (VE-821) and quantification of telomere fusions. Bars represent average number of fused chromosome ends. SDs were obtained from 3 independent experiments (>2,000 telomeres counted/condition/experiment). (**) $P < 0.01$, (*) $P < 0.01$, (ns) non significant as compared to WT; unpaired two-tailed Student's t-test.

Vancevska_Fig 5

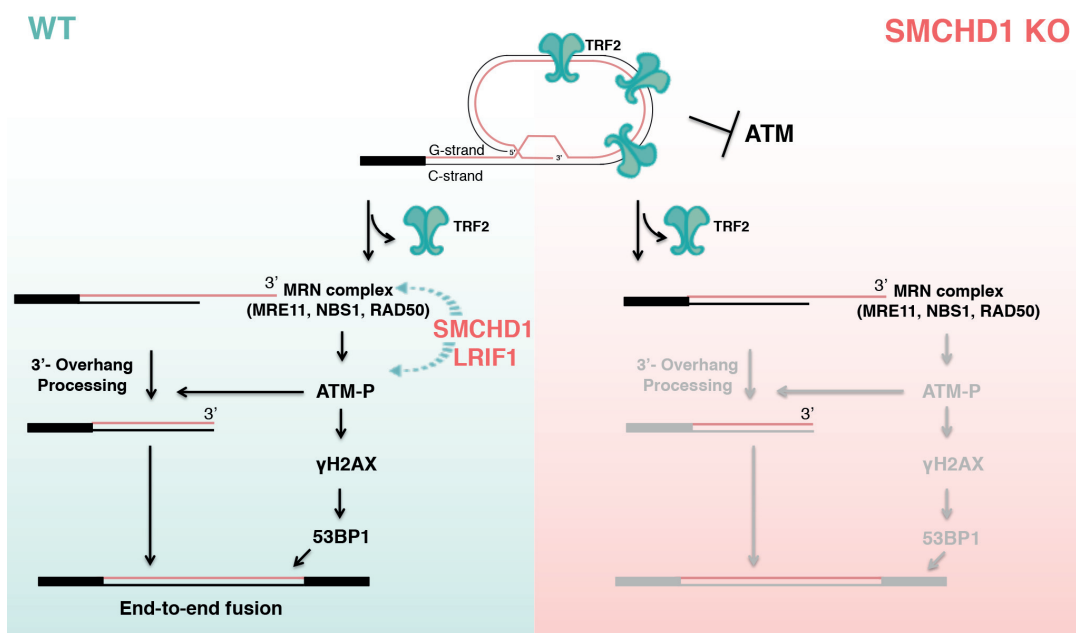


Figure 5. Schematic model of DNA damage response at uncapped telomeres in SMCHD1 wild type and knockout cells.

Loss of TRF2 leads to t-loop unwinding. In wild type cells, SMCHD1 may remodel the telomeric chromatin to promote MRN complex binding and/or ATM activation (dotted arrows). ATM activation is required for NHEJ at TRF2-depleted telomeres. In SMCHD1 knockout cells, ATM activation and DNA damage signaling is defective resulting in inefficient 3' overhang processing and impaired telomere end-to-end fusions. SMCHD1-loss and lack of ATM activation can be compensated for by ATR (not depicted).

Discussion

In this paper we demonstrate that loss of SMCHD1 abolishes efficient DNA damage signaling and NHEJ at telomeres that are depleted of TRF2. The defects of *SMCHD1* knockout cells in signaling and repair can be ascribed to its roles in DDR activation. Indeed, activation of ATR upon depletion of TPP1 was sufficient to suppress the defects of the *SMCHD1* knockout for NHEJ at TRF2-depleted telomeres suggesting that SMCHD1 is required for checkpoint signaling but it is not directly involved in NHEJ. Since SMCHD1 loss in TRF2-depleted cells prevented efficient ATM activation, our data indicate that SMCHD1 functions in the DDR cascade very early upstream of ATM. During canonical ATM-dependent DDR at DNA double strand breaks, the MRN complex binds and senses DNA ends recruiting and activating ATM, which then initiates the DNA damage signaling cascade (Paull 2015). At telomeres, the MRN complex is present even when telomeres are intact (Zhu et al. 2000). Indeed, NBS1 of the MRN complex interacts directly with TRF2 but in this context, ATM is not activated (Rai et al. 2017). TRF2 inhibits ATM signaling by several mechanisms involving its TRFH and hinge domains (Okamoto et al. 2013). The TRFH domain of TRF2 promotes formation of t-loops, which prevents exposure of the chromosome ends to the MRN complex not allowing ATM recruitment or activation (Doksani et al. 2013). In addition, the TRFH domain of TRF2 interacts at intact telomeres with a non-phosphorylated form of NBS1 preventing ATM activation (Rai et al. 2017). Second, through a portion of the hinge domain of TRF2 referred to as iDDR, TRF2 can sever the DDR at the level of the E3 ubiquitin ligase RNF168 which is required for 53BP1 localization to telomeres (Okamoto et al. 2013). Upon TRF2 removal, NBS1 is phosphorylated by CDK2 at Ser432 (Rai et al. 2017). The t-loops will unwind and MRE11/RAD50 may associate with the uncapped telomeres at their DNA ends possibly in a similar manner as it does with DNA double strand breaks (Syed and Tainer 2018). Phosphorylated NBS1 may bind to uncapped telomeres via MRE11 enabling ATM recruitment and activation (Rai et al. 2017).

Our data implicate SMCHD1 in ATM activation. Activation is likely to also involve the SMCHD1 binding partner LRIF1 as its depletion also prevented efficient NHEJ of TRF2-depleted telomeres. SMCHD1 contains an N-terminal ATPase domain and a C-terminal hinge domain mediating homodimerization (Brideau et al. 2015). We speculate that SMCHD1 may promote ATP-dependent chromatin remodeling at uncapped telomeres, in analogy to other SMC proteins which remodel chromosome architecture (van Ruiten and Rowland 2018). For example, SMCHD1 may modulate the telomere structure at TRF2-depleted telomeres at the molecular level to expose telomeric DNA ends and favor binding of MRE11. Alternatively, it may assist ATM recruitment or activation (Fig. 5). At the inactive X chromosome in females, SMCHD1 and LRIF1 had been implicated in chromosome compaction linking H3K9me3 rich with H3K27me3 rich domains (Nozawa et al. 2013). At, telomeres, however, we did not detect notable effects of SMCHD1 depletion on telomere compaction (data not shown). Thus, although H3K9me3 may be important for SMCHD1 binding to uncapped telomeres, SMCHD1/LRIF1 do not alter chromatin compaction at telomeres at detectable levels as seen at the inactive X chromosome.

ATM activation is not only required for NHEJ of uncapped telomeres but also for NHEJ of a subset of DNA breaks which occur in heterochromatic regions of the genome (Goodarzi et al. 2008). It has been proposed that ATM signaling at DNA breaks temporarily perturbs heterochromatin to promote processing of otherwise inflexible chromatin (Goodarzi et al. 2008). It is conceivable that SMCHD1/LRIF1 promotes also ATM activation at DNA breaks elsewhere in the genome, to help the repair of heterochromatin by NHEJ. Consistent with this notion are previous observations, which demonstrated recruitment of SMCHD1 to sites of DNA damage and inefficient repair and loss of viability upon DNA damage in the absence of SMCHD1 (Coker and Brockdorff 2014; Tang et al. 2014).

ATM activation upon telomere shortening and TRF2 depletion contributes to the induction of cell cycle arrest and cellular senescence (d'Adda di Fagagna et al. 2003). Our results implicate SMCHD1 and LRIF1 in damage signaling from unprotected telomeres. Mutations in SMCHD1 have been linked to several diseases including facioscapulohumeral muscular dystrophy (FSHD) and Bosmia arhinia (Jansz et al. 2017). It will be important to determine if disease mutations also impact on DNA damage signaling from telomeres and to what extent this may affect disease pathology.

Materials and methods

Cell culture

HeLa cells harbouring 11 kb long telomeres as well as the HeLa cells containing an inducible shTRF2 knockdown cassette cell lines were described previously (Grolimund et al. 2013). They were used for all transient transfection experiments and to derive *SMCHD1* knockout clones. Cells were maintained at 37°C with 5% CO₂ in Dulbecco's modified Eagle's medium supplemented with 10% FCS and penicillin/streptomycin.

Antibodies

The following primary antibodies were used: TRF2 (#05-521, Millipore, mouse, dilution 1:1,000, used for Western blots (WB)), γ H2AX (Millipore, #05-636, mouse, dilution 1:1,000, used for WB and IF), hnRNPA1 (4B10, #sc-32301, Santa Cruz Biotechnology, mouse, dilution 1:3,000, used for WB), 53BP1 (#NB100-304, Novus Biologicals, rabbit, dilution 1:2,000, used for IF), phospho-ATM-Ser1981 (#ab81292, Abcam, rabbit, dilution 1:1,000, used for WB and IF), SMCHD1 (#A302-871A, Bethyl Laboratories, N-terminal, rabbit, dilution 1:2,000, used for WB and ChIP), SMCHD1 (#A302-872A, Bethyl Laboratories, C-terminal, rabbit, dilution 1:2,000, used for WB and ChIP), TPP1 (#H00065057-M02, Abnova, rabbit, dilution 1:1,000, used for WB), MRE11 (#NB100-142, Novus Biologicals, rabbit, dilution 1:2,000, used for WB), normal rabbit IgG (#sc-2027, rabbit, used for ChIP).

Plasmids

Plasmids containing shRNAs used in this study were prepared by restriction cloning of annealed oligonucleotides into pSUPERpuro or pSUPERblast plasmid backbones (Oligoengine™). The target sequences of the shRNAs were: MRE11 5'-TGAGAACTCTTGGTTTAAC-3' cloned into pSUPERblast plasmid (Porro et al. 2014); TRF2 5'-GCGCATGACAATAAGCAGA-3' cloned into pSUPERblast and pSUPERpuro plasmid (Porro et al. 2014); sh1_SMCHD1 5'-ATTGGATAGCGGGTGATATTA-3' cloned into pSUPERpuro plasmid; sh2_SMCHD1 5'-TTATTCGAGTGCAACTAATTT-3' cloned into pSUPERpuro plasmid; shLRIF1 5'-GTAGGTGTGTTCTGAAAGT-3' cloned into pSUPERpuro plasmid; shTPP1 5'-GACTTAGATGTTTCAGAAAA-3' cloned into pSUPERblast plasmid (Abreu et al. 2010). The pSpCas9(BB)-2A-puro plasmid (a generous gift from Dr. Feng Zhang, Addgene plasmid #62988) was used for CRISPR/Cas9 mediated knockout of *SMCHD1*.

Transfection protocols

For depletion experiments HeLa cells were transfected in 6-well plates at 60-80% confluency using Lipofectamine 2000 according to the manufacturer's protocol (ThermoFisher, #11668019). Puromycin (conc. 1 μ g/mL, #ant-pr-1, Invivogen) and blasticidin (conc. 5 μ g/mL, #ant-bl-1, Invivogen) were added to the media 20-24h after transfection and the cells were expanded on 10cm dishes. Selection with the antibiotics was maintained for 3-5 days. Empty pSuperPURO and pSuperBLAST plasmids were used as control in all the experiments. For the experiment in Figure 4, ATRi (VE-821, Selleckchem, #S8007) was added to the cells 24 hour after addition of the selection antibiotics at 10 μ M concentration and the cells were maintained with the inhibitor for 4 days.

Immunoblotting

After harvesting, cells were counted using CASY Cell Counter and Analyzer, cell pellets with equal cell numbers were resuspended in 2x Laemmli buffer (20% glycerol, 4% sodium dodecyl sulphate, 10 mM Tris-Cl pH 6.8, 200 mM Dithiothreitol, 0.05% bromophenol blue) at final concentration of 10 000 cells/ μ L and boiled for 5min at 95°C. Protein extracts were fractionated on 4-20% Mini-PROTEAN® TGX™ Precast protein gels (Bio-

Rad), transferred to a nitrocellulose blotting membrane (Amersham™ Protran™, 0.2µm NC, GE Healthcare Life Sciences, #10600001), blocked in 3% BSA/1xPBS/0.1% Tween 20 for 30min and incubated with primary antibody overnight at 4°C. Membranes were then washed 3x5min in 1xPBS/0.1% Tween 20, incubated with anti-mouse or anti-rabbit HRP-conjugated secondary antibody for 30min (anti-mouse IgG HRP conjugate Promega #W402B, anti-rabbit IgG HRP conjugate Promega #W4011, 1:3000) and chemiluminescence was detected using Western Bright ECL spray (Advantia, #K-12049-D50). Detection of TPP1 was performed using a renaturation protocol as described (Loayza and De Lange 2003).

Telomere restriction fragment length analysis for detection of single stranded and double stranded telomeric DNA

Genomic DNA was isolated using the Wizard® Genomic DNA Purification kit (Promega, #A1120). Isolated DNA (5 µg) was subjected to digestion with 40U Exol (New England BioLabs, #M0293S) as control or non-digested and incubated for 8h at 37°C in CutSmart® Buffer in a final volume of 80µL. The samples were then heated at 80°C for 20min to inactivate the Exol enzyme. Following the inactivation, 20µL of digestion mix containing 125U HinfI (New England BioLabs, #R0155M) and 25U RsaI (New England BioLabs, #R0167L) was added to all the samples (Exo+ and Exo-) and the digestion mix was incubated overnight at 37°C. Digested DNA was loaded on a 1% agarose gel (35µL of the digestion mix was loaded for the Short run and 55µL for the Long run in Figure 2C) and separated by regular gel electrophoresis in 1 × TBE at 3 V cm⁻¹ for 1 h (Short run) and at 1.5 V cm⁻¹ for 16h (Long run). Gels were dried for 3h at 50°C, prehybridized at 50°C in Church buffer (1%BSA, 1mM EDTA, 0.5M phosphate buffer pH 7.5, 7%SDS) and hybridized at 50°C overnight to a [³²P]-labeled (CCCTAA)_n probe (Grolimund et al. 2013) for detection of single stranded (ss) telomeric DNA. After hybridization, the gel was rinsed in 4 × SSC and followed by successive 1 h washes at 50°C in 4 × SSC, 4 × SSC/0.5% SDS and 2 × SSC/0.5% SDS and exposed to a sensitive phosphorimager screen overnight. After the image was acquired the gel was denatured with 0.8 M NaOH and 150 mM NaCl, neutralized with 1.5 M NaCl, 0.5 M Tris-HCl pH 7.0, prehybridized in Church buffer at 50° for 1h and incubated with the same probe overnight at 50°C. The gel was again washed and exposed as above and the image was acquired using Amersham™ Typhoon™ Biomolecular imager (GE Healthcare). The images were quantified using Aida Image Analysis software. The single stranded-DNA signal was divided by the total denatured DNA signal in each lane and further normalized to -Dox samples.

CRISPR/Cas9 gene editing

The CRISPR/Cas9 gene editing system was used to create *SMCHD1* knockout cell lines. To target the *SMCHD1* gene locus (NC_000018.10; gene ID 23347), a region of 200 bp encompassing the ATG in Exon 1 was submitted to the Optimal CRISPR design tool (<http://crispr.mit.edu>). Three gRNAs with scores higher than 93 were chosen for further experiments (gRNA 1: 5'-CTTGTTTGATCGGCGCGAAA-3', gRNA2: 5'-GGG-GAGCGCTCGGACTACGC-3', gRNA 3: 5'-GCCGTCCGCCGCTGCCATAT-3'). Complementary oligonucleotides harbouring the guide RNA sequence and Bpil compatible overhangs were synthesized by Microsynth AG. The oligonucleotides were annealed and ligated into a Bpil (Thermo Fisher Scientific, ER1011) digested and dephosphorylated pSpCas9(BB)-2A-puro vector (Addgene, 62988). The resulting constructs were transfected into HeLa cells using Lipofectamine™ 2000 (Thermo Fisher Scientific, #11668019). Transfected cells were selected with 1µg/mL of puromycin for 4 days. Single-cell clones were obtained by limiting dilution and were screened for the absence of *SMCHD1* by Western blotting using the N-terminal anti-*SMCHD1* antibody. To verify the gene editing in positive clones, the PCR products obtained with 2 primers (AV48_SMCHD1_gPCR_F: 5'-AGGAGCGCGTTTGAATCGG-3', AV47_SMCHD1_gPCR_R 5'-CTTCGCG-TACCTGACACACAC-3') were TOPO- cloned (Thermo Fisher, #450071) and sent for sequencing.

Telomeric PNA-FISH on metaphase spreads

On the day of harvesting, cells were treated with 0.1 µg/mL demecolcine (Sigma Aldrich Chemie GmbH #D7385-10MG) for 2 h, cells were collected, resuspended in hypotonic solution (0.056 M KCl) and swollen for 7 min. Swollen cells were fixed in methanol:acetic acid (3:1) and stored overnight at 4°C. The next day cell suspensions were dropped onto slides to prepare metaphase spreads, incubated 1min at 70°C in a wet chamber and dried for 16–24 h before FISH. FISH staining of human telomeric DNA was performed as described (Vancevska et al. 2017). Slides were rehydrated in 1× PBS for 5 min, treated with 4% formaldehyde in PBS for 5 min, washed 3x with 1xPBS and dehydrated with increasing amounts of ethanol (70%, 95%, 100%). Dehydrated slides were then placed on coverslips containing 70 µL hybridization mix (10 mM Tris-HCl, 2% blocking reagent (Roche, #11096176001), 70% formamide and 0.1 µM Cy3 labeled (CCCTAA)₃ PNA probe (PNA Bio, #F1002)) and denatured at 80°C for 3 min in a hybridization oven. Subsequently, the hybridization was allowed to proceed for 3h in a light protected humidified chamber at 25 °C. The coverslip was then removed from the slide, washed twice for 15 min in buffer containing 70% formamide and 10 mM Tris-HCl pH 7.4 and 3 times for 15 min with 0.1 M Tris-HCl pH 7.2, 0.15 M NaCl, 0.08% Tween-20. For DNA staining, DAPI was added to 1 µg/ml in the second wash. After the washes slides were stored at 4°C in a dark place until imaging.

Indirect immunofluorescence and telomeric FISH (IF-FISH)

Indirect immunofluorescence detection of human ATM pS981, 53BP1 and γH2AX followed by telomeric FISH staining was performed as described (Vancevska et al. 2017). For detection of ATM pS1981 before crosslinking, cells were fractionated with an ice-cold preextraction buffer containing 0.5% Triton X-100, 20mM HEPES-OH pH 7.5, 50mM NaCl, 3mM MgCl₂ and 300mM sucrose for 7min. Subsequently cells were washed with 1xPBS and the same protocol was applied as for the other stainings.

RT-qPCR for measuring LRIF1 mRNA transcript levels

Total RNA was extracted with NucleoSpin® RNA isolation kit (Macherey-Nagel, #740955) from 2x10⁶ cells following the manufacturers protocol with three DNase treatment steps. cDNA from three biological replicates was synthesized using Invitrogen's SuperScript III Reverse Transcriptase (#18080044) from 2µg of total RNA. Reaction mixes in a total volume of 20µL contained: 2µg of total RNA, 0.5mM dNTP mix, 150ng random primers (Thermo Fisher #48190011), 250ng oligo (dT)₁₅ primer (Promega, #C1101), 1× First-Strand Buffer, 5 mM DTT, 20 U SUPERase IN (Ambion #AM2696) and 200 U SuperScript III RT (200 U/µl) or H₂O for no RT-control. The cDNA was then diluted to 40µL and stored at -20°C. Quantitative PCR (qPCR) was performed in Applied Biosystems 7900HT Fast Real-Time System using Power SYBR Green PCR Master Mix (Applied Biosystems #4368708) in a 384-well reaction plate (Applied Biosystems MicroAmp Optical 384-well reaction Plate with Barcode #4309849). Each sample was prepared in three biological and two technical replicates. The master-mix for each reaction is prepared as follows: 2 µl diluted cDNA, 5 pmol of forward primer, 5 pmol reverse primer, 1× Power SYBR Green PCR Master Mix and H₂O to a total volume of 10 µl. qPCR data were analysed using the relative ΔCt quantification method and GAPDH was used for normalization. Primers used for qPCR were as follows:

AV91_LRIF1_qPCR_F 5'-CTCGAATTCCTGACCATTGAC-3', AV92_LRIF1_qPCR_R 5'-CTCTCTCCTTCCTTCACCATAAAC-3', GAPDH_F 5'-AGCCACATCGCTCAGACA-3', GAPDH_R 5'-GCCAATACGACCAAATCC-3'.

Chromatin Immuno Precipitation (ChIP)

ChIP protocol for SMCHD1 and γH2AX was performed as described previously (Grolimund et al. 2013). Briefly, 10 million cells per condition were harvested and washed with 1xPBS pH 7.4. The cell pellet was then crosslinked in 1mL 1% formaldehyde in 1xPBS pH 7.4 for 15min at RT. Glycine pH 2.5 was added to 125mM

to quench the reaction, incubated for 5min and cells were then washed 3x with 1xPBS pH 7.4. Cells were subsequently incubated 5min in 1mL lysis buffer (1% SDS, 10mM EDTA pH 8.0, 50mM Tris-Cl pH 8.0, EDTA-free protease inhibitor complex (Roche, #11836170001)), centrifuged 5min at 2,000g and the chromatin enriched pellet was again resuspended in 500 μ L lysis buffer and subjected to sonication for 30min (30s ON, 30s OFF, total sonication time 15min) using Bioruptor[®] Twin Diogenode sonicator (#UCD-400). The sonicated lysate was centrifuged at 20,000g for 15min at 4°C. Per IP 100 μ L of the cleared lysate was diluted with 9 volumes of IP buffer (1.2mM EDTA pH 8.0, 1.1% Triton X-100, 16.7mM Tris pH 8.0, 300mM NaCl) and incubated with 5 μ g of the corresponding antibody (normal rabbit IgG, SMCHD1 or γ H2AX) and 30 μ L of preblocked Protein G Sepharose 4 Fast Flow 50% bead slurry (GE Healthcare, #17-0618-01) overnight at 4°C. The beads were then washed with once with wash buffer 1 (0.1% SDS, 1% Triton X-100, 2mM EDTA pH 8.0, 20mM Tris pH 8.0, 300mM NaCl), wash buffer 2 (0.1% SDS, 1% Triton X-100, 2mM EDTA pH 8.0, 20mM Tris pH 8.0, 500mM NaCl), wash buffer 3 (500mM LiCl, 1% NP-40, 1% Na-deoxycholate, 1mM EDTA, 10mM Tris pH 8.0) and twice with wash buffer 4 (1mM EDTA, 10mM Tris pH 8.0) at room temperature for 5 min. Elution and crosslink-reversal were performed at 65°C overnight in cross-link reversal buffer (1% SDS, 0.1 M NaHCO₃, 0.5mM EDTA pH 8.0, 20mM Tris-Cl pH 8.0, 10 μ g DNase-free RNase (Roche #11119915001)). For DNA extraction, the QIAquick PCR Purification kit (Qiagen, #28106) was used. Telomeric and Alu-repeat DNA were detected successively using the conditions described before. After the exposure the image was acquired using FujiFilm Fluorescent Image Analyzer FLA-3000 and the image quantification was done using AIDA Image Analyzer software v 4.06.

Acknowledgements

We thank Larissa Grolimund for initiating the work on SMCHD1 and LRIF1, Marianna Feretzaki for performing the RT-qPCR (Figure 1C) and for fruitful discussions, Jana Majerska and Galina Glousker for help in establishing the 3' overhang protocol and Wareed Ahmed for critical insight and helpful advice. Research in J.L.'s laboratory was supported by the Swiss National Science Foundation (SNSF), the SNSF funded NCCR RNA and disease network, the Swiss Cancer League and EPFL.

Author Contributions: J.L., A.V. and V.P. designed research, A.V. and V.P. carried out experiments, and J.L. and A.V. wrote the paper.

References

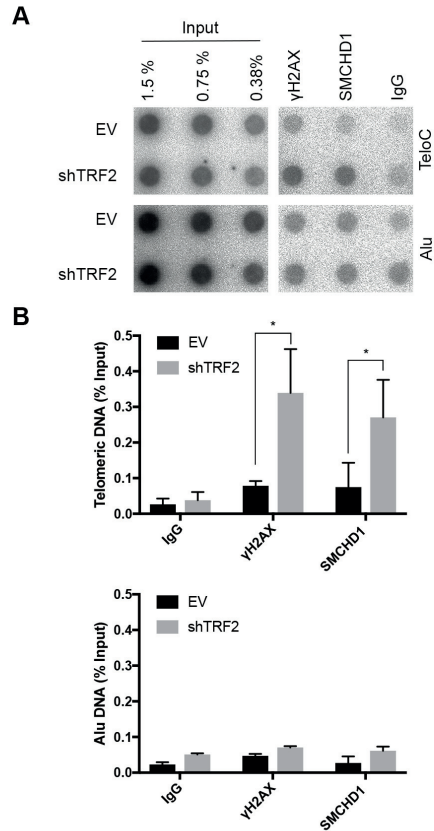
- Abreu E, Aritonovska E, Reichenbach P, Cristofari G, Culp B, Terns RM, Lingner J, Terns MP. 2010. TIN2-tethered TPP1 recruits human telomerase to telomeres in vivo. *Mol Cell Biol* **30**: 2971-2982.
- Bartocci C, Diedrich JK, Ouzounov I, Li J, Piunti A, Pasini D, Yates JR, 3rd, Lazzerini Denchi E. 2014. Isolation of chromatin from dysfunctional telomeres reveals an important role for Ring1b in NHEJ-mediated chromosome fusions. *Cell Rep* **7**: 1320-1332.
- Blewitt ME, Gendrel AV, Pang Z, Sparrow DB, Whitelaw N, Craig JM, Apedaile A, Hilton DJ, Dunwoodie SL, Brockdorff N et al. 2008. SmcHD1, containing a structural-maintenance-of-chromosomes hinge domain, has a critical role in X inactivation. *Nat Genet* **40**: 663-669.
- Brideau NJ, Coker H, Gendrel AV, Siebert CA, Bezstarosti K, Demmers J, Poot RA, Nesterova TB, Brockdorff N. 2015. Independent Mechanisms Target SMCHD1 to Trimethylated Histone H3 Lysine 9-Modified Chromatin and the Inactive X Chromosome. *Mol Cell Biol* **35**: 4053-4068.
- Celli GB, de Lange T. 2005. DNA processing is not required for ATM-mediated telomere damage response after TRF2 deletion. *Nat Cell Biol* **7**: 712-718.
- Cesare AJ, Hayashi MT, Crabbe L, Karlseder J. 2013. The telomere deprotection response is functionally distinct from the genomic DNA damage response. *Mol Cell* **51**: 141-155.
- Ciccio A, Elledge SJ. 2010. The DNA damage response: making it safe to play with knives. *Mol Cell* **40**: 179-204.

- Coker H, Brockdorff N. 2014. SMCHD1 accumulates at DNA damage sites and facilitates the repair of DNA double-strand breaks. *J Cell Sci* **127**: 1869-1874.
- d'Adda di Fagagna F, Reaper PM, Clay-Farrace L, Fiegler H, Carr P, Von Zglinicki T, Saretzki G, Carter NP, Jackson SP. 2003. A DNA damage checkpoint response in telomere-initiated senescence. *Nature* **426**: 194-198.
- de Lange T. 2009. How telomeres solve the end-protection problem. *Science* **326**: 948-952.
- Dejardin J, Kingston RE. 2009. Purification of proteins associated with specific genomic Loci. *Cell* **136**: 175-186.
- Denchi EL, de Lange T. 2007. Protection of telomeres through independent control of ATM and ATR by TRF2 and POT1. *Nature* **448**: 1068-1071.
- Denchi EL, Sfeir A. 2016. Stop pulling my strings-what telomeres taught us about the DNA damage response. *Nat Rev Mol Cell Biol* **17**: 364-378.
- Deng Y, Guo X, Ferguson DO, Chang S. 2009. Multiple roles for MRE11 at uncapped telomeres. *Nature* **460**: 914-918.
- Doksani Y, Wu JY, de Lange T, Zhuang X. 2013. Super-resolution fluorescence imaging of telomeres reveals TRF2-dependent T-loop formation. *Cell* **155**: 345-356.
- Frescas D, de Lange T. 2014. Binding of TPP1 protein to TIN2 protein is required for POT1a,b protein-mediated telomere protection. *J Biol Chem* **289**: 24180-24187.
- Goodarzi AA, Noon AT, Deckbar D, Ziv Y, Shiloh Y, Lobrich M, Jeggo PA. 2008. ATM signaling facilitates repair of DNA double-strand breaks associated with heterochromatin. *Mol Cell* **31**: 167-177.
- Grolimund L, Aeby E, Hamelin R, Armand F, Chiappe D, Moniatte M, Lingner J. 2013. A quantitative telomeric chromatin isolation protocol identifies different telomeric states. *Nature communications* **4**: 2848.
- Jansz N, Chen K, Murphy JM, Blewitt ME. 2017. The Epigenetic Regulator SMCHD1 in Development and Disease. *Trends Genet* **33**: 233-243.
- Jones RE, Oh S, Grimstead JW, Zimbric J, Roger L, Heppel NH, Ashelford KE, Liddiard K, Hendrickson EA, Baird DM. 2014. Escape from telomere-driven crisis is DNA ligase III dependent. *Cell Rep* **8**: 1063-1076.
- Kaidi A, Jackson SP. 2013. KAT5 tyrosine phosphorylation couples chromatin sensing to ATM signalling. *Nature* **498**: 70-74.
- Karlseder J, Smogorzewska A, de Lange T. 2002. Senescence induced by altered telomere state, not telomere loss. *Science* **295**: 2446-2449.
- Loayza D, De Lange T. 2003. POT1 as a terminal transducer of TRF1 telomere length control. *Nature* **424**: 1013-1018.
- Maciejowski J, de Lange T. 2017. Telomeres in cancer: tumour suppression and genome instability. *Nat Rev Mol Cell Biol* **18**: 175-186.
- Matsuoka S, Ballif BA, Smogorzewska A, McDonald ER, 3rd, Hurov KE, Luo J, Bakalarski CE, Zhao Z, Solimini N, Lerenthal Y et al. 2007. ATM and ATR substrate analysis reveals extensive protein networks responsive to DNA damage. *Science* **316**: 1160-1166.
- McClintock B. 1941. The Stability of Broken Ends of Chromosomes in Zea Mays. *Genetics* **26**: 234-282.
- Muller HJ. 1938. The remaking of chromosomes. *Collecting Net* **8**: 182-195.
- Nozawa RS, Nagao K, Igami KT, Shibata S, Shirai N, Nozaki N, Sado T, Kimura H, Obuse C. 2013. Human inactive X chromosome is compacted through a PRC2-independent SMCHD1-HBiX1 pathway. *Nature structural & molecular biology* **20**: 566-573.
- Okamoto K, Bartocci C, Ouzounov I, Diedrich JK, Yates JR, 3rd, Denchi EL. 2013. A two-step mechanism for TRF2-mediated chromosome-end protection. *Nature* **494**: 502-505.
- Panier S, Durocher D. 2013. Push back to respond better: regulatory inhibition of the DNA double-strand break response. *Nat Rev Mol Cell Biol* **14**: 661-672.
- Paull TT. 2015. Mechanisms of ATM Activation. *Annual review of biochemistry* **84**: 711-738.

- Porro A, Feuerhahn S, Lingner J. 2014. TERRA-reinforced association of LSD1 with MRE11 promotes processing of uncapped telomeres. *Cell Rep* **6**: 765-776.
- Rai R, Hu C, Broton C, Chen Y, Lei M, Chang S. 2017. NBS1 Phosphorylation Status Dictates Repair Choice of Dysfunctional Telomeres. *Mol Cell* **65**: 801-817 e804.
- Reaper PM, Griffiths MR, Long JM, Charrier JD, McCormick S, Charlton PA, Golec JM, Pollard JR. 2011. Selective killing of ATM- or p53-deficient cancer cells through inhibition of ATR. *Nature chemical biology* **7**: 428-430.
- Shay JW, Wright WE. 2011. Role of telomeres and telomerase in cancer. *Semin Cancer Biol* **21**: 349-353.
- Smogorzewska A, van Steensel B, Bianchi A, Oelmann S, Schaefer MR, Schnapp G, de Lange T. 2000. Control of human telomere length by TRF1 and TRF2. *Mol Cell Biol* **20**: 1659-1668.
- Sun Y, Jiang X, Xu Y, Ayrapetov MK, Moreau LA, Whetstine JR, Price BD. 2009. Histone H3 methylation links DNA damage detection to activation of the tumour suppressor Tip60. *Nat Cell Biol* **11**: 1376-1382.
- Syed A, Tainer JA. 2018. The MRE11-RAD50-NBS1 Complex Conducts the Orchestration of Damage Signaling and Outcomes to Stress in DNA Replication and Repair. *Annual review of biochemistry*.
- Takai H, Smogorzewska A, de Lange T. 2003. DNA damage foci at dysfunctional telomeres. *Curr Biol* **13**: 1549-1556.
- Tang M, Li Y, Zhang X, Deng T, Zhou Z, Ma W, Songyang Z. 2014. Structural maintenance of chromosomes flexible hinge domain containing 1 (SMCHD1) promotes non-homologous end joining and inhibits homologous recombination repair upon DNA damage. *J Biol Chem* **289**: 34024-34032.
- van Ruiten MS, Rowland BD. 2018. SMC Complexes: Universal DNA Looping Machines with Distinct Regulators. *Trends Genet* **34**: 477-487.
- Vancevska A, Douglass KM, Pfeiffer V, Manley S, Lingner J. 2017. The telomeric DNA damage response occurs in the absence of chromatin decompaction. *Genes Dev* **31**: 567-577.
- Wang CY, Jegu T, Chu HP, Oh HJ, Lee JT. 2018. SMCHD1 Merges Chromosome Compartments and Assists Formation of Super-Structures on the Inactive X. *Cell*.
- Zhu XD, Kuster B, Mann M, Petrini JH, Lange T. 2000. Cell-cycle-regulated association of RAD50/MRE11/NBS1 with TRF2 and human telomeres. *Nat Genet* **25**: 347-352.
- Zou L, Elledge SJ. 2003. Sensing DNA damage through ATRIP recognition of RPA-ssDNA complexes. *Science* **300**: 1542-1548.

Supplementary figures

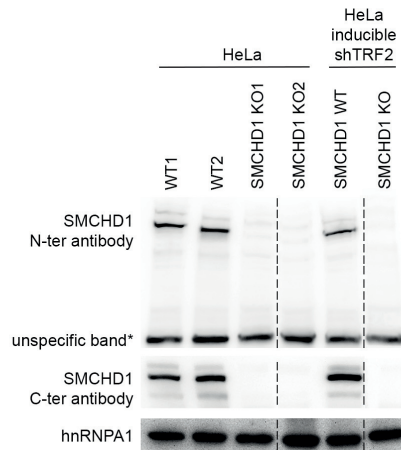
Vancevska_SuppFig1



Supplemental Figure S1: SMCHD1 association with telomeres is increased upon TRF2 removal.

(A) Telomeric DNA ChIP with antibodies against γ H2AX, SMCHD1 and rabbit IgG. Representative dot blot images of precipitated DNA detected with a (CCCTAA)_n or Alu probe. ChIPs were performed in HeLa cells transfected with shTRF2 or Empty Vector (EV) control (B) Bar graph for quantification of γ H2AX, SMCHD1 and rabbit IgG binding to telomeric or alu DNA. The bars represent average value from three independent experiments for telomeric DNA, and two independent experiments for Alu DNA. Error bars represent the standard deviation. P-values were calculated by unpaired two-tailed Student's t-test (*) P < 0.05

A

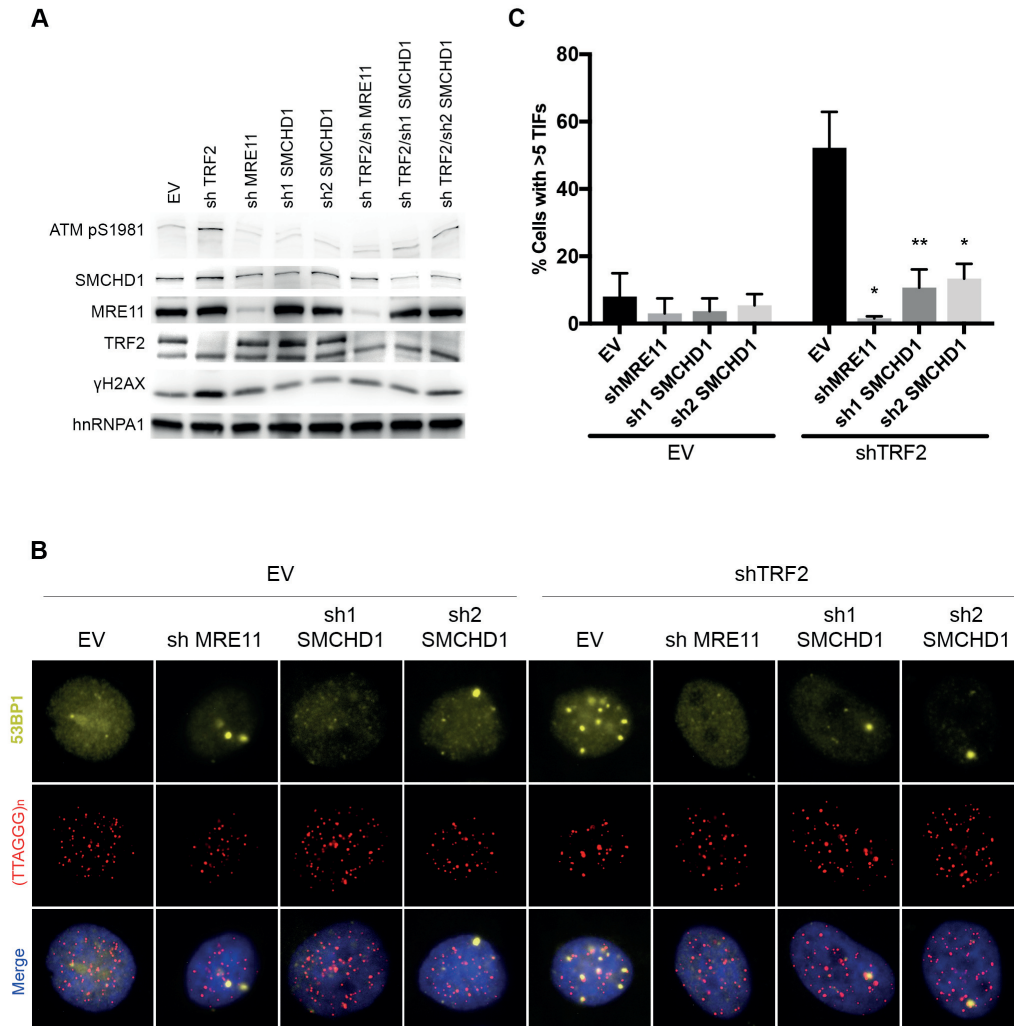


B

- a)** **gRNA 2**
 5'-GCTCGGGGACCGCCTCTGCAGGTCGGGGAGCGCTCGGACTACGGGGATTTTCGCGCCTG-3' **WT HeLa**
 5'-GCTCGGGGACCGCCTCTGCAGGTCGGGGAGCGCTCGGACTA-----GGATTTTCGCGCCTG-3' **SMCHD1 KO1 (8/8)**
 Deletion of 4 nucleotides at position +155 relative to the ATG in both alleles leading to translation termination at codon 53
- b)** **gRNA 3**
 5'-AGGCGTCGCTGTCTTTTCTCCTTTTCCCAATATGCGAGCGGCGGACGGCGGCGGGCCCTG-3' **WT HeLa**
 5'-AGGCGTCGCTGTCTTTTCTCCTTTTCCCA---TGGCAGCGGCGGACGGCGGCGGGCCCTG-3' **SMCHD1 KO2 (1/1)**
 208 bp insertion
 Insertion of 208 nucleotides and deletion of 3 nucleotides leading to disruption of the start codon (highlighted in green)
- c)** **gRNA 1**
 5'-CACAGGACGGTGTACTTGTTTGATCGGCGCGAAAAGGAGTCCGAGCTCGGGGACCGGCCT-3' **WT HeLa inducible shTRF2**
 5'-CACAGGACGGTGTACTTGTTTGATCGGCGCG-----TCCGAGCTCGGGGACCGGCCT-3' **SMCHD1 KO (3/6) Allele 1**
 5'-CACAGGACGGTGTACTTGTTTGATCGGCGCGAAAAGGAGTCCGAGCTCGGGGACCGGCCT-3' **SMCHD1 KO (3/6) Allele 2**
 G/T
Allele 1: Deletion of 8 nucleotides at position +100 relative to the ATG leading to translation termination at codon 65
Allele 2: Insertion of 1 nucleotide at position +100 relative to the ATG nucleotide leading to translation termination at codon 69

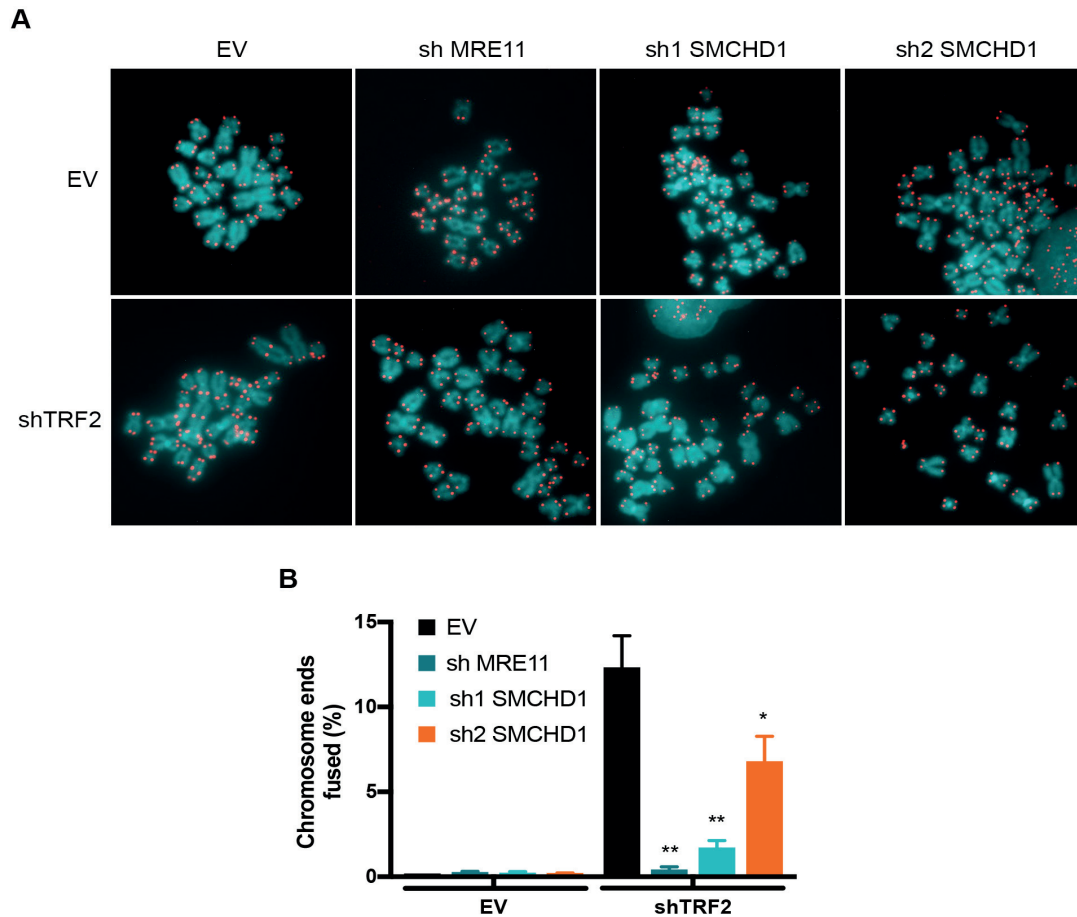
Supplemental Figure S2: Generation of SMCHD1 KO CRISPR-Cas9 cell lines.

(A) Western Blot detection of SMCHD1 with an antibody raised against the N-terminus (aa213-aa300) and the C-terminus of the protein (aa1955-2005) in *SMCHD1* knockout single cell clones of HeLa and HeLa inducible shTRF2 cell lines. (B) Sequence analysis of edited alleles in *SMCHD1* knockout single cell clones.



Supplemental Figure S3: SMCHD1 promotes DNA damage signaling at TRF2 depleted telomeres.

(A) Western Blot detection of ATM pS1981, SMCHD1, MRE11, TRF2, and γ H2AX, in HeLa cells transfected with the indicated shRNAs (shTRF2, shMRE11, sh1SMCHD1, sh2SMCHD1, shTRF2/shMRE11, shTRF2/sh1 SMCHD1, shTRF2/sh2 SMCHD1) and empty vector (EV) control (B) Representative images for detection of 53BP1 at telomeres in HeLa cells transfected with the indicated shRNAs. Immunofluorescence (IF) for 53BP1 (yellow) was combined with telomeric (CCCTAA)₃-FISH (red) and the DNA was stained with DAPI (C) Quantification of the number of cells containing >5 Telomere dysfunction Induced Foci (TIFs) detected as in (B). Data represent mean of 3 independent experiments \pm SD (>100 cells/condition/experiment). (*) $P > 0.05$, (**) $P > 0.01$, unpaired two tailed Student's t-test.



Supplemental Figure S4: SMCHD1 stimulates c-NHEJ at TRF2 depleted telomeres.

(A) Metaphase spreads from HeLa cells transfected with the indicated shRNAs (shTRF2, shMRE11, sh1SMCHD1, sh2SMCHD1, shTRF2/shMRE11, shTRF2/sh1 SMCHD1, shTRF2/sh2 SMCHD1) and empty vector (EV) control. Telomeric signals were detected with Cy3-(CCCTAA)₃ and are false colored in red (B) Quantification of telomere fusions in HeLa cells transfected with the indicated shRNAs and EV control. Bars represent average numbers of chromosome ends fused of 3 independent experiments with SDs (>6500 telomeres counted/ condition/ experiment). (**) $P < 0.01$; (*) $P < 0.05$, unpaired two-tailed Student's t-test.

Chapter 4 Conclusions and perspectives

Telomeres play principal roles in safeguarding genome stability by solving two major threats to linear genomes: the end replication and the end protection problem. Understanding the basic molecular mechanisms that are at the heart of this is of great importance for expanding our knowledge in how biological systems are organized and for providing treatments for individuals that have impaired genome and telomere integrity. Results presented in this thesis contribute to a deeper understanding of pathways that operate at dysfunctional telomeres and expand the repertoire of proteins that are involved in repair of toxic lesions in DNA. Importantly, we provide novel insights into how the early steps of DNA damage sensing at telomeres are orchestrated which is still an unresolved question in the fields of telomere biology and DNA damage repair.

Firstly, we have been able to clarify the question of how telomeric chromatin structure changes in response to telomere uncapping. To this end, we applied a state-of-the-art microscopy technique which enabled us to look at telomeres with improved resolution. Telomeres visualized in this way are clusters of discrete fluorophore position estimates which were used to infer telomere sizes by computing their Radius of gyration (R_g) or convex hull area. These two different assessments of telomere size correlated well with each other in our experiments. The measurements of the average R_g in telomere populations and telomere labeling efficiencies observed are in agreement with other studies that employ STORM measurement of telomere size (Bandaria et al., 2016; Doksani et al., 2013; Jaynes et al., 2017; Timashev et al., 2017) as well as with studies that visualize telomeres by immunogold staining of telomeric DNA and subsequent electron microscopy analysis (Luderus, 1996; Pierron and Puvion-Dutilleul, 1999). We have been able to benchmark the method by comparing cell lines with normal and extremely long telomeres. We detected changes in the Radius of gyration and convex hull area that are dependent on telomere length. Interestingly, we also observed that longer telomeres are more compacted than the short ones correlating with their heterochromatic status. Furthermore, we have explored telomere compaction state in HeLa cells depleted for TRF1, TRF2 and both TRF1 and TRF2 which should destabilize the whole shelterin complex (Sfeir and de Lange, 2012). To our surprise, shelterin proteins did not significantly remodel the three-dimensional structure of telomeric chromatin as assessed by our technique. We were able to stratify the telomere population by specifically examining the DNA damage positive telomeres using well-characterized DDR protein markers such as γ H2AX and 53BP1. Employing this experimental approach, we observed that upon shelterin removal there was an efficient DNA damage response activation but the change in average radius of gyration was driven by a small subset of damaged telomeres that had extremely large R_g , while the vast majority of telomeres were similar to the control condition. In addition, change in telomere size observed in the DDR positive population was always accompanied by a proportional increase in the number of FISH signals within the telomere clusters. We also employed a complementary approach for labeling the telomere by detecting the telomeric protein TRF1 in HeLa L cells. Similarly to the results obtained by FISH labeling, we observed that only a small subset of DDR positive telomeres upon TRF2 depletion were larger in size and had higher number of localizations albeit the fact that TRF1 levels should remain unchanged upon TRF2 removal (Hockemeyer et al., 2007). Thus, we proposed that these changes are due to telomere-telomere associations and therefore we have excluded the model that incorporated decompaction as a requirement for ATM and DNA damage signaling activation (Bandaria et al., 2016). Our data was in concordance with a jointly published study on mouse telomeres in which telomere decompaction upon uncapping was not observed by STORM microscopy nor by a complementary biochemical Assay for Transposase-Accessible Chromatin using sequencing (ATAC-seq). Furthermore, in this study the authors also suggest that the large telomeric foci are likely formed through 53BP1 dependent clustering of dysfunctional telomeres as they have observed that the average number of telomeric foci per cell is decreased upon telomere deprotection (Timashev et al., 2017). Several other studies are also in contrast with the idea that the major mechanism by which shelterin protects the telomere from illicit DNA damage signaling and repair is by maintaining the compact state of the telomere and restricting access to DDR and other proteins. Namely, when DSBs are made inside the telomeric repeat tract there is a robust DDR activation despite the presence of a functional shelterin complex (Cho et al., 2014a; Doksani and de Lange, 2016; Tang et al., 2013). In addition,

telomeres are frequently associated with large protein complexes such as telomerase in S phase or the MRN complex, ATM and ATR and other accessory factors even in the presence of the shelterin (Schmidt et al., 2016; Verdun and Karlseder, 2006; Zhu et al., 2000). Finally, removal of shelterin does not affect the sensitivity of the telomeric chromatin to MNase digestion (Tommerup et al., 1994) and does not alter the accessibility to Tn5 transposase integration (Timashev et al., 2017). Collectively, these studies support the model that DDR at deprotected telomeres is activated by a chain of molecular events unleashed by shelterin removal, rather than by physical change of telomeric chromatin.

We have also investigated whether SMCHD1 and LRIF1 would mediate telomere compaction similarly to their function at the inactive X chromosome. We did not observe any effect on higher order telomere structure after SMCHD1 and LRIF1 depletion. Thus, the proteins tested in our experiments including TRF1, TRF2, SMCHD1, and LRIF1 did not mediate the compacted state of the telomere. The question remains by which molecular mechanisms telomeres are compacted and how the organization of telomeric chromatin compares to the rest of the genome. As discussed earlier telomeric DNA is wrapped around nucleosomes and this is possibly one mechanism for compacting the ends of linear chromosomes (Tommerup et al., 1994). Additionally, these nucleosomes are decorated with repressive chromatin marks that mediate recruitment of heterochromatin proteins and organize the higher order compaction state of the telomere (reviewed in Blasco, 2007). It would be interesting to disrupt this molecular network by, for example, removal of HP1 and use the STORM-based method to assess changes in the volume of telomeres. The data acquired in our experiments can further be used to investigate the physical parameters of telomere compaction by modeling the telomeric chromatin fiber using computational approaches. Also, our experiments were performed in interphase cells and interesting avenues might be ahead if we looked at how telomeric chromatin is organized in other cell cycle stages especially in metaphase. Preliminary experiments have prompted us to think that another useful application of the established microscopy method would be to analyze fragile telomeres and possibly elucidate their molecular structure which is currently unknown.

Furthermore, we investigated compaction independent roles of previously uncharacterized proteins SMCHD1 and LRIF1 at telomeres. We observed that these factors bind to telomeres in a length dependent manner and that their binding is counteracted by the shelterin protein TRF2. We have discovered a yet undescribed requirement for these proteins in c-NHEJ at unprotected telomeres. We were able to show that this requirement is dependent on the function of SMCHD1 and possibly LRIF1 in activation of the DNA damage signaling cascade in the most upstream steps. As this step in the process is still mechanistically poorly understood, our results contribute to solving the puzzle of ATM activation. In addition, we observed that SMCHD1 removal delays the 3' overhang processing upon TRF2 depletion, a step that is critical for efficient telomere fusion process. Previously, LRIF1 had not been implicated in the DNA damage response. Thus, our results open up interesting paths for future investigation of the roles of LRIF1 in DDR. It would be important to create cell lines harboring LRIF1 knockout to deepen the understanding of how it contributes to promoting DNA damage repair. An important question that arises from our research is whether the two proteins act in a similar manner in the genome wide response to DNA damage and if they are important for efficient DNA repair at other heterochromatic loci whose repair is exclusively dependent on ATM (Goodarzi et al., 2008b; Noon et al., 2010). To tackle this question time course experiments in cells treated with different genotoxic stresses (e.g. γ -Irradiation, Camptothecin, Zeocin, Bleomycin, Hydroxyurea) are required. These experiments could help us to delineate what kind of DNA lesions (if any) require SMCHD1/LRIF1 for efficient DNA damage signaling and repair. Additionally, these experiments could help us understand if heterochromatin breaks that are repaired with slower dynamics rely on these two proteins for repair. Systems for more specific and thus cleaner double strand break induction, such as those based on FokI nuclease, could also contribute to elucidating the exact mechanisms by which these proteins function. These systems enable us to look at two very defined loci (telomeres and LacO array sequences) and compare how different chromatin contexts might influence DNA damage repair dynamics (Cho et al., 2014b; Shanbhag et al., 2010). Experiments in live cells with endogenously tagged shelterin proteins could shed light on the question if telomere mobility required for efficient DNA damage repair is affected by lack of SMCHD1 and LRIF1. These experiments would be interesting in the light of recent findings that SMC5/6 protein complex is required for relocalization of heterochromatic double strand

breaks to the nuclear periphery and for suppression of aberrant HR-mediated repair at repeated sequences (Caridi et al., 2018; Chiolo et al., 2011; Dion et al., 2012). Our experiments have been conducted in HeLa cells that have perturbed checkpoint signaling and it would also be important to test the effects of SMCHD1 and LRIF1 depletion on DDR in wildtype cells such as Retinal Pigment Epithelium (RPE1) or human fibroblasts. Although we have been able to very specifically narrow the steps in the DNA damage cascade that SMCHD1 and LRIF1 are required for, the exact mechanism of their action is still not clear. Further experiments that will reveal their interactors at uncapped telomeres and experiments that will tackle which protein domains are important for function in DDR might provide us with enough information to explain how these proteins perform their functions at telomeres and genome wide. We have been able to tag LRIF1 with tags used for proximity labeling techniques such as BioID (Roux et al., 2012) and we are interested in discovering its interactors at uncapped telomeres to better understand the exact mechanisms by which it helps DNA damage repair. Furthermore, we have cloned SMCHD1 rescue constructs that harbor a mutation in the ATPase domain and LRIF1 rescue constructs with mutations in the HP1 and SMCHD1 interacting domains to be able to delineate the exact interactions involved in the process of DDR. It would also be interesting to deplete chromatin modifiers such as HP1 and test if this phenocopies the effects observed upon SMCHD1 and LRIF1 removal at damaged telomeres. This would strengthen the conclusion that they act in activating the DNA damage signaling cascade by remodeling the chromatin structure. In addition, how modified chromatin structure affects DDR activation is unclear and experiments that test recruitment of ATM and the MRN complex to uncapped telomeres are required for further understanding of this mechanism. An alternative hypothesis for SMCHD1 and LRIF1 function in ATM dependent DDR is by modulating the amplification of the signal mediated by MDC1 (Dimitrova and de Lange, 2006b; Stewart et al., 2003; Stucki et al., 2005). To test this hypothesis analysis of the ATM signaling phenotype after MDC1 depletion in SMCHD1 KO cells is required. Altogether, the proposed experiments in addition to the already obtained experimental data could very precisely dissect the molecular functions and networks of SMCHD1 and LRIF1 at uncapped telomeres and genome wide and potentially help to understand the complex signaling cascade involved in response to DNA damage.

This study illustrates that unprotected telomeres are a very useful model to study DNA damage response pathways. On the other hand, this study reminds us that DNA damage response cascades are context dependent and that they might differ between heterochromatin and euchromatin. Thus, investigating phenomena occurring at deprotected telomeres has once again broadened our knowledge of how basic cellular processes occur. We have discovered novel factors involved in DNA damage signaling and expanded the current knowledge of how cells deal with toxic DNA lesions.

References

- Abreu, E., Aritonovska, E., Reichenbach, P., Cristofari, G., Culp, B., Terns, R.M., Lingner, J., and Terns, M.P. (2010). TIN2-tethered TPP1 recruits human telomerase to telomeres in vivo. *Mol. Cell. Biol.* *30*, 2971–2982.
- Akiyama, B.M., Parks, J.W., and Stone, M.D. (2015). The telomerase essential N-terminal domain promotes DNA synthesis by stabilizing short RNA-DNA hybrids. *Nucleic Acids Res.* *43*, 5537–5549.
- Arat, N.Ö., and Griffith, J.D. (2012). Human Rap1 interacts directly with telomeric DNA and regulates TRF2 localization at the telomere. *J. Biol. Chem.* *287*, 41583–41594.
- Arnoult, N., and Karlseder, J. (2015). Complex interactions between the DNA-damage response and mammalian telomeres. *Nat. Struct. Mol. Biol.* *22*, 859–866.
- Arnoult, N., Saintome, C., Ourliac-Garnier, I., Riou, J.-F., and Londoño-Vallejo, A. (2009). Human POT1 is required for efficient telomere C-rich strand replication in the absence of WRN. *Genes Dev.* *23*, 2915–2924.
- Arora, R., Lee, Y., Wischniewski, H., Brun, C.M., Schwarz, T., and Azzalin, C.M. (2014). RNaseH1 regulates TERRA-telomeric DNA hybrids and telomere maintenance in ALT tumour cells. *Nat. Commun.* *5*.
- Ashe, A., Morgan, D.K., Whitelaw, N.C., Bruxner, T.J., Vickaryous, N.K., Cox, L.L., Butterfield, N.C., Wicking, C., Blewitt, M.E., Wilkins, S.J., et al. (2008). A genome-wide screen for modifiers of transgene variegation identifies genes with critical roles in development. *Genome Biol.* *9*, R182.
- Ayoub, N., Jeyasekharan, A.D., Bernal, J.A., and Venkitaraman, A.R. (2008). HP1-beta mobilization promotes chromatin changes that initiate the DNA damage response. *Nature* *453*, 682–686.
- Azzalin, C.M., Reichenbach, P., Khoriantuli, L., Giulotto, E., and Lingner, J. (2007). Telomeric repeat containing RNA and RNA surveillance factors at mammalian chromosome ends. *Science* *318*, 798–801.
- Bakkenist, C.J., and Kastan, M.B. (2004). Initiating cellular stress responses. *Cell* *118*, 9–17.
- Balk, B., Maicher, A., Dees, M., Klermund, J., Luke-Glaser, S., Bender, K., and Luke, B. (2013). Telomeric RNA-DNA hybrids affect telomere-length dynamics and senescence. *Nat. Struct. Mol. Biol.* *20*, 1199–1205.
- Bandaria, J.N., Qin, P., Berk, V., Chu, S., and Yildiz, A. (2016). Shelterin Protects Chromosome Ends by Compacting Telomeric Chromatin. *Cell* *164*, 735–746.
- Barazas, M., Annunziato, S., Pettitt, S.J., de Krijger, I., Ghezraoui, H., Roobol, S.J., Lutz, C., Frankum, J., Song, F.F., Brough, R., et al. (2018). The CST Complex Mediates End Protection at Double-Strand Breaks and Promotes PARP Inhibitor Sensitivity in BRCA1-Deficient Cells. *Cell Rep.* *23*, 2107–2118.
- Baumann, P., and Cech, T.R. (2001). Pot1, the putative telomere end-binding protein in fission yeast and humans. *Science* *292*, 1171–1175.
- Benarroch-Popivker, D., Pisano, S., Mendez-Bermudez, A., Lototska, L., Kaur, P., Bauwens, S., Djerbi, N., Latrick, C.M., Fraiser, V., Pei, B., et al. (2016). TRF2-Mediated Control of Telomere DNA Topology as a Mechanism for Chromosome-End Protection. *Mol. Cell* *61*, 274–286.
- Bilaud, T., Brun, C., Ancelin, K., Koering, C.E., Laroche, T., and Gilson, E. (1997). Telomeric localization of TRF2, a novel human telobox protein. *Nat. Genet.* *17*, 236–239.
- Blackburn, E.H., and Gall, J.G. (1978). A tandemly repeated sequence at the termini of the extrachromosomal ribosomal RNA genes in Tetrahymena. *J. Mol. Biol.* *120*, 33–53.
- Blasco, M.A. (2007). The epigenetic regulation of mammalian telomeres. *Nat. Rev. Genet.* *8*, 299–309.
- Blewitt, M.E., Vickaryous, N.K., Hemley, S.J., Ashe, A., Bruxner, T.J., Preis, J.I., Arkell, R., and Whitelaw, E. (2005). An N-ethyl-N-nitrosourea screen for genes involved in variegation in the mouse. *Proc. Natl. Acad. Sci.* *102*, 7629–7634.
- Blewitt, M.E., Gendrel, A.-V., Pang, Z., Sparrow, D.B., Whitelaw, N., Craig, J.M., Apedaile, A., Hilton, D.J., Dunwoodie, S.L., Brockdorff, N., et al. (2008). SmcHD1, containing a structural-maintenance-of-chromosomes hinge domain, has a critical role in X inactivation. *Nat. Genet.* *40*, 663–669.

- Bodnar, A.G., Ouellette, M., Frolkis, M., Holt, S.E., Chiu, C.P., Morin, G.B., Harley, C.B., Shay, J.W., Lichtsteiner, S., and Wright, W.E. (1998). Extension of life-span by introduction of telomerase into normal human cells. *Science* *279*, 349–352.
- Boersma, V., Moatti, N., Segura-Bayona, S., Peuscher, M.H., van der Torre, J., Wevers, B.A., Orthwein, A., Durocher, D., and Jacobs, J.J.L. (2015). MAD2L2 controls DNA repair at telomeres and DNA breaks by inhibiting 5' end resection. *Nature* *521*, 537–540.
- Bolderson, E., Savage, K.I., Mahen, R., Pisupati, V., Graham, M.E., Richard, D.J., Robinson, P.J., Venkitaraman, A.R., and Khanna, K.K. (2012). Kruppel-associated Box (KRAB)-associated co-repressor (KAP-1) Ser-473 phosphorylation regulates heterochromatin protein 1 β (HP1- β) mobilization and DNA repair in heterochromatin. *J. Biol. Chem.* *287*, 28122–28131.
- Bombarde, O., Bobby, C., Gomez, D., Frit, P., Giraud-Panis, M.-J., Gilson, E., Salles, B., and Calsou, P. (2010). TRF2/RAP1 and DNA-PK mediate a double protection against joining at telomeric ends. *EMBO J.* *29*, 1573–1584.
- van den Boogaard, M.L., JFL Lemmers, R., Camaño, P., van der Vliet, P.J., Voermans, N., van Engelen, B.G., Lopez de Munain, A., Tapscott, S.J., van der Stoep, N., Tawil, R., et al. (2016). Double SMCHD1 variants in FSHD2: the synergistic effect of two SMCHD1 variants on D4Z4 hypomethylation and disease penetrance in FSHD2. *Eur. J. Hum. Genet.* *24*, 78–85.
- Bouwman, P., Aly, A., Escandell, J.M., Pieterse, M., Bartkova, J., van der Gulden, H., Hiddingh, S., Thanassoula, M., Kulkarni, A., Yang, Q., et al. (2010). 53BP1 loss rescues BRCA1 deficiency and is associated with triple-negative and BRCA-mutated breast cancers. *Nat. Struct. Mol. Biol.* *17*, 688–695.
- Brideau, N.J., Coker, H., Gendrel, A.-V., Siebert, C.A., Bezstarosti, K., Demmers, J., Poot, R.A., Nesterova, T.B., and Brockdorff, N. (2015). Independent Mechanisms Target SMCHD1 to Trimethylated Histone H3 Lysine 9-Modified Chromatin and the Inactive X Chromosome. *Mol. Cell. Biol.* *35*, 4053–4068.
- Broccoli, D., Smogorzewska, A., Chong, L., and de Lange, T. (1997). Human telomeres contain two distinct Myb-related proteins, TRF1 and TRF2. *Nat. Genet.* *17*, 231–235.
- Brown, E.J., and Baltimore, D. (2000). ATR disruption leads to chromosomal fragmentation and early embryonic lethality. *Genes Dev.* *14*, 397–402.
- Brown, E.J., and Baltimore, D. (2003). Essential and dispensable roles of ATR in cell cycle arrest and genome maintenance. *Genes Dev.* *17*, 615–628.
- Bryan, T.M., Englezou, A., Dalla-Pozza, L., Dunham, M.A., and Reddel, R.R. (1997). Evidence for an alternative mechanism for maintaining telomere length in human tumors and tumor-derived cell lines. *Nat. Med.* *3*, 1271–1274.
- Bryant, H.E., Schultz, N., Thomas, H.D., Parker, K.M., Flower, D., Lopez, E., Kyle, S., Meuth, M., Curtin, N.J., and Helleday, T. (2005). Specific killing of BRCA2-deficient tumours with inhibitors of poly(ADP-ribose) polymerase. *Nature* *434*, 913–917.
- Bunting, S.F., Callén, E., Wong, N., Chen, H.-T., Polato, F., Gunn, A., Bothmer, A., Feldhahn, N., Fernandez-Capetillo, O., Cao, L., et al. (2010). 53BP1 inhibits homologous recombination in Brca1-deficient cells by blocking resection of DNA breaks. *Cell* *141*, 243–254.
- Buxton, K.E., Kennedy-Darling, J., Shortreed, M.R., Zaidan, N.Z., Olivier, M., Scalf, M., Sridharan, R., and Smith, L.M. (2017). Elucidating Protein–DNA Interactions in Human Alphoid Chromatin via Hybridization Capture and Mass Spectrometry. *J. Proteome Res.* *16*, 3433–3442.
- Cao, L., Xu, X., Bunting, S.F., Liu, J., Wang, R.-H., Cao, L.L., Wu, J.J., Peng, T.-N., Chen, J., Nussenzweig, A., et al. (2009). A selective requirement for 53BP1 in the biological response to genomic instability induced by Brca1 deficiency. *Mol. Cell* *35*, 534–541.
- Caridi, C.P., D'Agostino, C., Ryu, T., Zapotoczny, G., Delabaere, L., Li, X., Khodaverdian, V.Y., Amaral, N., Lin, E., Rau, A.R., et al. (2018). Nuclear F-actin and myosins drive relocalization of heterochromatic breaks. *Nature* *559*, 54–60.
- Cash, D.D., and Feigon, J. (2017). Structure and folding of the *Tetrahymena* telomerase RNA pseudoknot. *Nucleic Acids Res.* *45*, 482–495.

Ceccaldi, R., Liu, J.C., Amunugama, R., Hajdu, I., Primack, B., Petalcorin, M.I.R., O'Connor, K.W., Konstantinopoulos, P.A., Elledge, S.J., Boulton, S.J., et al. (2015). Homologous-recombination-deficient tumours are dependent on Pol θ -mediated repair. *Nature* *518*, 258–262.

Chapman, J.R., Barral, P., Vannier, J.-B., Borel, V., Steger, M., Tomas-Loba, A., Sartori, A.A., Adams, I.R., Batista, F.D., and Boulton, S.J. (2013). RIF1 is essential for 53BP1-dependent nonhomologous end joining and suppression of DNA double-strand break resection. *Mol. Cell* *49*, 858–871.

Chen, K., Hu, J., Moore, D.L., Liu, R., Kessans, S.A., Breslin, K., Lucet, I.S., Keniry, A., Leong, H.S., Parish, C.L., et al. (2015). Genome-wide binding and mechanistic analyses of Smchd1-mediated epigenetic regulation. *Proc. Natl. Acad. Sci.* *112*, E3535–E3544.

Chen, K., Czabotar, P.E., Blewitt, M.E., and Murphy, J.M. (2016a). The hinge domain of the epigenetic repressor Smchd1 adopts an unconventional homodimeric configuration. *Biochem. J.* *473*, 733–742.

Chen, K., Dobson, R.C.J., Lucet, I.S., Young, S.N., Pearce, F.G., Blewitt, M.E., and Murphy, J.M. (2016b). The epigenetic regulator Smchd1 contains a functional GHKL-type ATPase domain. *Biochem. J.* *473*, 1733–1744.

Chen, L., Roake, C.M., Freund, A., Batista, P.J., Tian, S., Yin, Y.A., Gajera, C.R., Lin, S., Lee, B., Pech, M.F., et al. (2018). An Activity Switch in Human Telomerase Based on RNA Conformation and Shaped by TCAB1. *Cell* *174*, 218–230.e13.

Chen, L.-Y., Redon, S., and Lingner, J. (2012). The human CST complex is a terminator of telomerase activity. *Nature* *488*, 540–544.

Chiolo, I., Minoda, A., Colmenares, S.U., Polyzos, A., Costes, S.V., and Karpen, G.H. (2011). Double-strand breaks in heterochromatin move outside of a dynamic HP1a domain to complete recombinational repair. *Cell* *144*, 732–744.

Chiu, A., Revenkova, E., and Jessberger, R. (2004). DNA Interaction and Dimerization of Eukaryotic SMC Hinge Domains. *J. Biol. Chem.* *279*, 26233–26242.

Cho, N.W., Dilley, R.L., Lampson, M.A., and Greenberg, R.A. (2014a). Interchromosomal homology searches drive directional ALT telomere movement and synapsis. *Cell* *159*, 108–121.

Cho, N.W., Dilley, R.L., Lampson, M.A., and Greenberg, R.A. (2014b). Interchromosomal homology searches drive directional ALT telomere movement and synapsis. *Cell* *159*, 108–121.

Chong, L., van Steensel, B., Broccoli, D., Erdjument-Bromage, H., Hanish, J., Tempst, P., and de Lange, T. (1995). A human telomeric protein. *Science* *270*, 1663–1667.

Cohen, S.B., Graham, M.E., Lovrecz, G.O., Bache, N., Robinson, P.J., and Reddel, R.R. (2007). Protein Composition of Catalytically Active Human Telomerase from Immortal Cells. *Science* *315*, 1850–1853.

Coker, H., and Brockdorff, N. (2014). SMCHD1 accumulates at DNA damage sites and facilitates the repair of DNA double-strand breaks. *J. Cell Sci.* *127*, 1869–1874.

Cong, Y.S., Wen, J., and Bacchetti, S. (1999). The human telomerase catalytic subunit hTERT: organization of the gene and characterization of the promoter. *Hum. Mol. Genet.* *8*, 137–142.

Cong, Y.-S., Wright, W.E., and Shay, J.W. (2002). Human Telomerase and Its Regulation. *Microbiol. Mol. Biol. Rev.* *66*, 407–425.

Cortez, D., Guntuku, S., Qin, J., and Elledge, S.J. (2001). ATR and ATRIP: partners in checkpoint signaling. *Science* *294*, 1713–1716.

Cotta-Ramusino, C., McDonald, E.R., Hurov, K., Sowa, M.E., Harper, J.W., and Elledge, S.J. (2011). A DNA damage response screen identifies RHINO, a 9-1-1 and TopBP1 interacting protein required for ATR signaling. *Science* *332*, 1313–1317.

Crabbe, L., Verdun, R.E., Haggblom, C.I., and Karlseder, J. (2004). Defective telomere lagging strand synthesis in cells lacking WRN helicase activity. *Science* *306*, 1951–1953.

Cristofari, G., Adolf, E., Reichenbach, P., Sikora, K., Terns, R.M., Terns, M.P., and Lingner, J. (2007). Human telomerase RNA accumulation in Cajal bodies facilitates telomerase recruitment to telomeres and telomere elongation. *Mol. Cell* *27*, 882–889.

- Déjardin, J., and Kingston, R.E. (2009). Purification of Proteins Associated with Specific Genomic Loci. *Cell* *136*, 175–186.
- Delacroix, S., Wagner, J.M., Kobayashi, M., Yamamoto, K., and Karnitz, L.M. (2007). The Rad9-Hus1-Rad1 (9-1-1) clamp activates checkpoint signaling via TopBP1. *Genes Dev.* *21*, 1472–1477.
- Denchi, E.L., and de Lange, T. (2007). Protection of telomeres through independent control of ATM and ATR by TRF2 and POT1. *Nature* *448*, 1068–1071.
- Deng, Z., Wang, Z., Stong, N., Plasschaert, R., Moczan, A., Chen, H.-S., Hu, S., Wikramasinghe, P., Davuluri, R.V., Bartolomei, M.S., et al. (2012). A role for CTCF and cohesin in subtelomere chromatin organization, TERRA transcription, and telomere end protection. *EMBO J.* *31*, 4165–4178.
- Dev, H., Chiang, T.-W.W., Lescale, C., de Krijger, I., Martin, A.G., Pilger, D., Coates, J., Sczaniecka-Clift, M., Wei, W., Ostermaier, M., et al. (2018). Shieldin complex promotes DNA end-joining and counters homologous recombination in BRCA1-null cells. *Nat. Cell Biol.* *20*, 954–965.
- Difilippantonio, S., Gapud, E., Wong, N., Huang, C.-Y., Mahowald, G., Chen, H.T., Kruhlak, M.J., Callen, E., Livak, F., Nussenzweig, M.C., et al. (2008). 53BP1 facilitates long-range DNA end-joining during V(D)J recombination. *Nature* *456*, 529–533.
- Dilley, R.L., and Greenberg, R.A. (2015). ALternative Telomere Maintenance and Cancer. *Trends Cancer* *1*, 145–156.
- Dimitrova, N., and de Lange, T. (2006a). MDC1 accelerates nonhomologous end-joining of dysfunctional telomeres. *Genes Dev.* *20*, 3238–3243.
- Dimitrova, N., and de Lange, T. (2006b). MDC1 accelerates nonhomologous end-joining of dysfunctional telomeres. *Genes Dev.* *20*, 3238–3243.
- Dion, V., Kalck, V., Horigome, C., Towbin, B.D., and Gasser, S.M. (2012). Increased mobility of double-strand breaks requires Mec1, Rad9 and the homologous recombination machinery. *Nat. Cell Biol.* *14*, 502–509.
- Doil, C., Mailand, N., Bekker-Jensen, S., Menard, P., Larsen, D.H., Pepperkok, R., Ellenberg, J., Panier, S., Durocher, D., Bartek, J., et al. (2009). RNF168 binds and amplifies ubiquitin conjugates on damaged chromosomes to allow accumulation of repair proteins. *Cell* *136*, 435–446.
- Doksani, Y., and de Lange, T. (2016). Telomere-Internal Double-Strand Breaks Are Repaired by Homologous Recombination and PARP1/Lig3-Dependent End-Joining. *Cell Rep.* *17*, 1646–1656.
- Doksani, Y., Wu, J.Y., de Lange, T., and Zhuang, X. (2013). Super-Resolution Fluorescence Imaging of Telomeres Reveals TRF2-Dependent T-loop Formation. *Cell* *155*, 345–356.
- Dunham, M.A., Neumann, A.A., Fasching, C.L., and Reddel, R.R. (2000). Telomere maintenance by recombination in human cells. *Nat. Genet.* *26*, 447–450.
- Ellison, V., and Stillman, B. (2003). Biochemical characterization of DNA damage checkpoint complexes: clamp loader and clamp complexes with specificity for 5' recessed DNA. *PLoS Biol.* *1*, E33.
- d'Adda di Fagagna, F., Reaper, P.M., Clay-Farrace, L., Fiegler, H., Carr, P., Von Zglinicki, T., Saretzki, G., Carter, N.P., and Jackson, S.P. (2003). A DNA damage checkpoint response in telomere-initiated senescence. *Nature* *426*, 194–198.
- d'Adda di Fagagna, F., Teo, S.-H., and Jackson, S.P. (2004). Functional links between telomeres and proteins of the DNA-damage response. *Genes Dev.* *18*, 1781–1799.
- Falck, J., Coates, J., and Jackson, S.P. (2005). Conserved modes of recruitment of ATM, ATR and DNA-PKcs to sites of DNA damage. *Nature* *434*, 605–611.
- Farmer, H., McCabe, N., Lord, C.J., Tutt, A.N.J., Johnson, D.A., Richardson, T.B., Santarosa, M., Dillon, K.J., Hickson, I., Knights, C., et al. (2005). Targeting the DNA repair defect in BRCA mutant cells as a therapeutic strategy. *Nature* *434*, 917–921.
- Feuerhahn, S., Iglesias, N., Panza, A., Porro, A., and Lingner, J. (2010). TERRA biogenesis, turnover and implications for function. *FEBS Lett.* *584*, 3812–3818.

Flynn, R.L., Centore, R.C., O'Sullivan, R.J., Rai, R., Tse, A., Songyang, Z., Chang, S., Karlseder, J., and Zou, L. (2011). TERRA and hnRNPA1 orchestrate an RPA-to-POT1 switch on telomeric single-stranded DNA. *Nature* *471*, 532–536.

Freund, A., Zhong, F.L., Venteicher, A.S., Meng, Z., Veenstra, T.D., Frydman, J., and Artandi, S.E. (2014). Proteostatic Control of Telomerase Function through TRiC-Mediated Folding of TCAB1. *Cell* *159*, 1389–1403.

Galati, A., Micheli, E., Alicata, C., Ingegnere, T., Cicconi, A., Pusch, M.C., Giraud-Panis, M.-J., Gilson, E., and Cacchione, S. (2015). TRF1 and TRF2 binding to telomeres is modulated by nucleosomal organization. *Nucleic Acids Res.* *43*, 5824–5837.

Garcia-Exposito, L., Bournique, E., Bergoglio, V., Bose, A., Barroso-Gonzalez, J., Zhang, S., Roncaioli, J.L., Lee, M., Wallace, C.T., Watkins, S.C., et al. (2016). Proteomic Profiling Reveals a Specific Role for Translesion DNA Polymerase η in the Alternative Lengthening of Telomeres. *Cell Rep.* *17*, 1858–1871.

Gendrel, A.-V., Tang, Y.A., Suzuki, M., Godwin, J., Nesterova, T.B., Grealley, J.M., Heard, E., and Brockdorff, N. (2013). Epigenetic Functions of Smchd1 Repress Gene Clusters on the Inactive X Chromosome and on Autosomes. *Mol. Cell. Biol.* *33*, 3150–3165.

Ghezraoui, H., Oliveira, C., Becker, J.R., Bilham, K., Moralli, D., Anzilotti, C., Fischer, R., Deobagkar-Lele, M., Sanchiz-Calvo, M., Fueyo-Marcos, E., et al. (2018). 53BP1 cooperation with the REV7-shieldin complex underpins DNA structure-specific NHEJ. *Nature*.

Goodarzi, A.A., Noon, A.T., Deckbar, D., Ziv, Y., Shiloh, Y., Löbrich, M., and Jeggo, P.A. (2008a). ATM signaling facilitates repair of DNA double-strand breaks associated with heterochromatin. *Mol. Cell* *31*, 167–177.

Goodarzi, A.A., Noon, A.T., Deckbar, D., Ziv, Y., Shiloh, Y., Löbrich, M., and Jeggo, P.A. (2008b). ATM Signaling Facilitates Repair of DNA Double-Strand Breaks Associated with Heterochromatin. *Mol. Cell* *31*, 167–177.

Goodarzi, A.A., Jeggo, P., and Lobrich, M. (2010). The influence of heterochromatin on DNA double strand break repair: Getting the strong, silent type to relax. *DNA Repair* *9*, 1273–1282.

Gordon, C.T., Xue, S., Yigit, G., Filali, H., Chen, K., Rosin, N., Yoshiura, K., Oufadem, M., Beck, T.J., McGowan, R., et al. (2017). De novo mutations in SMCHD1 cause Bosma arhinia microphthalmia syndrome and abrogate nasal development. *Nat. Genet.* *49*, 249–255.

Graf, M., Bonetti, D., Lockhart, A., Serhal, K., Kellner, V., Maicher, A., Jolivet, P., Teixeira, M.T., and Luke, B. (2017). Telomere Length Determines TERRA and R-Loop Regulation through the Cell Cycle. *Cell* *170*, 72–85.e14.

Greenberg, R.A. (2018). Assembling a protective shield. *Nat. Cell Biol.* *20*, 862–863.

Greider, C.W., and Blackburn, E.H. (1985). Identification of a specific telomere terminal transferase activity in tetrahymena extracts. *Cell* *43*, 405–413.

Greider, C.W., and Blackburn, E.H. (1987). The telomere terminal transferase of Tetrahymena is a ribonucleoprotein enzyme with two kinds of primer specificity. *Cell* *51*, 887–898.

Greider, C.W., and Blackburn, E.H. (1989). A telomeric sequence in the RNA of Tetrahymena telomerase required for telomere repeat synthesis. *Nature* *337*, 331–337.

Griffith, J.D., Comeau, L., Rosenfield, S., Stansel, R.M., Bianchi, A., Moss, H., and de Lange, T. (1999). Mammalian telomeres end in a large duplex loop. *Cell* *97*, 503–514.

Grolimund, L., Aeby, E., Hamelin, R., Armand, F., Chiappe, D., Moniatte, M., and Lingner, J. (2013). A quantitative telomeric chromatin isolation protocol identifies different telomeric states. *Nat. Commun.* *4*.

Gupta, R., Somyajit, K., Narita, T., Maskey, E., Stanlie, A., Kremer, M., Typas, D., Lammers, M., Mailand, N., Nussenzweig, A., et al. (2018). DNA Repair Network Analysis Reveals Shieldin as a Key Regulator of NHEJ and PARP Inhibitor Sensitivity. *Cell* *173*, 972–988.e23.

Hanahan, D., and Weinberg, R.A. (2000). The hallmarks of cancer. *Cell* *100*, 57–70.

Hayashi, M.T., Cesare, A.J., Rivera, T., and Karlseder, J. (2015). Cell death during crisis is mediated by mitotic telomere deprotection. *Nature* *522*, 492–496.

- Hayflick, L. (1965). THE LIMITED IN VITRO LIFETIME OF HUMAN DIPLOID CELL STRAINS. *Exp. Cell Res.* **37**, 614–636.
- Henderson, E.R., and Blackburn, E.H. (1989). An overhanging 3' terminus is a conserved feature of telomeres. *Mol. Cell. Biol.* **9**, 345–348.
- Hockemeyer, D., Palm, W., Else, T., Daniels, J.-P., Takai, K.K., Ye, J.Z.-S., Keegan, C.E., de Lange, T., and Hammer, G.D. (2007). Telomere protection by mammalian Pot1 requires interaction with Tpp1. *Nat. Struct. Mol. Biol.* **14**, 754–761.
- Huen, M.S.Y., Grant, R., Manke, I., Minn, K., Yu, X., Yaffe, M.B., and Chen, J. (2007). RNF8 transduces the DNA-damage signal via histone ubiquitylation and checkpoint protein assembly. *Cell* **131**, 901–914.
- Hustedt, N., and Durocher, D. (2017). The control of DNA repair by the cell cycle. *Nat. Cell Biol.* **19**, 1–9.
- Jackson, S.P., and Bartek, J. (2009). The DNA-damage response in human biology and disease. *Nature* **461**, 1071–1078.
- Jády, B.E., Bertrand, E., and Kiss, T. (2004). Human telomerase RNA and box H/ACA scaRNAs share a common Cajal body-specific localization signal. *J. Cell Biol.* **164**, 647–652.
- Jády, B.E., Richard, P., Bertrand, E., and Kiss, T. (2006). Cell cycle-dependent recruitment of telomerase RNA and Cajal bodies to human telomeres. *Mol. Biol. Cell* **17**, 944–954.
- Janoušková, E., Nečasová, I., Pavloušková, J., Zimmermann, M., Hluchý, M., Marini, V., Nováková, M., and Hofr, C. (2015). Human Rap1 modulates TRF2 attraction to telomeric DNA. *Nucleic Acids Res.* **43**, 2691–2700.
- Jansz, N., Chen, K., Murphy, J.M., and Blewitt, M.E. (2017). The Epigenetic Regulator SMCHD1 in Development and Disease. *Trends Genet.* **33**, 233–243.
- Jazayeri, A., Falck, J., Lukas, C., Bartek, J., Smith, G.C.M., Lukas, J., and Jackson, S.P. (2006). ATM- and cell cycle-dependent regulation of ATR in response to DNA double-strand breaks. *Nat. Cell Biol.* **8**, 37–45.
- Jeynes, J.C.G., Geraki, K., Jeynes, C., Zhaohong, M., Bettiol, A.A., Latorre, E., Harries, L.W., and Soeller, C. (2017). Nanoscale Properties of Human Telomeres Measured with a Dual Purpose X-ray Fluorescence and Super Resolution Microscopy Gold Nanoparticle Probe. *ACS Nano* **11**, 12632–12640.
- Karlseder, J., Broccoli, D., Dai, Y., Hardy, S., and de Lange, T. (1999). p53- and ATM-dependent apoptosis induced by telomeres lacking TRF2. *Science* **283**, 1321–1325.
- Karlseder, J., Hoke, K., Mirzoeva, O.K., Bakkenist, C., Kastan, M.B., Petrini, J.H.J., and Lange, T. de (2004). The Telomeric Protein TRF2 Binds the ATM Kinase and Can Inhibit the ATM-Dependent DNA Damage Response. *PLoS Biol.* **2**, e240.
- Kelleher, C., Kurth, I., and Lingner, J. (2005). Human protection of telomeres 1 (POT1) is a negative regulator of telomerase activity in vitro. *Mol. Cell. Biol.* **25**, 808–818.
- Kent, T., Chandramouly, G., McDevitt, S.M., Ozdemir, A.Y., and Pomerantz, R.T. (2015). Mechanism of microhomology-mediated end-joining promoted by human DNA polymerase θ . *Nat. Struct. Mol. Biol.* **22**, 230–237.
- Kim, N.W., Piatyszek, M.A., Prowse, K.R., Harley, C.B., West, M.D., Ho, P.L., Coviello, G.M., Wright, W.E., Weinrich, S.L., and Shay, J.W. (1994). Specific association of human telomerase activity with immortal cells and cancer. *Science* **266**, 2011–2015.
- de Klein, A., Muijtjens, M., van Os, R., Verhoeven, Y., Smit, B., Carr, A.M., Lehmann, A.R., and Hoeijmakers, J.H. (2000). Targeted disruption of the cell-cycle checkpoint gene ATR leads to early embryonic lethality in mice. *Curr. Biol. CB* **10**, 479–482.
- Klobutcher, L.A., Swanton, M.T., Donini, P., and Prescott, D.M. (1981). All gene-sized DNA molecules in four species of hypotrichs have the same terminal sequence and an unusual 3' terminus. *Proc. Natl. Acad. Sci. U. S. A.* **78**, 3015–3019.
- Kolas, N.K., Chapman, J.R., Nakada, S., Ylanko, J., Chahwan, R., Sweeney, F.D., Panier, S., Mendez, M., Wildenhain, J., Thomson, T.M., et al. (2007). Orchestration of the DNA-damage response by the RNF8 ubiquitin ligase. *Science* **318**, 1637–1640.

- Konishi, A., and de Lange, T. (2008). Cell cycle control of telomere protection and NHEJ revealed by a ts mutation in the DNA-binding domain of TRF2. *Genes Dev.* *22*, 1221–1230.
- Lambert, S., and Carr, A.M. (2013). Impediments to replication fork movement: stabilisation, reactivation and genome instability. *Chromosoma* *122*, 33–45.
- de Lange, T. (2005). Shelterin: the protein complex that shapes and safeguards human telomeres. *Genes Dev.* *19*, 2100–2110.
- Lansdorp, P.M. (2009). Telomeres and disease. *EMBO J.* *28*, 2532–2540.
- Larsen, M., Rost, S., El Hajj, N., Ferbert, A., Deschauer, M., Walter, M.C., Schoser, B., Tacik, P., Kress, W., and Müller, C.R. (2015). Diagnostic approach for FSHD revisited: SMCHD1 mutations cause FSHD2 and act as modifiers of disease severity in FSHD1. *Eur. J. Hum. Genet.* *23*, 808–816.
- Latrick, C.M., and Cech, T.R. (2010). POT1-TPP1 enhances telomerase processivity by slowing primer dissociation and aiding translocation. *EMBO J.* *29*, 924–933.
- Lazzerini-Denchi, E., and Sfeir, A. (2016). Stop pulling my strings — what telomeres taught us about the DNA damage response. *Nat. Rev. Mol. Cell Biol.* *17*, 364–378.
- Lee, J., and Dunphy, W.G. (2010). Rad17 plays a central role in establishment of the interaction between TopBP1 and the Rad9-Hus1-Rad1 complex at stalled replication forks. *Mol. Biol. Cell* *21*, 926–935.
- Lee, J.-H., and Paull, T.T. (2004). Direct activation of the ATM protein kinase by the Mre11/Rad50/Nbs1 complex. *Science* *304*, 93–96.
- Lee, J.-H., and Paull, T.T. (2005). ATM activation by DNA double-strand breaks through the Mre11-Rad50-Nbs1 complex. *Science* *308*, 551–554.
- Lee, J.-H., Ghirlando, R., Bhaskara, V., Hoffmeyer, M.R., Gu, J., and Paull, T.T. (2003). Regulation of Mre11/Rad50 by Nbs1: EFFECTS ON NUCLEOTIDE-DEPENDENT DNA BINDING AND ASSOCIATION WITH ATAXIA-TELANGIECTASIA-LIKE DISORDER MUTANT COMPLEXES. *J. Biol. Chem.* *278*, 45171–45181.
- Lei, M., Zaug, A.J., Podell, E.R., and Cech, T.R. (2005). Switching human telomerase on and off with hPOT1 protein in vitro. *J. Biol. Chem.* *280*, 20449–20456.
- Lemmers, R.J.L.F., Tawil, R., Petek, L.M., Balog, J., Block, G.J., Santen, G.W.E., Amell, A.M., van der Vliet, P.J., Almomani, R., Straasheijm, K.R., et al. (2012). Digenic inheritance of an SMCHD1 mutation and an FSHD-permissive D4Z4 allele causes facioscapulohumeral muscular dystrophy type 2. *Nat. Genet.* *44*, 1370–1374.
- Lempiäinen, H., and Halazonetis, T.D. (2009). Emerging common themes in regulation of PIKKs and PI3Ks. *EMBO J.* *28*, 3067–3073.
- Lendvay, T.S., Morris, D.K., Sah, J., Balasubramanian, B., and Lundblad, V. (1996). Senescence mutants of *Saccharomyces cerevisiae* with a defect in telomere replication identify three additional EST genes. *Genetics* *144*, 1399–1412.
- Leong, H.S., Chen, K., Hu, Y., Lee, S., Corbin, J., Pakusch, M., Murphy, J.M., Majewski, I.J., Smyth, G.K., Alexander, W.S., et al. (2013). Epigenetic Regulator Smchd1 Functions as a Tumor Suppressor. *Cancer Res.* *73*, 1591–1599.
- Li, H.J., Haque, Z.K., Chen, A., and Mendelsohn, M. (2007). RIF-1, a novel nuclear receptor corepressor that associates with the nuclear matrix. *J. Cell. Biochem.* *102*, 1021–1035.
- Li, J.S.Z., Miralles Fusté, J., Simavorian, T., Bartocci, C., Tsai, J., Karlseder, J., and Lazzerini Denchi, E. (2017). TZAP: A telomere-associated protein involved in telomere length control. *Science* *355*, 638–641.
- Lin, J., Ly, H., Hussain, A., Abraham, M., Pearl, S., Tzfati, Y., Parslow, T.G., and Blackburn, E.H. (2004). A universal telomerase RNA core structure includes structured motifs required for binding the telomerase reverse transcriptase protein. *Proc. Natl. Acad. Sci. U. S. A.* *101*, 14713–14718.
- Lingner, J., and Cech, T.R. (1996). Purification of telomerase from *Euplotes aediculatus*: requirement of a primer 3' overhang. *Proc. Natl. Acad. Sci. U. S. A.* *93*, 10712–10717.

- Lingner, J., Cooper, J., and Cech, T. (1995). Telomerase and DNA end replication: no longer a lagging strand problem? *Science* *269*, 1533–1534.
- Lingner, J., Hughes, T.R., Shevchenko, A., Mann, M., Lundblad, V., and Cech, T.R. (1997). Reverse transcriptase motifs in the catalytic subunit of telomerase. *Science* *276*, 561–567.
- Liu, Q., Guntuku, S., Cui, X.S., Matsuoka, S., Cortez, D., Tamai, K., Luo, G., Carattini-Rivera, S., DeMayo, F., Bradley, A., et al. (2000). Chk1 is an essential kinase that is regulated by Atr and required for the G(2)/M DNA damage checkpoint. *Genes Dev.* *14*, 1448–1459.
- Liu, R., Chen, K., Jansz, N., Blewitt, M.E., and Ritchie, M.E. (2016). Transcriptional profiling of the epigenetic regulator Smchd1. *Genomics Data* *7*, 144–147.
- Liu, S., Shiotani, B., Lahiri, M., Maréchal, A., Tse, A., Leung, C.C.Y., Glover, J.N.M., Yang, X.H., and Zou, L. (2011). ATR autophosphorylation as a molecular switch for checkpoint activation. *Mol. Cell* *43*, 192–202.
- Lorković, Z.J., Naumann, U., Matzke, A.J.M., and Matzke, M. (2012). Involvement of a GHKL ATPase in RNA-Directed DNA Methylation in *Arabidopsis thaliana*. *Curr. Biol.* *22*, 933–938.
- Losada, A. (2005). Dynamic molecular linkers of the genome: the first decade of SMC proteins. *Genes Dev.* *19*, 1269–1287.
- Lotterberger, F., Karssemeijer, R.A., Dimitrova, N., and de Lange, T. (2015). 53BP1 and the LINC Complex Promote Microtubule-Dependent DSB Mobility and DNA Repair. *Cell* *163*, 880–893.
- Lovejoy, C.A., and Cortez, D. (2009). Common mechanisms of PIKK regulation. *DNA Repair* *8*, 1004–1008.
- Luderus, M.E. (1996). Structure, subnuclear distribution, and nuclear matrix association of the mammalian telomeric complex. *J. Cell Biol.* *135*, 867–881.
- Lue, N.F. (2005). A physical and functional constituent of telomerase anchor site. *J. Biol. Chem.* *280*, 26586–26591.
- Lukas, J., Lukas, C., and Bartek, J. (2011). More than just a focus: The chromatin response to DNA damage and its role in genome integrity maintenance. *Nat. Cell Biol.* *13*, 1161–1169.
- Lukaszewicz, A., Lange, J., Keeney, S., and Jasin, M. (2018). Control of meiotic double-strand-break formation by ATM: local and global views. *Cell Cycle* *1*–18.
- Lundblad, V., and Blackburn, E.H. (1993). An alternative pathway for yeast telomere maintenance rescues est1- senescence. *Cell* *73*, 347–360.
- Lundblad, V., and Szostak, J.W. (1989). A mutant with a defect in telomere elongation leads to senescence in yeast. *Cell* *57*, 633–643.
- Maciejowski, J., Li, Y., Bosco, N., Campbell, P.J., and de Lange, T. (2015). Chromothripsis and Kataegis Induced by Telomere Crisis. *Cell* *163*, 1641–1654.
- Mailand, N., Falck, J., Lukas, C., Syljuåsen, R.G., Welcker, M., Bartek, J., and Lukas, J. (2000). Rapid destruction of human Cdc25A in response to DNA damage. *Science* *288*, 1425–1429.
- Mailand, N., Bekker-Jensen, S., Fastrup, H., Melander, F., Bartek, J., Lukas, C., and Lukas, J. (2007). RNF8 ubiquitylates histones at DNA double-strand breaks and promotes assembly of repair proteins. *Cell* *131*, 887–900.
- Majerska, J., Feretzaki, M., Glousker, G., and Lingner, J. (2018). Transformation-induced stress at telomeres is counteracted through changes in the telomeric proteome including SAMHD1. *Life Sci. Alliance* *1*, e201800121.
- Marcand, S., Gilson, E., and Shore, D. (1997). A protein-counting mechanism for telomere length regulation in yeast. *Science* *275*, 986–990.
- Marechal, A., and Zou, L. (2013). DNA Damage Sensing by the ATM and ATR Kinases. *Cold Spring Harb. Perspect. Biol.* *5*, a012716–a012716.
- Maréchal, A., and Zou, L. (2015). RPA-coated single-stranded DNA as a platform for post-translational modifications in the DNA damage response. *Cell Res.* *25*, 9–23.

- Margalef, P., Kotsantis, P., Borel, V., Bellelli, R., Panier, S., and Boulton, S.J. (2018). Stabilization of Reversed Replication Forks by Telomerase Drives Telomere Catastrophe. *Cell* *172*, 439–453.e14.
- Massah, S., Hollebakken, R., Labrecque, M.P., Kolybaba, A.M., Beischlag, T.V., and Prefontaine, G.G. (2014). Epigenetic Characterization of the Growth Hormone Gene Identifies SmcHD1 as a Regulator of Autosomal Gene Clusters. *PLoS ONE* *9*, e97535.
- Mateos-Gomez, P.A., Gong, F., Nair, N., Miller, K.M., Lazzerini-Denchi, E., and Sfeir, A. (2015). Mammalian polymerase θ promotes alternative NHEJ and suppresses recombination. *Nature* *518*, 254–257.
- Mateos-Gomez, P.A., Kent, T., Deng, S.K., McDevitt, S., Kashkina, E., Hoang, T.M., Pomerantz, R.T., and Sfeir, A. (2017). The helicase domain of Pol θ counteracts RPA to promote alt-NHEJ. *Nat. Struct. Mol. Biol.* *24*, 1116–1123.
- Matsuoka, S., Huang, M., and Elledge, S.J. (1998). Linkage of ATM to cell cycle regulation by the Chk2 protein kinase. *Science* *282*, 1893–1897.
- Mattioli, F., Vissers, J.H.A., van Dijk, W.J., Ikpa, P., Citterio, E., Vermeulen, W., Martejijn, J.A., and Sixma, T.K. (2012). RNF168 ubiquitinates K13-15 on H2A/H2AX to drive DNA damage signaling. *Cell* *150*, 1182–1195.
- McClintock, B. (1939). The Behavior in Successive Nuclear Divisions of a Chromosome Broken at Meiosis. *Proc. Natl. Acad. Sci. U. S. A.* *25*, 405–416.
- McClintock, B. (1941). The Stability of Broken Ends of Chromosomes in Zea Mays. *Genetics* *26*, 234–282.
- Meier, A., Fiegler, H., Muñoz, P., Ellis, P., Rigler, D., Langford, C., Blasco, M.A., Carter, N., and Jackson, S.P. (2007). Spreading of mammalian DNA-damage response factors studied by ChIP-chip at damaged telomeres. *EMBO J.* *26*, 2707–2718.
- Miller, K.M., Rog, O., and Cooper, J.P. (2006). Semi-conservative DNA replication through telomeres requires Taz1. *Nature* *440*, 824–828.
- Mirman, Z., Lottersberger, F., Takai, H., Kibe, T., Gong, Y., Takai, K., Bianchi, A., Zimmermann, M., Durocher, D., and de Lange, T. (2018). 53BP1-RIF1-shieldin counteracts DSB resection through CST- and Pola-dependent fill-in. *Nature*.
- Mitchell, J.R., and Collins, K. (2000). Human telomerase activation requires two independent interactions between telomerase RNA and telomerase reverse transcriptase. *Mol. Cell* *6*, 361–371.
- Moudry, P., Lukas, C., Macurek, L., Hanzlikova, H., Hodny, Z., Lukas, J., and Bartek, J. (2012). Ubiquitin-activating enzyme UBA1 is required for cellular response to DNA damage. *Cell Cycle Georget. Tex* *11*, 1573–1582.
- MOYZIS, R.K., JONES, M.D., MEYNE, J., RATLIFF, R.L., and WU, J.-R. (1988). A highly conserved repetitive DNA sequence, (TTAGGG)_n, present at the telomeres of human chromosomes. *Proc Natl Acad Sci USA* *5*.
- Müller, Hermann (1938). The remaking of Chromosomes. *Collect. Net* *8* 182–195.
- Myers, J.S., and Cortez, D. (2006). Rapid activation of ATR by ionizing radiation requires ATM and Mre11. *J. Biol. Chem.* *281*, 9346–9350.
- Nakamura, T.M., Morin, G.B., Chapman, K.B., Weinrich, S.L., Andrews, W.H., Lingner, J., Harley, C.B., and Cech, T.R. (1997). Telomerase catalytic subunit homologs from fission yeast and human. *Science* *277*, 955–959.
- Nam, E.A., Zhao, R., Glick, G.G., Bansbach, C.E., Friedman, D.B., and Cortez, D. (2011). Thr-1989 phosphorylation is a marker of active ataxia telangiectasia-mutated and Rad3-related (ATR) kinase. *J. Biol. Chem.* *286*, 28707–28714.
- Nandakumar, J., Bell, C.F., Weidenfeld, I., Zaugg, A.J., Leinwand, L.A., and Cech, T.R. (2012). The TEL patch of telomere protein TPP1 mediates telomerase recruitment and processivity. *Nature* *492*, 285–289.
- Nasmyth, K., and Haering, C.H. (2009). Cohesin: Its Roles and Mechanisms. *Annu. Rev. Genet.* *43*, 525–558.
- Nergadze, S.G., Farnung, B.O., Wischniewski, H., Khoriauli, L., Vitelli, V., Chawla, R., Giulotto, E., and Azzalin, C.M. (2009). CpG-island promoters drive transcription of human telomeres. *RNA* *15*, 2186–2194.

- Noon, A.T., Shibata, A., Rief, N., Löbrich, M., Stewart, G.S., Jeggo, P.A., and Goodarzi, A.A. (2010). 53BP1-dependent robust localized KAP-1 phosphorylation is essential for heterochromatic DNA double-strand break repair. *Nat. Cell Biol.* *12*, 177–184.
- Noordermeer, S.M., Adam, S., Setiawati, D., Barazas, M., Pettitt, S.J., Ling, A.K., Olivieri, M., Álvarez-Quilón, A., Moatti, N., Zimmermann, M., et al. (2018). The shieldin complex mediates 53BP1-dependent DNA repair. *Nature*.
- Nozawa, R.-S., Nagao, K., Masuda, H.-T., Iwasaki, O., Hirota, T., Nozaki, N., Kimura, H., and Obuse, C. (2010). Human POGZ modulates dissociation of HP1 α from mitotic chromosome arms through Aurora B activation. *Nat. Cell Biol.* *12*, 719–727.
- Nozawa, R.-S., Nagao, K., Igami, K.-T., Shibata, S., Shirai, N., Nozaki, N., Sado, T., Kimura, H., and Obuse, C. (2013). Human inactive X chromosome is compacted through a PRC2-independent SMCHD1-HBiX1 pathway. *Nat. Struct. Mol. Biol.* *20*, 566–573.
- Okamoto, K., Bartocci, C., Ouzounov, I., Diedrich, J.K., Yates III, J.R., and Denchi, E.L. (2013). A two-step mechanism for TRF2-mediated chromosome-end protection. *Nature* *494*, 502–505.
- Olovnikov, A.M. (1971). [Principle of marginotomy in template synthesis of polynucleotides]. *Dokl. Akad. Nauk SSSR* *201*, 1496–1499.
- Olovnikov, A.M. (1973). A theory of marginotomy. The incomplete copying of template margin in enzymic synthesis of polynucleotides and biological significance of the phenomenon. *J. Theor. Biol.* *41*, 181–190.
- Orthwein, A., Fradet-Turcotte, A., Noordermeer, S.M., Canny, M.D., Brun, C.M., Strecker, J., Escibano-Diaz, C., and Durocher, D. (2014). Mitosis Inhibits DNA Double-Strand Break Repair to Guard Against Telomere Fusions. *Science* *344*, 189–193.
- Palm, W., and de Lange, T. (2008). How shelterin protects mammalian telomeres. *Annu. Rev. Genet.* *42*, 301–334.
- Pardue, M.L., Danilevskaya, O.N., Lowenhaupt, K., Slot, F., and Traverse, K.L. (1996). *Drosophila* telomeres: new views on chromosome evolution. *Trends Genet. TIG* *12*, 48–52.
- Parks, J.W., and Stone, M.D. (2014). Coordinated DNA dynamics during the human telomerase catalytic cycle. *Nat. Commun.* *5*.
- Pfeiffer, V., and Lingner, J. (2013). Replication of telomeres and the regulation of telomerase. *Cold Spring Harb. Perspect. Biol.* *5*, a010405.
- Pickett, H.A., and Reddel, R.R. (2015). Molecular mechanisms of activity and derepression of alternative lengthening of telomeres. *Nat. Struct. Mol. Biol.* *22*, 875–880.
- Pierron, G., and Puvion-Dutilleul, F. (1999). An anchorage nuclear structure for telomeric DNA repeats in HeLa cells. *Chromosome Res. Int. J. Mol. Supramol. Evol. Asp. Chromosome Biol.* *7*, 581–592.
- Pisano, S., Marchioni, E., Galati, A., Mechelli, R., Savino, M., and Cacchione, S. (2007). Telomeric nucleosomes are intrinsically mobile. *J. Mol. Biol.* *369*, 1153–1162.
- Porro, A., Feuerhahn, S., Reichenbach, P., and Lingner, J. (2010a). Molecular dissection of telomeric repeat-containing RNA biogenesis unveils the presence of distinct and multiple regulatory pathways. *Mol. Cell. Biol.* *30*, 4808–4817.
- Porro, A., Feuerhahn, S., Reichenbach, P., and Lingner, J. (2010b). Molecular dissection of telomeric repeat-containing RNA biogenesis unveils the presence of distinct and multiple regulatory pathways. *Mol. Cell. Biol.* *30*, 4808–4817.
- Porro, A., Feuerhahn, S., Delafontaine, J., Riethman, H., Rougemont, J., and Lingner, J. (2014a). Functional characterization of the TERRA transcriptome at damaged telomeres. *Nat. Commun.* *5*, 5379.
- Porro, A., Feuerhahn, S., and Lingner, J. (2014b). TERRA-reinforced association of LSD1 with MRE11 promotes processing of uncapped telomeres. *Cell Rep.* *6*, 765–776.
- Prescott, D.M. (1994). The DNA of ciliated protozoa. *Microbiol. Rev.* *58*, 233–267.
- Qiao, F., and Cech, T.R. (2008). Triple-helix structure in telomerase RNA contributes to catalysis. *Nat. Struct. Mol. Biol.* *15*, 634–640.

- Reinhardt, H.C., Aslanian, A.S., Lees, J.A., and Yaffe, M.B. (2007). p53-deficient cells rely on ATM- and ATR-mediated checkpoint signaling through the p38MAPK/MK2 pathway for survival after DNA damage. *Cancer Cell* *11*, 175–189.
- Ribes-Zamora, A., Indiviglio, S.M., Mihalek, I., Williams, C.L., and Bertuch, A.A. (2013). TRF2 interaction with Ku heterotetramerization interface gives insight into c-NHEJ prevention at human telomeres. *Cell Rep.* *5*, 194–206.
- Rippe, K., and Luke, B. (2015). TERRA and the state of the telomere. *Nat. Struct. Mol. Biol.* *22*, 853–858.
- Roberts, A.R., Blewitt, M.E., Youngson, N.A., Whitelaw, E., and Chong, S. (2011). Reduced dosage of the modifiers of epigenetic reprogramming Dnmt1, Dnmt3L, SmcHD1 and Foxo3a has no detectable effect on mouse telomere length in vivo. *Chromosoma* *120*, 377–385.
- Rogakou, E.P., Pilch, D.R., Orr, A.H., Ivanova, V.S., and Bonner, W.M. (1998). DNA Double-stranded Breaks Induce Histone H2AX Phosphorylation on Serine 139. *J. Biol. Chem.* *273*, 5858–5868.
- Roux, K.J., Kim, D.I., Raida, M., and Burke, B. (2012). A promiscuous biotin ligase fusion protein identifies proximal and interacting proteins in mammalian cells. *J. Cell Biol.* *196*, 801–810.
- Saldivar, J.C., Cortez, D., and Cimprich, K.A. (2017). The essential kinase ATR: ensuring faithful duplication of a challenging genome. *Nat. Rev. Mol. Cell Biol.* *18*, 622–636.
- Sanchez, Y., Wong, C., Thoma, R.S., Richman, R., Wu, Z., Piwnicka-Worms, H., and Elledge, S.J. (1997). Conservation of the Chk1 checkpoint pathway in mammals: linkage of DNA damage to Cdk regulation through Cdc25. *Science* *277*, 1497–1501.
- Sarek, G., Vannier, J.-B., Panier, S., Petrini, J.H.J., and Boulton, S.J. (2015). TRF2 Recruits RTEL1 to Telomeres in S Phase to Promote T-Loop Unwinding. *Mol. Cell* *57*, 622–635.
- Sartori, A.A., Lukas, C., Coates, J., Mistrik, M., Fu, S., Bartek, J., Baer, R., Lukas, J., and Jackson, S.P. (2007). Human CtIP promotes DNA end resection. *Nature* *450*, 509–514.
- Schiller, C.B., Lammens, K., Guerini, I., Cordes, B., Feldmann, H., Schlauderer, F., Möckel, C., Schele, A., Strässer, K., Jackson, S.P., et al. (2012). Structure of Mre11-Nbs1 complex yields insights into ataxia-telangiectasia-like disease mutations and DNA damage signaling. *Nat. Struct. Mol. Biol.* *19*, 693–700.
- Schmidt, J.C., Zaugg, A.J., and Cech, T.R. (2016). Live Cell Imaging Reveals the Dynamics of Telomerase Recruitment to Telomeres. *Cell* *166*, 1188–1197.e9.
- Schmutz, I., Timashev, L., Xie, W., Patel, D.J., and de Lange, T. (2017). TRF2 binds branched DNA to safeguard telomere integrity. *Nat. Struct. Mol. Biol.* *24*, 734–742.
- Sexton, A.N., Regalado, S.G., Lai, C.S., Cost, G.J., O’Neil, C.M., Urnov, F.D., Gregory, P.D., Jaenisch, R., Collins, K., and Hockemeyer, D. (2014). Genetic and molecular identification of three human TPP1 functions in telomerase action: recruitment, activation, and homeostasis set point regulation. *Genes Dev.* *28*, 1885–1899.
- Sfeir, A., and de Lange, T. (2012). Removal of shelterin reveals the telomere end-protection problem. *Science* *336*, 593–597.
- Sfeir, A., Kosiyatrakul, S.T., Hockemeyer, D., MacRae, S.L., Karlseder, J., Schildkraut, C.L., and de Lange, T. (2009). Mammalian Telomeres Resemble Fragile Sites and Require TRF1 for Efficient Replication. *Cell* *138*, 90–103.
- Sfeir, A.J., Chai, W., Shay, J.W., and Wright, W.E. (2005). Telomere-end processing the terminal nucleotides of human chromosomes. *Mol. Cell* *18*, 131–138.
- Shampay, J., Szostak, J.W., and Blackburn, E.H. (1984). DNA sequences of telomeres maintained in yeast. *Nature* *310*, 154–157.
- Shanbhag, N.M., Rafalska-Metcalf, I.U., Balane-Bolivar, C., Janicki, S.M., and Greenberg, R.A. (2010). ATM-Dependent Chromatin Changes Silence Transcription In cis to DNA Double-Strand Breaks. *Cell* *141*, 970–981.

- Shaw, N.D., Brand, H., Kupchinsky, Z.A., Bengani, H., Plummer, L., Jones, T.I., Erdin, S., Williamson, K.A., Rainger, J., Stortchevoi, A., et al. (2017). SMCHD1 mutations associated with a rare muscular dystrophy can also cause isolated arhinia and Bosma arhinia microphthalmia syndrome. *Nat. Genet.* *49*, 238–248.
- Shiloh, Y., and Ziv, Y. (2013). The ATM protein kinase: regulating the cellular response to genotoxic stress, and more. *Nat. Rev. Mol. Cell Biol.* *14*, 197–210.
- Shiotani, B., and Zou, L. (2009). Single-stranded DNA orchestrates an ATM-to-ATR switch at DNA breaks. *Mol. Cell* *33*, 547–558.
- Smogorzewska, A., van Steensel, B., Bianchi, A., Oelmann, S., Schaefer, M.R., Schnapp, G., and de Lange, T. (2000). Control of human telomere length by TRF1 and TRF2. *Mol. Cell. Biol.* *20*, 1659–1668.
- van Steensel, B., Smogorzewska, A., and de Lange, T. (1998). TRF2 protects human telomeres from end-to-end fusions. *Cell* *92*, 401–413.
- Stewart, G.S., Wang, B., Bignell, C.R., Taylor, A.M.R., and Elledge, S.J. (2003). MDC1 is a mediator of the mammalian DNA damage checkpoint. *Nature* *421*, 961–966.
- Stiff, T., Walker, S.A., Cerosaletti, K., Goodarzi, A.A., Petermann, E., Concannon, P., O’Driscoll, M., and Jeggo, P.A. (2006). ATR-dependent phosphorylation and activation of ATM in response to UV treatment or replication fork stalling. *EMBO J.* *25*, 5775–5782.
- Stucki, M., Clapperton, J.A., Mohammad, D., Yaffe, M.B., Smerdon, S.J., and Jackson, S.P. (2005). MDC1 directly binds phosphorylated histone H2AX to regulate cellular responses to DNA double-strand breaks. *Cell* *123*, 1213–1226.
- Sun, Y., Jiang, X., Chen, S., Fernandes, N., and Price, B.D. (2005). A role for the Tip60 histone acetyltransferase in the acetylation and activation of ATM. *Proc. Natl. Acad. Sci. U. S. A.* *102*, 13182–13187.
- Szostak, J.W., and Blackburn, E.H. (1982). Cloning yeast telomeres on linear plasmid vectors. *Cell* *29*, 245–255.
- Takai, H., Smogorzewska, A., and de Lange, T. (2003). DNA damage foci at dysfunctional telomeres. *Curr. Biol. CB* *13*, 1549–1556.
- Takai, K.K., Kibe, T., Donigian, J.R., Frescas, D., and de Lange, T. (2011). Telomere protection by TPP1/POT1 requires tethering to TIN2. *Mol. Cell* *44*, 647–659.
- Takeda, S., Nakamura, K., Taniguchi, Y., and Paull, T.T. (2007). Ctp1/CtIP and the MRN complex collaborate in the initial steps of homologous recombination. *Mol. Cell* *28*, 351–352.
- Tang, J., Cho, N.W., Cui, G., Manion, E.M., Shanbhag, N.M., Botuyan, M.V., Mer, G., and Greenberg, R.A. (2013). Acetylation limits 53BP1 association with damaged chromatin to promote homologous recombination. *Nat. Struct. Mol. Biol.* *20*, 317–325.
- Tang, M., Li, Y., Zhang, X., Deng, T., Zhou, Z., Ma, W., and Songyang, Z. (2014). Structural Maintenance of Chromosomes Flexible Hinge Domain Containing 1 (SMCHD1) Promotes Non-homologous End Joining and Inhibits Homologous Recombination Repair upon DNA Damage. *J. Biol. Chem.* *289*, 34024–34032.
- Timashev, L.A., Babcock, H., Zhuang, X., and de Lange, T. (2017). The DDR at telomeres lacking intact shelterin does not require substantial chromatin decompaction. *Genes Dev.* *31*, 578–589.
- Tomimatsu, N., Mukherjee, B., Deland, K., Kurimasa, A., Bolderson, E., Khanna, K.K., and Burma, S. (2012). Exo1 plays a major role in DNA end resection in humans and influences double-strand break repair and damage signaling decisions. *DNA Repair* *11*, 441–448.
- Tomlinson, R.L., Ziegler, T.D., Supakorndej, T., Terns, R.M., and Terns, M.P. (2006). Cell cycle-regulated trafficking of human telomerase to telomeres. *Mol. Biol. Cell* *17*, 955–965.
- Tommerup, H., Dousmanis, A., and de Lange, T. (1994). Unusual chromatin in human telomeres. *Mol. Cell. Biol.* *14*, 5777–5785.
- Townsley, D.M., Dumitriu, B., and Young, N.S. (2014). Bone marrow failure and the telomeropathies. *Blood* *124*, 2775–2783.
- Vancevska, A., Douglass, K.M., Pfeiffer, V., Manley, S., and Lingner, J. (2017). The telomeric DNA damage response occurs in the absence of chromatin decompaction. *Genes Dev.* *31*, 567–577.

- Vannier, J.-B., Pavicic-Kaltenbrunner, V., Petalcorin, M.I.R., Ding, H., and Boulton, S.J. (2012). RTEL1 Disassembles T Loops and Counteracts Telomeric G4-DNA to Maintain Telomere Integrity. *Cell* *149*, 795–806.
- Venteicher, A.S., Abreu, E.B., Meng, Z., McCann, K.E., Terns, R.M., Veenstra, T.D., Terns, M.P., and Artandi, S.E. (2009). A human telomerase holoenzyme protein required for Cajal body localization and telomere synthesis. *Science* *323*, 644–648.
- Verdun, R.E., and Karlseder, J. (2006). The DNA damage machinery and homologous recombination pathway act consecutively to protect human telomeres. *Cell* *127*, 709–720.
- Walmsley, R.W., Chan, C.S., Tye, B.K., and Petes, T.D. (1984). Unusual DNA sequences associated with the ends of yeast chromosomes. *Nature* *310*, 157–160.
- Wang, C.-Y., Jégu, T., Chu, H.-P., Oh, H.J., and Lee, J.T. (2018). SMCHD1 Merges Chromosome Compartments and Assists Formation of Super-Structures on the Inactive X. *Cell* *174*, 406–421.e25.
- Wang, F., Podell, E.R., Zaug, A.J., Yang, Y., Baciu, P., Cech, T.R., and Lei, M. (2007). The POT1-TPP1 telomere complex is a telomerase processivity factor. *Nature* *445*, 506–510.
- Watson, J.D. (1972). Origin of concatemeric T7 DNA. *Nature. New Biol.* *239*, 197–201.
- Wawrousek, K.E., Fortini, B.K., Polaczek, P., Chen, L., Liu, Q., Dunphy, W.G., and Campbell, J.L. (2010). *Xenopus* DNA2 is a helicase/nuclease that is found in complexes with replication proteins And-1/Ctf4 and Mcm10 and DSB response proteins Nbs1 and ATM. *Cell Cycle Georget. Tex* *9*, 1156–1166.
- Weinert, T.A., and Hartwell, L.H. (1988). The RAD9 gene controls the cell cycle response to DNA damage in *Saccharomyces cerevisiae*. *Science* *241*, 317–322.
- Wilkie, A.O.M. (2017). Many faces of SMCHD1. *Nat. Genet.* *49*, 176–178.
- Wright, W.E., Piatyszek, M.A., Rainey, W.E., Byrd, W., and Shay, J.W. (1996). Telomerase activity in human germline and embryonic tissues and cells. *Dev. Genet.* *18*, 173–179.
- Wu, N. (2012). The Smc complexes in DNA damage response. *11*.
- Xu, G., Chapman, J.R., Brandsma, I., Yuan, J., Mistrik, M., Bouwman, P., Bartkova, J., Gogola, E., Warmerdam, D., Barazas, M., et al. (2015). REV7 counteracts DNA double-strand break resection and affects PARP inhibition. *Nature* *521*, 541–544.
- Yu, G.L., Bradley, J.D., Attardi, L.D., and Blackburn, E.H. (1990). In vivo alteration of telomere sequences and senescence caused by mutated *Tetrahymena* telomerase RNAs. *Nature* *344*, 126–132.
- Yu, T.-Y., Kao, Y., and Lin, J.-J. (2014). Telomeric transcripts stimulate telomere recombination to suppress senescence in cells lacking telomerase. *Proc. Natl. Acad. Sci. U. S. A.* *111*, 3377–3382.
- Zhang, C.-Z., Leibowitz, M.L., and Pellman, D. (2013). Chromothripsis and beyond: rapid genome evolution from complex chromosomal rearrangements. *Genes Dev.* *27*, 2513–2530.
- Zhang, C.-Z., Spektor, A., Cornils, H., Francis, J.M., Jackson, E.K., Liu, S., Meyerson, M., and Pellman, D. (2015). Chromothripsis from DNA damage in micronuclei. *Nature* *522*, 179–184.
- Zhong, Z., Shiue, L., Kaplan, S., and de Lange, T. (1992). A mammalian factor that binds telomeric TTAGGG repeats in vitro. *Mol. Cell. Biol.* *12*, 4834–4843.
- Zhu, X.D., Küster, B., Mann, M., Petrini, J.H., and de Lange, T. (2000). Cell-cycle-regulated association of RAD50/MRE11/NBS1 with TRF2 and human telomeres. *Nat. Genet.* *25*, 347–352.
- Zhu, Y., Tomlinson, R.L., Lukowiak, A.A., Terns, R.M., and Terns, M.P. (2004). Telomerase RNA accumulates in Cajal bodies in human cancer cells. *Mol. Biol. Cell* *15*, 81–90.
- Zimmermann, M., Lottersberger, F., Buonomo, S.B., Sfeir, A., and de Lange, T. (2013). 53BP1 regulates DSB repair using Rif1 to control 5' end resection. *Science* *339*, 700–704.
- Zimmermann, M., Kibe, T., Kabir, S., and de Lange, T. (2014). TRF1 negotiates TTAGGG repeat-associated replication problems by recruiting the BLM helicase and the TPP1/POT1 repressor of ATR signaling. *Genes Dev.* *28*, 2477–2491.
- Zou, L. (2003). Sensing DNA Damage Through ATRIP Recognition of RPA-ssDNA Complexes. *Science* *300*, 1542–1548.

Aleksandra Vančevska –CV

NAME: Aleksandra Vančevska
BIRTHDATE: 11/16/1990, Belgrade, Serbia
ADDRESS: Chemin de la Foret 6, CH-1024, Lausanne, Switzerland
TEL: +41 78 636 73 22
E-MAIL: aleksandra.vancevska@epfl.ch



EDUCATION

2013 – 2018 PhD student in Prof. Joachim Lingner's group, EPFL, Switzerland
2009 – 2013 Student of Biochemistry at the Faculty of Chemistry, University of Belgrade, graduated *summa cum laude*

RESEARCH EXPERIENCE

2013 Summer Research Program for undergraduate students, Project: *Characterization of ubiquitin deficient TPP1 mutants*, Supervisor: Dr. Ivo Zemp, Joachim Lingner's laboratory, EPFL Switzerland
2011 Summer internship at Laboratory for molecular biology, Project: *DNase activity assay*, supervisor: Dr. Aleksandra Nikolic, Institute for molecular genetics and genetic engineering, Serbia
2010 Kupcinet-Getz International Science Summer School for undergraduate students, Project: *Activator of Dronc with E3 ubiquitin ligase complex*, Eli Arama's laboratory, Weizmann Institute of Science, Israel
2009 Participant of XLAB Goettingen Experimental Laboratory for young people, Goettingen, Germany
2008 – 2009 Participant of Molecular Biomedicine educational program at Petnica Science Centre, Serbia

PUBLICATIONS

Vancevska A., Douglass KM, Pfeiffer V., Manley S., Lingner J. (2017). The telomeric DNA damage response occurs in the absence of chromatin decompaction. *Genes Dev*, 31: 567-577.

Vancevska A., Nikolic A., Bonaci-Nikolic B., Sikijevic D., Radojkovic D. (2016) Assessment of Deoxyribonuclease activity in serum samples of patients with systemic lupus erythematosus: Fluorescence-Based Method Versus ELISA. *J Clin Lab Anal.*, 30(6):797-803

Vancevska A., Nikolic A. (2013) Method for assessment of deoxyribonuclease activity in biological samples. *Laboratory Medicine*, 44(2):125-128

MANUSCRIPTS IN PREPARATION

Vancevska A., Pfeiffer V., Lingner J. (2018) SMCHD1 and LRIF1 Promote ATM-dependent DNA Damage Signaling and Repair of Uncapped Telomeres. (*in preparation*)

CONFERENCE PRESENTATIONS

Vancevska A., Pfeiffer V., Lingner J., Poster presentation, EMBO meeting: Telomere biology in health and human disease, Portugal, May 01-06, 2018.

Vancevska A., Pfeiffer V., Lingner J., Poster presentation, Global Young Scientists Summit, Singapore, January 21-26, 2018.

Vancevska A., Douglass K.M., Pfeiffer V., Manley S., Lingner J., Poster presentation, CSHL Telomeres & Telomerase meeting at CSHL, New York, May 02-06, 2017.

Aleksandra Vančevska –CV

Vancevska A., Douglass K.M., Pfeiffer V., Manley S., Lingner J., Poster presentation, EpiGeneSwiss Kick-off meeting in Weggis, Switzerland, June 6-7, 2016.

Vancevska A., Douglass K.M., Pfeiffer V., Manley S., Lingner J., Oral and poster presentation, Swiss Summer School on Molecular and Chemical Mechanisms in Epigenetics in Arolla, Switzerland, July 12-17, 2015. **Invited speaker**

Vancevska A., Douglass K.M., Pfeiffer V., Manley S., Lingner J., Oral and poster presentation, CSHL Telomeres & Telomerase meeting at CSHL, New York, April 28-May 02, 2015. **Invited speaker**

Vancevska A., Nikolic A., Poster presentation, Leiden International Medical Students Conference in Leiden, Netherlands, March 13-17, 2013.

Vancevska A. Oral and poster presentation, Petnica Students' Science Conference, Petnica Science school for gifted high school students, December 2008. **Invited speaker**

ORGANIZATION OF CONFERENCES

2015 July Summer school in translational biology. <http://archiveweb.epfl.ch/sstb2015.epfl.ch/>, Organizers: Wen-bin Alfred Chng (EPFL), Allan Lamontanara (EPFL), Oleg Mikhajlov (EPFL), **Aleksandra Vancevska (EPFL)**, Nino Jejelava (ETHZ), Natalie Russi (ETHZ/UZH)

STUDENT SUPERVISION AND TEACHING

2017
Sept- Dec Internship student co-supervision with Marianna Feretzaki
Student name: Nicolas Séne
Project: **Endogenous tagging of shelterin proteins TRF1 and TRF2 with mCherry in HeLa cells using CRISPR/Cas9 mediated genome editing**

2016
Feb-May Lab immersion student co-supervision with Gérald Lossaint
Student name: Lorenzo Archetti
Project: **Effects of TRF1 depletion on mitosis dynamics in HeLa cells**

2015
Sept- Dec Lab immersion student co-supervision with Gérald Lossaint
Student name: Numa Piot
Project: **Effects of CDK1 inhibition on TRF1-dependent telomere fragility**

2014 April High school student supervision as part of the program Swiss Youth in Science (<https://sjf.ch/>)
Student name: Jasmin Steudler
Project: **Cloning and expression of YFP donor plasmid for assessment of CRISPR-Cas9 mediated genome editing efficiency**

2014 – 2015 Laboratoire intégré en sciences de la vie I&II- EPFL undergraduate course teaching assistant
http://edu.epfl.ch/coursebook/en/integrated-labo-in-life-sciences-ii-BIO-204?cb_cycle=bama_cyclebachelor&cb_section=sv

2010 – 2013 Junior assistant in Molecular Biomedicine educational program at Petnica Science Centre, Serbia

PERSONAL INTERESTS

- Serbian traditional dancing
- Yoga
- Crocheting
- Hiking

LANGUAGES

- Serbian (native), Macedonian (native), English, Spanish, French

